Quantum violation of classical physics in macroscopic systems

Lucas Clemente

Ludwig Maximilian University of Munich

Max Planck Institute of Quantum Optics

Quantum violation of classical physics in macroscopic systems

Lucas Clemente

Dissertation
an der Fakultät für Physik
der Ludwig-Maximilians-Universität
München

vorgelegt von Lucas Clemente
aus München

München, im November 2015

Tag der mündlichen Prüfung: 26. Januar 2016

Erstgutachter: Prof. J. Ignacio Cirac, PhD

Zweitgutachter: Prof. Dr. Jan von Delft

Weitere Prüfungskommissionsmitglieder: Prof. Dr. Harald Weinfurter, Prof. Dr. Armin Scrinzi

> *Reality is that which, when you stop believing in it, doesn't go away.*
>
> — **Philip K. Dick**
>
> *How To Build A Universe That Doesn't Fall Apart Two Days Later*, a speech published in the collection *I Hope I Shall Arrive Soon*

Contents

Abstract

While quantum theory has been tested to an incredible degree on microscopic scales, quantum effects are seldom observed in our everyday macroscopic world. The curious results of applying quantum mechanics to macroscopic objects are perhaps best illustrated by Erwin Schrödinger's famous thought experiment, where a cat can be put into a superposition state of being both dead and alive. Obviously, these quantum predictions are in stark contradiction to our common experience. Even with plenty of theoretical explanations put forward to explain this discrepancy, a large number of questions about the frontier between the quantum and the classical world remain unanswered.

To distinguish between classical and quantum behavior, two fundamental concepts inherent to classical physics have been established over the years: The world view of *local realism* limits the power of classical experiments to establish correlations over space, while the world view of *macroscopic realism* (or *macrorealism*) restricts temporal correlations. Necessary conditions for both world views have been formulated in the form of Bell and Leggett-Garg inequalities, and Bell inequalities have been shown to be violated by quantum mechanics through increasingly conclusive experiments. Furthermore, many challenging steps towards convincing violations of macrorealism have been taken in a number of recent experiments.

In the first part of this thesis, conditions for macrorealism are analyzed in detail. Two necessary conditions for macrorealism, the original Leggett-Garg inequality and the recently proposed *no-signaling in time* condition, are presented. It is then shown that a combination of no-signaling in time conditions is not only necessary but also sufficient for the existence of a macrorealistic description. Finally, an operational formulation of no-signaling in time, in terms of positive-operator valued measurements and Hamiltonians, is derived.

In the next part, we argue that these results lead to a suitable definition of classical behavior. In particular, we provide a formalism to judge the classicality of measurements and time evolutions. We then proceed to apply it to a number of exemplary

measurement operators and Hamiltonians. Finally, we argue for the importance of spontaneously realized Hamiltonians in our intuition of classical behavior.

Next, differences between local realism and macrorealism are analyzed. For this purpose, the probability polytopes for spatially and temporally separated experiments are compared, and a fundamental difference in the power of quantum mechanics to build both types of correlations is discovered. This result shows that Fine's theorem, which states that a set of Bell inequalities is necessary and sufficient for local realism, is not transferable to macrorealism. Thus, (Leggett-Garg) inequalities are in principle not well-suited for tests of macrorealism, as they can never form a necessary and sufficient condition, and unnecessarily restrict the violating parameter space. No-signaling in time is both better suited and more strongly motivated from the underlying physical theory.

In the final part of this thesis, a concrete experimental setup for implementing quantum experiments with macroscopic objects is proposed. It consists of a superconducting micro-sphere in the Meißner state, which is levitated by magnetic fields. Through its expelled magnetic field, the sphere's center-of-mass motion couples to a superconducting quantum circuit. Properly tuned, ground state cooling can be realized, since the sphere's motion is extremely well isolated from the surrounding environment. This setup therefore is a promising candidate for the observation of quantum effects in macroscopic systems.

Zusammenfassung

Obwohl Quantenmechanik auf mikroskopischen Skalen Vorhersagen trifft, die mit unglaublicher Präzision experimentell bestätigt sind, beobachten wir in unserer alltäglichen makroskopischen Welt kaum ihren Einfluss. Die Anwendung von Quantentheorie auf makroskopische Objekte liefert vielmehr außerordentlich seltsame Ergebnisse. Das bekannte Beispiel, Erwin Schrödinger's Gedankenexperiment, in dem eine Katze in einen Überlagerungszustand aus tot und lebendig gebracht werden kann, illustriert dies anschaulich. Offensichtlicherweise entspricht das nicht unseren alltäglichen Erfahrungen. Obwohl unzählige Theorien versuchen, diesen Unterschied zwischen Quantenmechanik und klassischer Physik zu erklären, bleiben viele Fragen über die Grenze zwischen diesen beiden Welten offen.

Im Laufe des letzten Jahrhunderts wurden zwei fundamentale Charakteristika von klassischer Physik identifiziert, die eine Unterscheidung von klassischem und quantenmechanischem Verhalten ermöglichen: Die Weltbilder *lokaler Realismus* und *makroskopischer Realismus* (oder *Makrorealismus*) setzen dem Aufbau von räumlichen bzw. zeitlichen Korrelationen in klassischen Theorien prinzipielle Grenzen. Notwendige Bedingungen für beide Weltbilder wurden in Form von Bell-Ungleichungen und Leggett-Garg-Ungleichungen formuliert. Die Verletzung von Bell-Ungleichungen (und damit von lokalem Realismus) durch Quantenmechanik ist durch Experimente mit zunehmender Zuverlässigkeit bestätigt, und wichtige Schritte hin zu experimentellen Tests von Makrorealismus wurden in den letzten Jahren unternommen.

Im ersten Teil dieser Dissertation werden Bedingungen für Makrorealismus im Detail analysiert. Zwei notwendige Bedingungen, die ursprüngliche Leggett-Garg-Ungleichung und die kürzlich vorgeschlagene Bedingung namens *no-signaling in time* werden vorgestellt. Es wird ferner gezeigt, dass eine Kombination aus *no-signaling in time* und Kausalitätsbedingungen sowohl hinreichend als auch notwendig für die Existenz einer makrorealistischen Beschreibung eines Experiments ist. Zuletzt wird eine operationelle Formulierung von *no-signaling in time* als Forderungen an POVM-Messoperatoren und den Hamiltonoperator hergeleitet.

Der nächste Teil legt dar, dass sich aus den obigen Ergebnissen eine passende Definition von klassischem Verhalten ergibt. Wir definieren die Klassizität von Messungen und Zeitentwicklungen, und wenden unsere Ergebnisse auf einige beispielhafte Messoperatoren und Hamiltonoperatoren an. Ferner wird die Wichtigkeit der in der Natur spontan realisierten Wechselwirkungen für jede Definition von klassischem Verhalten diskutiert.

Im dritten Teil werden Unterschiede zwischen lokalem Realismus und makroskopischem Realismus analysiert. Wir betrachten hierfür die Form der Räume, die durch die Wahrscheinlichkeitsverteilungen in beiden Fällen aufgespannt werden. Wir finden fundamentale Unterschiede in der Struktur beider Polytope, insbesondere in Bezug auf Quantenmechanik. Unsere Ergebnisse belegen, dass Fines Theorem, welches besagt, dass Bell-Ungleichungen hinreichend und notwendig für lokalen Realismus sind, nicht auf Makrorealismus übertragbar ist. Daraus folgern wir, dass (Leggett-Garg-)Ungleichungen prinzpiell nicht optimal für experimentelle Tests von Makrorealismus sind, da sie niemals hinreichend sein können, und den verletzenden Parameterraum unnötig einschränken. *No-signaling in time* ist somit sowohl mächtiger, als auch besser durch die zugrundeliegende Theorie motiviert.

Im letzten Teil dieser Dissertation schlagen wir einen konkreten experimentellen Aufbau für Quantenexperimente mit makroskopischen Objekten vor. Er besteht aus einer supraleitenden Kugel im Mikrometerbereich im Meißner-Zustand. Die Kugel wird durch ein starkes Magnetfeld in der Schwebe gehalten und gefangen. Über das verdrängte Magnetfeld koppelt die Schwerpunktsposition der Kugel an einen supraleitenden Quantenstromkreis. Mit einem passenden Antriebsfeld kann die Schwerpunktsbewegung dann in den Quantengrundzustand gekühlt werden, da die Kugel extrem gut von der Umgebug isoliert ist. Unser Vorschlag ist damit ein vielversprechender Kandidat für die Beobachtung von Quanteneffekten in makroskopischen Systemen.

List of publications

Publications relevant to this thesis

- [1]: L. Clemente and J. Kofler, 'Necessary and sufficient conditions for macroscopic realism from quantum mechanics', Phys. Rev. A **91**, 062103 (2015)
  See chapters 1 and 2

- [2]: L. Clemente and J. Kofler, 'The emergence of macroscopic classical dynamics from microscopic quantum behavior', (in preparation)
  See chapter 2

- [3]: L. Clemente and J. Kofler, 'No Fine theorem for macrorealism: Retiring the Leggett-Garg inequality', (2015), arXiv:1509.00348 [quant-ph]
  See chapter 3

- [4]: O. Romero-Isart, L. Clemente, C. Navau, A. Sanchez, and J. I. Cirac, 'Quantum Magnetomechanics with Levitating Superconducting Microspheres', Phys. Rev. Lett. **109**, 147205 (2012)
  See chapter 4

Other publications

- [5]: W. Assmann, R. Becker, H. Otto, M. Bader, L. Clemente, S. Reinhardt, C. Schäfer, J. Schirra, S. Uschold, A. Welzmüller, and R. Sroka, '32P-haltige Folien als Implantate für die LDR-Brachytherapie gutartiger Stenosen in der Urologie und Gastroenterologie', Zeit. Med. Phys. **23**, 21 (2013)

- [6]: F. Pastawski, L. Clemente, and J. I. Cirac, 'Quantum memories based on engineered dissipation', Phys. Rev. A **83**, 012304 (2011)

• [7]: C. Hoeschen, H. Schlattl, M. Zankl, T. Seggebrock, L. Clemente, and F. Grüner, 'Simulating Mammographic Absorption Imaging and Its Radiation Protection Properties', in *World Congress on Medical Physics and Biomedical Engineering, September 7 - 12, 2009, Munich, Germany* (Springer Berlin Heidelberg, Berlin, Heidelberg, 2009), pp. 355–358

Acknowledgments

First and foremost, I am deeply indebted to my supervisor Ignacio Cirac for the privilege of doing research with him. With his extraordinary knowledge, incredible understanding, and wonderful passion for physics, he has assembled a group of inspiring scientists, who manage day by day to expand our understanding of the quantum world. I thank him in particular for his trust, his patience and guidance during my time at MPQ.

I am very grateful to have been able to work with my co-advisor Johannes Kofler. His astonishing knowledge and extraordinarily precise way of thinking have inspired me from the start, and led to countless sparkling discussions, spanning from foundational physics problems to more worldly topics. I will sorely miss working with him.

I would also like to thank Oriol Romero-Isart for co-advising me during the first part of my PhD. His passion for physics made our many discussions about novel physical systems fun and inspiring.

Further, I want to thank our collaborators from Barcelona, Àlvar Sànchez and Carles Navau, for their great pedagogical skills in teaching us about superconductivity, and their detailed contributions to our joint work.

Special thanks go to Guido Bacciagaluppi, Chris Timpson and Owen Maroney for fruitful scientific and philosophical discussions.

I also thank Jan von Delft for kindly agreeing to act as a referee for this thesis.

I am thankful to all authors of free and open source software that I used during my work.

Moreover, I am very thankful to all former and current members of our group, who made working at MPQ incredibly inspiring and joyful. In particular, I want to thank Eric Kessler, Maita Schade and Ivan Glasser for being great office-mates, Heike Schwager for many fun and inspiring discussions, Géza Giedke for his countless

contributions to our group, both scientific and organizational, Xiaotong Ni for interesting discussions about machine learning, and both Veronika Lechner and Andrea Kluth for their always helpful administrative assistance.

Certainly, this thesis would not have been possible without the generous and unconditional support from my family. I am deeply grateful to my parents, my sister and my grandparents for all their love.

Finally, I thank Patricia Kammerer for her love and support.

0 Introduction

> *Das Typische an solchen Fällen ist, daß eine ursprünglich auf den Atombereich beschränkte Unbestimmtheit sich in grobsinnliche Unbestimmtheit umsetzt, die sich dann durch direkte Beobachtung entscheiden läßt. Das hindert uns, in so naiver Weise ein „verwaschenes Modell" als Abbild der Wirklichkeit gelten zu lassen. An sich enthielte es nichts Unklares oder Widerspruchsvolles.* ***Es ist ein Unterschied zwischen einer verwackelten oder unscharf eingestellten Photographie und einer Aufnahme von Wolken und Nebelschwaden.***
>
> *It is typical of these cases that an indeterminacy originally restricted to the atomic domain becomes transformed into macroscopic indeterminacy, which can then be resolved by direct observation. That prevents us from so naively accepting as valid a "blurred model" for representing reality. In itself, it would not embody anything unclear or contradictory.* ***There is a difference between a shaky or out-of-focus photograph and a snapshot of clouds and fog banks.***
>
> **— Erwin Schrödinger**
> On macroscopic superpositions in *Die gegenwärtige Situation in der Quantenmechanik* [8], translation from ref. [9], highlighting added

0.1 History and motivation

It is one of nature's subtle ironies that quantum mechanics, the perhaps best-tested modern physical theory[1], gives rise to a plethora of unanswered foundational questions. Issues like the measurement problem [11, 12], quantum violations of local realism [13], and the vivid debate about different interpretations of quantum mechanics [14–16], have kept both physicists and philosophers busy for almost a century. Among these problems is one (inadvertently) put forward by Erwin Schrödinger in 1935 [8], with his famous cat-based thought experiment (see fig. 0.1): the question of the validity of quantum mechanics for macroscopic systems.

Many quantum mechanical peculiarities are in stark contrast to the behavior of our macroscopic everyday world. While microscopic particles, such as photons, electrons or even large molecules, can nowadays be put into superposition or entangled states [17–19], the concept that a macroscopic object, such as a cat, could be in a superposition state, seems, in Schrödinger's words, *burlesque*. So, if quantum mechanics provides such an excellent description of effects on the micro-scale, *why are quantum phenomena not a commonplace banality in our macroscopic world?*

Over the past decades, various attempts have been made to answer this question. While *quantum decoherence* [20–24] explains how strong interaction between quantum systems and its environment leads to classical behavior[2], it does not by itself set an upper limit to the size of systems that can still exhibit quantum behavior. Alternatively, a variety of novel theories have been put format to address this issue. Through (in principle) observable changes to quantum physics, they impose fundamental limits to the maximum scales of quantum behavior. Since they introduce novel, real physical processes leading to an accelerated collapse of the wave function, they are called *objective collapse theories*. Perhaps the best-known example is the Ghirardi-Rimini-Weber-Pearle model of continuous spontaneous localization [25–28], which proposes a fundamental (non-quantum) source of "decoherence" with two free parameters: a fundamental frequency for localization events, and characteristic length scale for the localization distance. Another direction is the application of gravitational concepts or string theory to quantum mechanics, e.g. by Penrose and Diósi [29–33] or by Ellis, Mohanty, Nanopoulos, and Mavromatos [34, 35].

[1] Precision tests of quantum electrodynamics find agreement between the measured and theorized value of the fine structure constant with a relative error of about 10^{-10} [10].

[2] Here one should distinguish between decoherence, which explains how a system gets entangled with the environment, and the subsequent collapse of the wave function. The question of how and when the actual collapse occurs (and the role of the observer in the process) is called the *quantum measurement problem*.

Figure 0.1: The absurdity of Schrödinger's cat thought experiment has spawned an overwhelming amount of references in popular culture. The above drawing from the *Oatmeal* webcomic [37] puts a curious twist on its setup.

Since the mentioned theories modify quantum behavior and present fundamental limits to the reach of quantum mechanics, they can in principle be falsified by the observation of quantum behavior on the macro scale. Experiments are quickly approaching the regime where first tests are feasible [36]. A novel experimental setup with some promising features is discussed in this thesis in chapter 4.

While the proposals mentioned above modify quantum mechanics to include additional, dynamic processes, recently, an orthogonal approach was proposed by Kofler and Brukner [38–40]. Investigating the measurement process itself, they showed that using solely suitably coarse-grained measurements, one cannot observe quantum behavior for a large class of Hamiltonian time evolutions. On the other hand, sharp measurements (in principle) allow the observation of quantum effects even on macroscopic systems, but are exceedingly hard to realize. In this thesis, their work is extended from spins to arbitrary systems in chapter 1, and applied to various measurement operators and Hamiltonians in chapter 2.

Before we[3] go into depth on tests of quantum mechanics in macroscopic systems, let us first give a brief introduction to *local realism*, one particularly important classical concept that is violated on the microscopic level. While the rest of this thesis focuses more on the related concept of *macroscopic realism*, a discussion of local realism is interesting from a historical perspective and will be of use in chapter 3.

0.2 Local realism and Bell's theorem

In 1935, Einstein, Podolsky and Rosen (EPR) published a seminal paper on the completeness of quantum theory [41]. Using the effects of what is now known as *quantum entanglement*, they attempted to show that the quantum wave function cannot be considered a complete description of *physical reality*[4]. Their proof is best illustrated by Bohm and Aharonov's example [43]: Consider two spin $1/2$ particles are emitted from a single spin 0 particle and sent to two observers, Alice and Bob. Alice then measures the spin of her particle in a random direction. Due to conservation of angular momentum, she can now predict with certainty the result of Bob's measurement, if both measurement directions are aligned. However, since Alice could have chosen any measurement direction, and assuming locality, i.e. the absence of "spooky action at a distance" [42], the result of any of Bob's possible measurements must already have been predetermined. Since these predetermined values are not part of the quantum description, EPR concluded that the wave function must be an incomplete description of reality. As a solution, they argued for the extension of quantum mechanics with these predetermined values, which were later called *hidden variables*.

Today, the conjunction of locality and realism is usually called *local realism*. It is the world view that all physical properties always exist independent of measurements (i.e. the existence of hidden variables), and that events at one point in space cannot have an instantaneous influence on a distant point in space. In Scott Aaronson's words [44], "it's the thing you believe in, if you believe all the physicists babbling about 'quantum entanglement' just missed something completely obvious."

Motivated by EPR's proposal, in 1964 John S. Bell presented his famous theorem [45][5]: local hidden-variable models are fundamentally limited and cannot reproduce truly quantum mechanical behavior. More technically, theories fulfilling local realism

[3] Throughout this thesis, plural pronouns ("we", "us", "our") are used for simplicity. Depending on the context, they are meant to include the co-authors of the presented studies.

[4] The meaning of the term *physical reality* was often illustrated by Einstein with the question [42] "is the moon there when nobody is looking?"

[5] For reviews of Bell's theorem and violations of local realism, see refs. [13, 46].

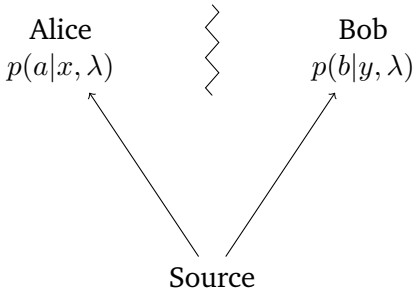

Figure 0.2: A sketch of an experiment testing local realism. A source generates two particles, that are, after some initial interaction, sent to Alice and Bob. If no communication between them is possible during the measurement process, as stylized by the zigzag line, then local realism demands that their probability distributions for the outcomes a, b must only depend on their own individual settings x, y, and the hidden variables λ.

must also fulfill all so-called *Bell inequalities*, while quantum entangled states are able to violate them. This allows for an explicit experimental test of whether nature follows local realism or behaves in agreement with quantum mechanics[6].

In the following decades until today, many alternative and, in some cases, more general inequalities have been found [48–52]. The *CHSH inequality*, perhaps the most important Bell inequality today, was proposed by Clauser, Horne, Shimony and Holt ("CHSH") in 1969 [48]. Let us now briefly recapitulate its derivation. We follow the calculations in ref. [13].

Consider the experimental setup sketched in fig. 0.2: Two physical systems (e.g. two particles), that have initially been allowed to interact with each other, are now separated. The first system is sent to Alice, the second system is sent to Bob. Both observers have the capability to perform different measurements on their individual system. We denote the choice of measurement (setting) of Alice by x, and the one of Bob by y. Their outcomes are called a and b, respectively. If the experiment is repeated a sufficient number of times, we obtain a probability distribution $p(ab|xy)$ for the outcomes given the respective measurement settings. Note that in general this probability does not factorize,

$$p(ab|xy) \neq p(a|x)p(b|y). \tag{0.1}$$

Let us now assume the existence of hidden variables λ, which completely capture the state of the system. The probability distributions then depend only on λ, their re-

[6] While an experimental violation of Bell's inequality disproves all local realistic theories, it certainly does not prove *quantum mechanics*, as, in the sense of Popper, physical theories can only be falsified [47].

spective measurement settings, and the other party's outcome; we write $p(a|xy,b,\lambda)$, $p(b|xy,a,\lambda)$ and $p(ab|xy,\lambda)$.

Additionally, assume locality, i.e. that Alice and Bob cannot communicate their measurement settings and results between each other. In an experiment, this requirement may be realized by space-like separation of both observers, and by randomly selecting the settings and performing the measurements in a time shorter than information (light) would need to travel the distance from Alice to Bob. Then, the joint probability factorizes into

$$p(ab|xy,\lambda) = p(a|x,\lambda)p(b|y,\lambda). \tag{0.2}$$

If the experiment is repeated multiple times, initial states with different λ may be produced by the source. Hence, we introduce a probability distribution $q(\lambda)$. Furthermore assuming that x, y can be chosen independently from λ, the *freedom of choice* assumption, we can write the joint probability distribution as

$$p(ab|xy) = \int \mathrm{d}\lambda\, q(\lambda)p(a|x,\lambda)p(b|y,\lambda). \tag{0.3}$$

For simplicity, let us now consider the case of only two measurement settings $x, y \in \{0,1\}$ and dichotomic outcomes $a, b \in \{-1,+1\}$. The expectation value of ab, given settings x, y, is defined as $\langle a_x b_y\rangle = \sum_{a,b} ab\, p(ab|xy)$, and can take values from -1 to 1. Using eq. (0.3), we can write this expectation value in terms of the local expectation values,

$$\langle a_x b_y\rangle = \int \mathrm{d}\lambda\, q(\lambda)\, \langle a_x\rangle_\lambda \langle b_y\rangle_\lambda\,, \tag{0.4}$$

where we introduced $\langle a_x\rangle_\lambda = \sum_a a\, p(a|x,\lambda)$ and $\langle b_y\rangle_\lambda = \sum_b b\, p(b|y,\lambda)$.

Consider now the expression

$$S \equiv \langle a_0 b_0\rangle + \langle a_0 b_1\rangle + \langle a_1 b_0\rangle - \langle a_1 b_1\rangle\,, \tag{0.5}$$

which we can, assuming local realism, also write as $S = \int \mathrm{d}\lambda\, q(\lambda) S_\lambda$, where

$$S_\lambda \equiv \langle a_0\rangle_\lambda \langle b_0\rangle_\lambda + \langle a_0\rangle_\lambda \langle b_1\rangle_\lambda + \langle a_1\rangle_\lambda \langle b_0\rangle_\lambda - \langle a_1\rangle_\lambda \langle b_1\rangle_\lambda\,. \tag{0.6}$$

Since $|\langle a_x\rangle_\lambda| \leq 1$, we have

$$\begin{aligned} S_\lambda &\leq |\langle a_0\rangle_\lambda (\langle b_0\rangle_\lambda + \langle b_1\rangle_\lambda)| + |\langle a_1\rangle_\lambda (\langle b_0\rangle_\lambda - \langle b_1\rangle_\lambda)| \\ &\leq |\langle b_0\rangle_\lambda + \langle b_1\rangle_\lambda| + |\langle b_0\rangle_\lambda - \langle b_1\rangle_\lambda|. \end{aligned} \tag{0.7}$$

Without loss of generality we can permute the settings and outcomes such that $\langle b_0\rangle_\lambda \geq \langle b_1\rangle_\lambda \geq 0$. We obtain

$$S_\lambda \leq 2\langle b_0\rangle_\lambda \leq 2, \tag{0.8}$$

or, equivalently,

$$S = \langle a_0 b_0\rangle + \langle a_0 b_1\rangle + \langle a_1 b_0\rangle - \langle a_1 b_1\rangle \leq 2. \tag{0.9}$$

This is the famous CHSH inequality, first shown in ref. [48].

Let us now consider a simple quantum implementation of this experiment, following ref. [13]. Two quantum systems (e.g. two spins) can occupy two individual states, called $|-1\rangle$ and $|+1\rangle$, and form a joint product state, written e.g. as $|+1\rangle \otimes |-1\rangle = |+1,-1\rangle$. Initially, the systems are prepared in the singlet state $|\psi\rangle = (|-1,+1\rangle - |+1,-1\rangle)/\sqrt{2}$. Let the measurement settings be described by 3-dimensional vectors $\boldsymbol{x}, \boldsymbol{y}$, and the measurement operators be $\boldsymbol{x}\cdot\boldsymbol{\sigma}$ for the first qubit, and $\boldsymbol{y}\cdot\boldsymbol{\sigma}$ for the second qubit. Here, $\boldsymbol{\sigma} = (\sigma_x, \sigma_y, \sigma_z)$ is the vector of Pauli matrices. Then, the expectation value $\langle a_x b_y\rangle = -\boldsymbol{x}\cdot\boldsymbol{y}$. Now we choose the two settings for Alice, $\boldsymbol{x} \in \{\hat{e}_x, \hat{e}_y\}$, and for Bob, $\boldsymbol{y} \in \{-(\hat{e}_x + \hat{e}_y)/\sqrt{2}, (-\hat{e}_x + \hat{e}_y)/\sqrt{2}\}$. This yields $\langle a_0 b_0\rangle = \langle a_0 b_1\rangle = \langle a_1 b_0\rangle = 1/\sqrt{2}$ and $\langle a_1 b_1\rangle = -1/\sqrt{2}$. We obtain a violation of the CHSH inequality (0.9),

$$S = 2\sqrt{2} > 2. \tag{0.10}$$

We have thus shown that quantum mechanics violates the assumption of local realism.

Interestingly, neither a violation of solely locality or solely realism can be inferred from the joint violation of locality and realism. The question which of the two concepts is untenable is one of the main subjects in the great debate between different interpretations of quantum mechanics [14–16].

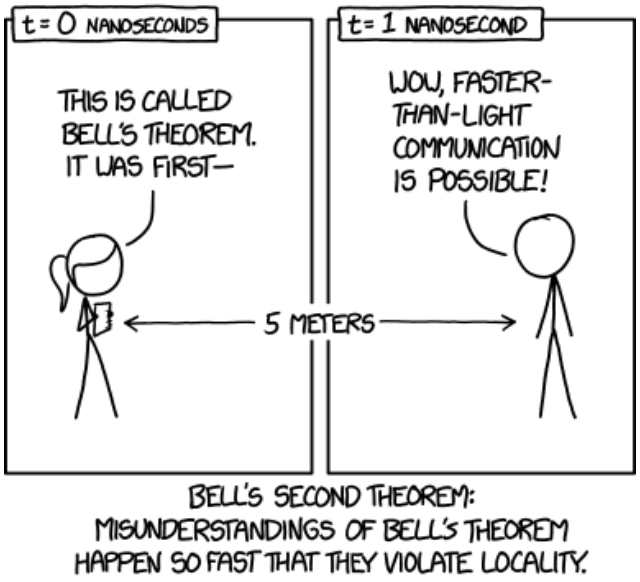

Figure 0.3: A common misinterpretation of Bell's result is the idea that quantum physics allows faster-than-light communication, as shown in the above webcomic from xkcd [70]. Online, its title text reads: *"The no-communication theorem states that no communication about the no-communication theorem can clear up the misunderstanding quickly enough to allow faster-than-light signaling."*

Furthermore, it is important to note that this does not mean that quantum mechanics violates special relativity. The *no-signaling* conditions, which can be formalized as

$$\forall y : p(a|x) = \sum_b p(ab|xy), \tag{0.11}$$

are still satisfied (c.f. fig. 0.3).

Experimental violations of Bell-like inequalities have been achieved in a variety of systems [53–67]. While these experiments will always leave open a number of fundamental loopholes [68], recent experiments [65–67] manage to close all that are considered relevant by the community [68, 69].

An interesting follow-up question is the degree of the Bell inequality violation admitted by quantum mechanics. While discussed briefly in chapter 3, the topic of quantum violations of local realism is out of the scope of this thesis. The reader is referred to refs. [13, 71] for a detailed review.

0.3 Contents of this thesis

As discussed in the previous section, quantum physics and classical (local realistic) theories differ vastly in their potential to establish spatial correlations. How, on the other hand, do quantum and classical models differ when we look at measurements separated in time?

In this thesis we will mainly look at these temporal correlations, i.e. measurements performed on a single macroscopic system at multiple times. **Chapter 1** starts with a definition of macrorealism, roughly the analogue of local realism in time. We show how the Leggett-Garg inequality [72], a condition similar to the Bell inequality, can be derived. We then discuss no-signaling in time, a recently proposed necessary condition for macrorealism [73], its relationship to the Leggett-Garg inequalities, and prove that a combination of no-signaling in time and arrow of time conditions is both necessary and sufficient for macrorealism. We also introduce a formulation of no-signaling in time in terms of measurement operators and Hamiltonians.

Next, in **chapter 2**, we use this formalism to obtain a definition of the "classicality" of measurement operators and Hamiltonians. We apply our definition to a number of exemplary systems, and discuss the importance of spontaneously realized Hamiltonians for a definition of classical behavior.

In **chapter 3** we compare the results from chapter 1 to tests of local realism and look at the structure of probability space in quantum mechanics, local realism and macrorealism. A fundamental difference of the role of quantum mechanics is identified, which leads to the conclusion that the Leggett-Garg inequalities are generally not well-suited to serve as a condition for macrorealism.

Chapter 4 discusses a novel *magnetomechanical* system for implementing, amongst other experiments, tests of macrorealism. To bring a macroscopic object into the quantum regime, we propose to use magnetostatics to couple a superconducting quantum device to the motion of a superconducting sphere. We show that ground state cooling, the fundamental requirement for many quantum protocols, can be realized in this system. A key characteristic of our proposal is the almost perfect isolation of the mechanical motion from the environment.

Finally, we draw some conclusions in **chapter 5**, and discuss possible future work.

1 Conditions for macrorealism

> *The Hitchhiker's Guide to the Galaxy is an indispensable companion to all those who are keen to make sense of life in an infinitely complex and confusing Universe, for though it cannot hope to be useful or informative on all matters, it does at least make the reassuring claim, that where it is inaccurate it is at least definitively inaccurate. In cases of major discrepancy it's always reality that's got it wrong.*
>
> **— Douglas Adams**
> *The Hitchhiker's Guide to the Galaxy* [74]

Abstract

Macroscopic realism (or macrorealism) is a world view common to all classical theories, enforcing that macroscopic properties of macroscopic objects exist independently of and are not influenced by measurements. In analogue to the world view of local realism, classical physics fulfills macrorealism, while quantum mechanics violates it. This makes macrorealism an interesting subject for the study of the quantum-to-classical transition.

Macrorealism is usually tested using *Leggett-Garg inequalities* [72, 75, 76]. Recently, another necessary condition called *no-signaling in time* has been proposed as an alternative witness for non-classical behavior [73]. It has been argued that no-signaling in time may be a more robust condition than the Leggett-Garg inequalities [39, 73, 77, 78].

In this chapter, we expand on previous analyses of no-signaling in time, and formulate operational conditions for macrorealism. After an introduction to macrorealism (**section 1.1**) and a discussion about the relation between its two constituents, macrorealism per se and non-invasive measurability (**section 1.2**), we introduce the Leggett-Garg inequality (**section 1.3**). We then present the condition of no-signaling

in time (**section 1.4**), and show that a combination of no-signaling in time and arrow-of-time conditions is necessary and sufficient for macrorealism (**section 1.5**). Subsequently, we derive an operational formulation for NSIT in terms of positive operator-valued measurements and the system Hamiltonian (**section 1.6**).

This chapter is based on and uses parts of ref. [1]:

- L. Clemente and J. Kofler, 'Necessary and sufficient conditions for macroscopic realism from quantum mechanics', Phys. Rev. A **91**, 062103 (2015)

1.1 Macroscopic realism

The direct application of quantum mechanical principles to macroscopic systems usually results in curios predictions, perhaps best illustrated by the famous Schrödinger's cat thought experiment [8]. As mentioned before (c.f. chapter 0), the question whether macroscopic[1] quantum effects can in principle be observed in macroscopic systems remains unsolved to date. An answer to this questions would have vast impact on a multitude of fundamental issues, such as the quantum measurement problem [11, 12]. It is therefore interesting to explore how—assuming their existence—quantum effects on the macroscale could be experimentally demonstrated.

In 1985, Leggett and Garg [72] put forward *macroscopic realism* (or *macrorealism*), a world view common to all classical physical theories which enforce that macroscopic properties of macroscopic objects exist independently of, and are not influenced by measurements. Macrorealism can be regarded as a close analogue to local realism (as discussed in section 0.2), but with temporal correlations taking the role of spatial correlations. Quantum violations of macrorealism can thus serve as an experimental witness of non-classicality.

Let us start our discussion with the definition[2] of macrorealism (MR), originally presented in ref. [72]. Quoting Leggett's revised version from 2002, macrorealism is defined as the conjunction of three postulates [75]:

> (1) *Macrorealism per se.* A macroscopic object which has available to it two or more macroscopically distinct states is at any given time in a definite one of those states.
>
> (2) *Non-invasive measurability.* It is possible in principle to determine which of these states the system is in without any effect on the state itself or on the subsequent system dynamics.
>
> (3) *Induction.* The properties of ensembles are determined exclusively by initial conditions (and in particular not by final conditions).

[1] Here and in the following discussion, we are interested in truly macroscopic quantum superpositions, not in microscopic quantum effects giving rise to macroscopic phenomena (as e.g. in superconductivity).

[2] Alternative definitions of macrorealism, and in particular macrorealism per se, have recently been proposed, see refs. [78, 79] for more details.

In the following, we will also refer to postulate (3) as the *arrow of time*[3].

Here, we will not discuss the question of how to define the term *macroscopic* in detail. Let us note that there exist two problems: The quantification of the macroscopicity of a system itself, and the quantification of the *macroscopic distinctness* of the states in a quantum superposition. The latter arises in particular since quantum states of a macroscopic object can be orthogonal, even though they are not macroscopically distinct: Paraphrasing an example from Peres [87], the quantum states of a pen, and of the same pen with one atom removed, are macroscopically practically indistinguishable, but orthogonal in quantum theory. Some notable contributions towards a general definition of macroscopic distinctness can be found in refs. [75, 88–100].

Analyzing the present definition of macrorealism, it can readily be seen that orthodox[4] quantum mechanics fulfills postulate (3), but violates postulates (1) and (2). Classical physics obviously satisfies postulate (1), as superposition states are confined to the realm of quantum physics, and (3) due to causality. However, at first glance, it seems that classical physics can violate postulate (2) if imperfect measurements are performed. Various approaches to close this so-called *clumsiness loophole* have been discussed [72, 101]. The original solution proposed by Leggett and Garg requires performing solely *negative ideal measurements* [72]. In that case, the measurement process is constructed such that the measurement device interacts with the system if and only if the system has one particular value (e.g. a double-slit experiment with a detector blocking only one slit). The absence of a measurement result (no click of the detector) then indicates the opposite outcome (the photon went through the other slit). Classically, the system cannot have been influenced by a negative measurement outcome. We conclude that classical physics, with its possibility of performing non-invasive measurements, fulfills all postulates, and therefore is a macrorealistic theory.

Exactly how the everyday macrorealism around us arises out of quantum behavior can be regarded as an open question of quantum foundations. While theories such as objective collapse models (briefly introduced in chapter 0) propose novel physical processes, recent studies have investigated the possibility of obtaining classical behavior from within quantum mechanics. They discovered that the restriction to coarse-grained ("classical") measurements alone already leads to the emergence of

[3]The question of how the arrow of time arises in quantum mechanics has been extensively discussed in the literature. Some notable contributions are refs. [80–86]. Interestingly, a possible explanation stems from coarse-graining, see refs. [85, 86].

[4]Here we consider the "orthodox" interpretation of quantum theory. There are interpretations (e.g. Bohmian mechanics) where postulate (1) is obeyed.

classicality [38, 102, 103], unless a certain type of ("non-classical") Hamiltonian is governing the object's time evolution [39]. Although challenged by recent work [104], further investigations have confirmed the intuition that these Hamiltonians are hard to engineer and require a very high control precision in the experimental setup [105–107]. In the current and the following chapter, we extend this work, and obtain conditions for classicality from measurements and Hamiltonians.

Although setups such as superconducting devices, heavy molecules, and quantum-optical systems are promising candidates in the race towards an experimental violation of macrorealism, non-classical effects have so far only been observed either for microscopic objects or microscopic properties of larger objects [19, 76, 108–129]. The experimental realization of Schrödinger cat states is highly challenging, and so far only possible for single-digit numbers of atoms or photons [130–141]. However, a genuine violation of macroscopic realism—with its reference to macroscopically distinct states—requires using solely measurements of macroscopically coarse-grained observables. Thus far, the required parameter ranges lie outside of the experimentally feasible domain. A proposal for a novel experimental setup that may extend the experimentalist's reach is discussed in chapter 4.

1.2 Macrorealism per se following from strong non-invasive measurability

We start our analysis by first showing that a strong reading of non-invasive measurability implies macrorealism per se.

In this section, we assume that the state space of a macroscopic object is split into macroscopically distinct *non-overlapping* states (macrostates). Consider a macro-observable $Q(t)$ with a one-to-one mapping between its values and the macrostates. Further consider measurements of the macro-observable that enforce a definite post-measurement macrostate and report the corresponding value as the outcome.

Macrorealism per se (MRps) is fulfilled if $Q(t)$ has a definite value at all times t, prior to and independent of measurement:

$$\forall t : \exists \text{ definite } Q(t). \tag{1.1}$$

Probabilistic predictions for $Q(t)$ are merely due to ignorance of the observer. Even in cases where $Q(t)$ evolves unpredictably (e.g. in classical chaos) or even indeterministically, it is still assumed to have a definite value at all times.

On top of MRps, the assumption of non-invasive measurability (NIM) in principle allows a measurement at every instant of time, revealing the macrostate without disturbance. NIM guarantees that

$$\forall t\colon Q(t) = Q_H(t), \tag{1.2}$$

where H denotes the history of past non-invasive measurements on the system: In order for measurements to be non-invasive, the time evolution of Q must not depend on the history of the experiment[5]. Note that all non-invasive measurements are repeatable, i.e. when performing the same measurement immediately again, the same outcome is obtained with probability 1.

In the literature, NIM is often treated as a necessary condition for macrorealism per se. It is argued that NIM is "so natural a corollary of [MRps] that the latter is virtually meaningless in its absence" [75]. As some others before [73, 78, 79], we do not adhere to this position. A counter example to the statement MRps $\Rightarrow$ NIM is given by the de Broglie–Bohm theory, where measurements are invasive, as they affect the guiding field and thus the subsequent (position) state, but MRps is fulfilled, as the (position) state is well-defined at all times. In fact, we now argue that there exist two different ways of reading the postulate of NIM in [75]:

- *Weak NIM*. Given a macroscopic object is in a definite one of its macrostates, it is possible to determine this state without any effect on the state itself or on the subsequent system dynamics.

- *Strong NIM (sNIM)*. It is always possible to measure the macrostate of an object without any effect on the state itself or on the subsequent system dynamics.

Let us now argue that sNIM actually implies MRps. Assuming sNIM, a hypothetical non-invasive measurement can be performed at every instant of time, determining the value of the macro-observable Q. Due to its non-invasive nature, Q must have

[5] Let us now assume the existence of hidden parameters $\lambda(t)$ that define all physical properties. MRps is fulfilled if the macro-observable is a deterministic function $Q = Q(\lambda(t))$. There are two conceivable scenarios: (i) *Deterministic time evolution* of λ, causing deterministic time evolution of the macro-observable $Q(\lambda(t))$. (ii) *Stochastic time evolution* of λ, where some intrinsic randomness generates random jumps in λ. We still have a deterministic dependency $Q(\lambda)$, but $Q(\lambda(t))$ *appears* stochastic. In both cases MRps is fulfilled, since the system is in a single macrostate, as described by $Q = Q(\lambda(t))$, at all times. The condition for NIM then reads $Q(\lambda(t)) = Q(\lambda_H(t))$, where $\lambda_H(t)$ are the hidden parameters after a history H of non-invasive measurements.

had a definite value already before the measurement. This ensures that Q has a definite value at all times, giving rise to a "trajectory" $Q(t)$. Therefore,

$$\text{sNIM} \Rightarrow \text{MRps}. \tag{1.3}$$

Another way of establishing this implication is the following: Assume that MRps fails, i.e. the object is not in a definite macrostate. A measurement leaves the object in a definite macrostate, creating a definite state out of an indefinite one, and therefore does not satisfy sNIM. We thus have $\neg$MRps $\Rightarrow$ $\neg$sNIM, which is equivalent to (1.3).

Note that (1.3) holds even if sNIM is made less stringent, allowing measurements to change the subsequent time evolution, while still determining the macrostate.

In this thesis, we implicitly assume the arrow of time and freedom of choice concerning the initial states and measurement times (including whether a measurement takes place at all). Then, sNIM alone is sufficient for macrorealism:

$$\text{sNIM} \Leftrightarrow \text{MRps} \wedge \text{NIM} \Leftrightarrow \text{MR}. \tag{1.4}$$

1.3 The Leggett-Garg inequality

In their 1985 paper, Leggett and Garg proposed a necessary condition for macrorealism, called the *Leggett-Garg inequality* (LGI) [72]. Similarly to the Bell inequalities discussed in section 0.2, which serve as a witness for violations of local realism, the violation of an LGI serves as a witness for violations of macrorealism. Let us now briefly recapitulate its derivation, following ref. [76].

Consider a simple experimental setup where a system undergoes time evolution. At times t_0, t_1, t_2, the experimenter may choose to perform (or not perform) a dichotomic measurement. We denote with $P_i(Q_i)$ the probability for obtaining measurement result $Q_i \in \{+1, -1\}$ when measuring at time t_i, with $i \in \{0, 1, 2\}$. Let us now define the correlation functions

$$\langle Q_i Q_j \rangle = \sum_{Q_i, Q_j} Q_i Q_j P_{ij}(Q_i, Q_j), \tag{1.5}$$

where $P_{ij}(Q_i, Q_j)$ is the joint probability of Q_i and Q_j. Note that the subscripts of the probability distributions here are important, as they distinguish different

experiments: E.g. $P_{12}(Q_2)$ belongs to an experiment where measurements are performed at times t_1 *and* t_2, and, in general, $P_2(Q_2) \neq P_{12}(Q_2)$.

Under the the assumption of macrorealism per se, the well-defined value of Q_k exists, whether or not a measurement was performed at t_i. We can therefore write the two-time joint probability distribution as marginal of a three-time probability distribution:

$$P_{ij}(Q_i, Q_j) = \sum_{Q_{k\neq i,j}} P_{ij}(Q_i, Q_j, Q_k). \tag{1.6}$$

With macrorealism per se alone, the probabilities P_{01}, P_{02}, P_{12} do not necessarily follow from a joint probability distribution, since earlier measurements can be invasive and change the future time evolution towards the next measurement. With the assumption of non-invasive measurability, this possibility is forbidden, and the probabilities become equal:

$$\begin{aligned} P_{01}(Q_0, Q_1, Q_2) = P_{02}(Q_0, Q_1, Q_2) = P_{12}(Q_0, Q_1, Q_2) \\ = P_{012}(Q_0, Q_1, Q_2) \equiv P(Q_0, Q_1, Q_2). \end{aligned} \tag{1.7}$$

Using the short notation $P(+,+,+) = P(+1,+1,+1)$ (others accordingly), we can calculate all pairwise joint probability distributions:

$$\begin{aligned} \langle Q_0 Q_1 \rangle = {} & P(+,+,+) + P(+,+,-) + P(-,-,+) + P(-,-,-) \\ & - P(+,-,+) - P(+,-,-) - P(-,+,+) - P(-,+,-), \end{aligned} \tag{1.8}$$

$$\begin{aligned} \langle Q_0 Q_2 \rangle = {} & P(+,+,+) + P(+,-,+) + P(-,+,-) + P(-,-,-) \\ & - P(+,+,-) - P(+,-,-) - P(-,+,+) - P(-,-,+), \end{aligned} \tag{1.9}$$

$$\begin{aligned} \langle Q_1 Q_2 \rangle = {} & P(+,+,+) + P(-,+,+) + P(+,-,-) + P(-,-,-) \\ & - P(+,+,-) - P(-,+,-) - P(+,-,+) - P(-,-,+). \end{aligned} \tag{1.10}$$

Adding and applying the normalization of probabilities, and introducing $C_{ij} = \langle Q_i Q_j \rangle$, we can write

$$K \equiv C_{01} + C_{02} - C_{12} = 1 - 4[P(+,-,+) + P(-,+,-)]. \tag{1.11}$$

Choosing $P(+,-,+) = P(-,+,-) = 0$ we obtain the upper bound for eq. (1.11), $K \leq 1$, while $P(+,-,+) + P(-,+,-) = 1$ (the maximum due to normalization) yields the lower bound, $K \geq -3$. We thus obtain the *Leggett-Garg inequality*,

$$\text{LGI}_{012}\colon -3 \leq C_{01} + C_{02} - C_{12} \leq 1. \tag{1.12}$$

As with the Bell inequalities, quantum mechanics is able to violate this inequality. As an example [38], consider a spin $1/2$, evolving under Hamiltonian $\hat{H} = \hbar\omega\hat{\sigma}_x/2$, and subject to possible $\hat{\sigma}_z$ measurements with outcomes Q_1, Q_2, Q_3 at times t_0, t_1, t_2. Then, the correlation functions are $\langle Q_i Q_j \rangle = \cos[\omega(t_j - t_i)]$. Choosing measurement times separated by $\Delta t = \pi/(3\omega)$, we obtain $K = 3/2 > 1$. Quantum mechanics therefore does not behave according to macrorealism.

Leggett-Garg inequalities have so far been violated in a number of experimental realizations in microscopic systems [110–112, 114–119, 121, 122, 126–128]. However, all of the experimentally feasible systems so far are microscopic in size (e.g. single spins or a single flux quanta), and therefore cannot implement a real test of *macroscopic* realism. Promising schemes for experiments with more macroscopic systems are quantum optomechanics and quantum magnetomechanics, which will be discussed in chapter 4.

There exist many other Leggett-Garg inequalities involving more than three possible measurement times or more than two outcomes [76]. Quantum mechanical experiments are able to violate ineq. (1.12) up to $3/2$ for a qubit and, as shown in ref. [142], up to the algebraic maximum 3 for higher-dimensional systems still using dichotomic measurements $Q_i = \pm 1$.

For a review of Leggett-Garg inequalities and current experimental work see ref. [76].

1.4 No-signaling in time

Recently, a necessary condition alternative to the Leggett-Garg inequalities, *no-signaling in time* (NSIT), was proposed[6] by Kofler and Brukner [73]. The condition can be seen as a temporal analogue to the no-signaling conditions in Bell experiments (c.f. eq. (0.11) of section 0.2), or, alternatively, as a statistical version of NIM (c.f. eq. (1.2)). It requires that the outcome probabilities $P_j(Q_j)$ of result Q_j measured at time t_j are the same, no matter whether or not a measurement was performed at some earlier time $t_i < t_j$:

$$\text{NSIT}_{(i)j}: P_j(Q_j) = P_{ij}(Q_j) \equiv \sum_{Q_i'} P_{ij}(Q_i', Q_j). \tag{1.13}$$

Note again that the probability distributions on both sides of the equation, P_i and P_{ij}, correspond to *different* physical experiments: While P_j is established by measuring

[6] While *no-signaling in time* appeared in some forms already in earlier works [39, 72, 143, 144], its potential was not fully realized until ref. [73].

only at t_j, P_{ij} is obtained by measuring both at t_i and t_j. Unlike in the LGI in (1.12), one is not limited to only two outcomes.

If it is the later measurement at t_j which may or may not be performed, $\text{NSIT}_{i(j)}$ reduces to an instance of the arrow of time and is therefore fulfilled by both macrorealism and quantum mechanics.

While $\text{NSIT}_{(1)2}$ is a promising condition that is usually able to detect violations of MR more reliably than LGI_{012} [39, 73, 77, 78], it fails for particular initial states, where the invasiveness is able to "hide" in the statistics of the experiment (see the discussion below). We can however make $\text{NSIT}_{(1)2}$ robust against such cases, by always performing a measurement at t_0. We call the resulting condition

$$\begin{aligned}\text{NSIT}_{0(1)2}\colon P_{02}(Q_0,Q_2) &= P_{012}(Q_0,Q_2)\\ &\equiv \sum_{Q_1'} P_{012}(Q_0,Q_1',Q_2).\end{aligned} \tag{1.14}$$

$\text{NSIT}_{0(1)2}$ alone is not sufficient for LGI_{012}. Hence, we also introduce the condition

$$\begin{aligned}\text{NSIT}_{(0)12}\colon P_{12}(Q_1,Q_2) &= P_{012}(Q_1,Q_2)\\ &\equiv \sum_{Q_0'} P_{012}(Q_0',Q_1,Q_2).\end{aligned} \tag{1.15}$$

As was recently shown in [78], a combination of $\text{NSIT}_{(0)12}$, $\text{NSIT}_{0(1)2}$ and the arrow of time (AoT) is sufficient for LGI_{012}:

$$\text{NSIT}_{0(1)2} \wedge \text{NSIT}_{(0)12} \wedge \text{AoT} \Rightarrow \text{LGI}_{012}. \tag{1.16}$$

Importantly, the inverse is not true, and, moreover the left-hand side is not sufficient for macrorealism. In fact, we will show in chapter 3 that Leggett-Garg inequalities can fundamentally never be necessary and sufficient for macrorealism.

We further remark that one can also write a condition similar to $\text{NSIT}_{0(1)2}$ in a more intuitive form that we call non-invaded correlations (NIC),

$$\text{NIC}_{0(1)2}\colon C_{02} = C_{02|1}, \tag{1.17}$$

where $C_{02|1}$ denotes the correlation $\langle Q_0 Q_2\rangle$ given that an additional measurement was performed at t_1. It is shown in appendix 1.A that $\text{NIC}_{0(1)2}$ follows from $\text{NSIT}_{0(1)2}$.

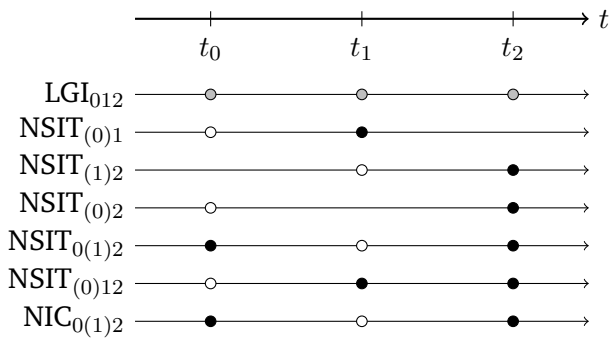

Figure 1.1: The setup for macrorealism tests with different necessary conditions for MR in a system with possible measurements at three points in time. Black filled circles denote measurements that always take place, white filled circles measurements that may or may not be performed. A pair of measurements is always performed for the LGI, shown with gray filled circles.

Fig. 1.1 presents a graphical summary of the conditions that have been discussed in this and the previous section.

1.5 Necessary and sufficient conditions for macrorealism

In the following, we will show that the combination of various NSIT conditions and the arrow of time (AoT) guarantees the existence of a unique global probability distribution $P_{012}(Q_0, Q_1, Q_2)$, which is equivalent to macrorealism evaluated at t_0, t_1, t_2. Let us start by writing all single-measurement probabilities in terms of P_{012}. Once again, note that joint probabilities P with different subscripts correspond to different experimental setups (e.g. $P_2(Q_2)$ is obtained by measuring only at t_2, while $P_{12}(Q_1, Q_2)$ is obtained by measuring at times t_1 and t_2):

$$P_2(Q_2) = \sum_{Q_1'} P_{12}(Q_1', Q_2) = \sum_{Q_0'} \sum_{Q_1'} P_{012}(Q_0', Q_1', Q_2), \tag{1.18}$$

where we have used $\mathrm{NSIT}_{(1)2}$ for the first equality and $\mathrm{NSIT}_{(0)12}$ for the second one. Furthermore,

$$P_1(Q_1) = \sum_{Q_2'} P_{12}(Q_1, Q_2') = \sum_{Q_0'} \sum_{Q_2'} P_{012}(Q_0', Q_1, Q_2'), \tag{1.19}$$

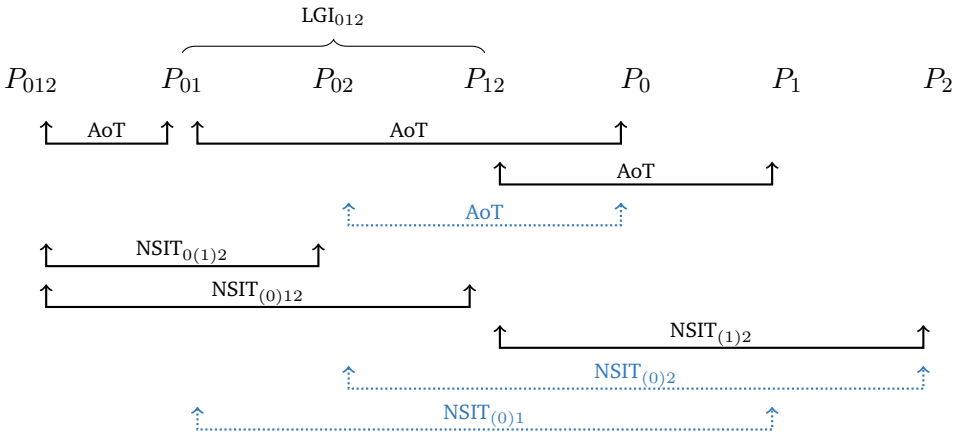

Figure 1.2: Different combinations of NSIT and AoT conditions are sufficient for guaranteeing that all probability distributions P_i, P_{ij} are the marginals of a unique global probability distribution P_{012}. There are multiple ways of obtaining a sufficient set. The black arrows correspond to one particular choice, and additional conditions are printed for completeness in blue. Note that the existence of a classical explanation for the pairwise joint probabilities P_{ij} is sufficient for fulfilling LGI_{012}, but not for MR_{012}.

where for the first equality we assumed AoT [i.e. Q_i are (statistically) independent of Q_j for $j > i$], and $\text{NSIT}_{(0)12}$ for the second one. Moreover, we see that

$$P_0(Q_0) = \sum_{Q_1'} \sum_{Q_2'} P_{012}(Q_0, Q_1', Q_2'), \tag{1.20}$$

where AoT was used twice. Next, the pairwise joint probability functions can be constructed:

$$P_{01}(Q_0, Q_1) = \sum_{Q_2'} P_{012}(Q_0, Q_1, Q_2') \tag{1.21}$$

follows from AoT. Using $\text{NSIT}_{0(1)2}$ one obtains

$$P_{02}(Q_0, Q_2) = \sum_{Q_1'} P_{012}(Q_0, Q_1', Q_2). \tag{1.22}$$

Finally, using $\text{NSIT}_{(0)12}$, we obtain

$$P_{12}(Q_1, Q_2) = \sum_{Q_0'} P_{012}(Q_0', Q_1, Q_2). \tag{1.23}$$

We have thus shown that there exists a combination of NSIT conditions, whose fulfillment guarantees that all probability distributions in any experiment can be written as the marginals of a unique global probability distribution $P_{012}(Q_0, Q_1, Q_2)$. This is equivalent to the existence of a macrorealistic model for measurements at

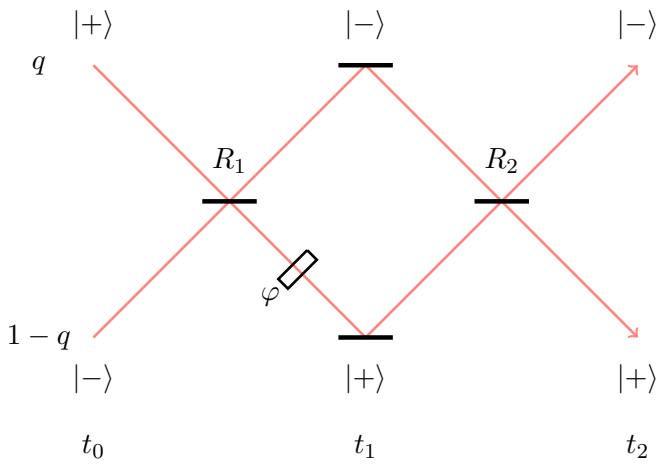

Figure 1.3: The Mach-Zehnder setup [145] described in the main text. Which-path measurements may be performed at times t_0, t_1 and t_2. The reflectivities are R_1 and R_2; a phase plate with phase a shift of φ is added to the lower beam. The initial occupation fraction of the upper beam is given by q.

times t_0, t_1, t_2 (MR_{012}). Note that while MR_{012} cannot prove the world view of MR in general, it implies that no experimental procedure (with measurements at t_0, t_1, t_2) can detect a violation of MR. Let us now write a *necessary and sufficient* condition for MR_{012},

$$\text{NSIT}_{(1)2} \wedge \text{NSIT}_{0(1)2} \wedge \text{NSIT}_{(0)12} \wedge \text{AoT} \Leftrightarrow \text{MR}_{012}. \tag{1.24}$$

This set of conditions is not unique: We can e.g. substitute $\text{NSIT}_{(1)2}$ by $\text{NSIT}_{(0)2}$, as can easily be seen from a graphical representation of all conditions in fig. 1.2. We remark that even the combination of all two-time NSIT conditions, $\text{NSIT}_{(0)1} \wedge \text{NSIT}_{(1)2} \wedge \text{NSIT}_{(0)2}$, is sufficient neither for MR_{012} nor for LGI_{012}. Note that LGIs only test for non-classicalities of the pairwise joint probability distributions. A smaller set of conditions is therefore sufficient for fulfilling all LGIs using two-time correlation functions or probabilities [such as ineq. (1.12) or the so-called Wigner LGIs [77]], see expression (1.16).

To illustrate these conditions for a qubit, in table 1.1 we show the individual conditions evaluated for a Mach-Zehnder setup with arbitrary initial state and time evolution (see fig. 1.3 for explanation). The three possible measurements are which-path measurements before the first beamsplitter (t_0), between the two beamsplitters (t_1), and after the second beamsplitter (t_2), respectively. We can easily find cases where LGI_{012} is always fulfilled, but various NSIT conditions still witness a violation of MR, e.g. for $R_1 = R_2 = 1/2, \varphi \neq (n + 1/2)\pi$. As discussed above, it is possible for LGI_{012} to be violated with $\text{NSIT}_{(1)2}$ fulfilled, e.g. for $R_1 = 1/4, R_2 = 3/4, q = 1/2, \varphi = \pi$. For mixed initial states, $\text{NSIT}_{0(1)2}$ reduces to the condition $\varphi = (n + 1/2)\pi$ with

		LGI_{012}	$\mathrm{NSIT}_{(1)2}$	$\mathrm{NSIT}_{0(1)2}$	$\mathrm{NSIT}_{(0)12}$
$\hat{\rho}_{\mathrm{mix}}$:	$R_1 = R_2 = \frac{1}{2}$	✓	$q = \frac{1}{2}$ or $\varphi = (n+\frac{1}{2})\pi$	$\varphi = (n+\frac{1}{2})\pi$	✓
	$R_1 = \frac{1}{4}, R_2 = \frac{3}{4}$	$1 + 3\cos\varphi \geq 0$	$q = \frac{1}{2}$ or $\varphi = (n+\frac{1}{2})\pi$	$\varphi = (n+\frac{1}{2})\pi$	✓
	R_1, R_2	$R_1 + \alpha\cos\varphi - R_1 R_2 \geq 0$	$q = \frac{1}{2}$ or $\varphi = (n+\frac{1}{2})\pi$ or $\alpha = 0$	$\varphi = (n+\frac{1}{2})\pi$ or $\alpha = 0$	✓
$\hat{\rho}_{\mathrm{sup}}$:	$R_1 = R_2 = \frac{1}{2}$	✓	$2q\cos\varphi = \cos\varphi + 2\,\mathrm{Re}(c)\sin\varphi$	$\varphi = (n+\frac{1}{2})\pi$	$c \in \mathbb{R}$
	$R_1 = \frac{1}{4}, R_2 = \frac{3}{4}$	$1 + 3\cos\varphi \geq 0$	$[*]$	$\varphi = (n+\frac{1}{2})\pi$	$c \in \mathbb{R}$
	R_1, R_2	$R_1 + \alpha\cos\varphi - R_1 R_2 \geq 0$	$[**]$	$\varphi = (n+\frac{1}{2})\pi$ or $\alpha = 0$	$c \in \mathbb{R}$ or $R_1 = 0, 1$

Table 1.1: Different necessary conditions for macrorealism evaluated for a Mach-Zehnder (qubit) experiment [145], c.f. fig. 1.3. The reflectivity of the first beamsplitter is R_1, and of the second one is R_2. In one path of the interferometer, a phase φ is added. Which-path measurements may be performed before, between and after the beamsplitters. The initial states are $\hat{\rho}_{\mathrm{mix}} = \left(\begin{smallmatrix} q & 0 \\ 0 & 1-q \end{smallmatrix}\right)$ and $\hat{\rho}_{\mathrm{sup}} = \left(\begin{smallmatrix} q & c \\ c^* & 1-q \end{smallmatrix}\right)$. The symbol "✓" means that the condition holds for all values of the free parameters. For brevity, $\alpha \equiv \sqrt{R_1 R_2 (1-R_1)(1-R_2)}$. Equation $[*]$ reads $(2i\sqrt{3}c + 6q - 3)\cos\varphi - 2i\sqrt{3}\,\mathrm{Re}(c)(\cos\varphi - 2i\sin\varphi) = 0$, equation $[**]$ reads $\cos\varphi[(2q-1)\alpha + ic(1-2R_1)\sqrt{-(R_2-1)R_2}] + i\sqrt{-(R_2-1)R_2}\,\mathrm{Re}(c)[(2R_1-1)\cos\varphi + i\sin\varphi] = 0$. See main text for discussion.

$n \in \mathbb{N}_0$ and is sufficient for MR_{012}, as no interference is possible in this case. For general superposition states, $\text{NSIT}_{(0)12}$ can be violated with $\text{NSIT}_{0(1)2}$ fulfilled. Moreover, NSIT conditions still allow detecting violations of MR if $R_1 = 0, 1$ or $R_2 = 0, 1$.

1.6 No-signaling in time for quantum measurements

In the following, we will look at $\text{NSIT}_{(0)T}$ in an archetypal quantum experiment. A system has been prepared at $t = 0$ in an initial state $\hat{\rho}_0$. Then, at $t = 0$, a POVM $\{\hat{A}_a^\dagger \hat{A}_a\}_a$ with outcomes a is carried out. After the measurement, the system evolves according to a unitary $\hat{U}_t = e^{-i\hat{H}t}$. At time $t = T$ a second, possibly different POVM $\{\hat{B}_b^\dagger \hat{B}_b\}_b$ with outcomes b is performed.

To determine the effect of the first measurement $\hat{A}_a^\dagger \hat{A}_a$ on the system's state and its subsequent dynamics, we will compare the results of the final measurement with a different experiment, where no measurement was performed at $t = 0$ (or, equivalently, a measurement $\hat{A}_a = \mathbb{1}$ was performed). The two setups are shown in fig. 1.4.

The probabilities for obtaining outcome b in the second and first setup are called $P_{\hat{B}}(b)$ and $P_{\hat{B}|\hat{A}}(b)$, respectively. They can be calculated as

$$P_{\hat{B}}(b) = \text{tr}(\hat{B}_b \hat{U}_T \hat{\rho}_0 \hat{U}_T^\dagger \hat{B}_b^\dagger) \tag{1.25}$$

$$P_{\hat{B}|\hat{A}}(b) = \int \text{d}a \;\; \text{tr}(\hat{B}_b \hat{U}_T \hat{A}_a \hat{\rho}_0 \hat{A}_a^\dagger \hat{U}_T^\dagger \hat{B}_b^\dagger), \tag{1.26}$$

with the integral replaced by a sum if the number of outcomes is countable. $\text{NSIT}_{(0)T}$ is fulfilled if the test measurement has no detectable effect on the system, i.e. if $P_{\hat{B}} = P_{\hat{B}|\hat{A}}$:

$$\forall b \colon \text{tr}(\hat{B}_b \hat{U}_T \hat{\rho}_0 \hat{U}_T^\dagger \hat{B}_b^\dagger) = \int \text{d}a \;\; \text{tr}(\hat{B}_b \hat{U}_T \hat{A}_a \hat{\rho}_0 \hat{A}_a^\dagger \hat{U}_T^\dagger \hat{B}_b^\dagger). \tag{1.27}$$

Note that the equality sign in eq. (1.27) will often be fulfilled only approximately, even by non-invasive measurements. In practice, one can choose from a variety of error measures and corresponding reasonable error thresholds. However, to simplify notation, we will continue to use the equality sign in the following calculations.

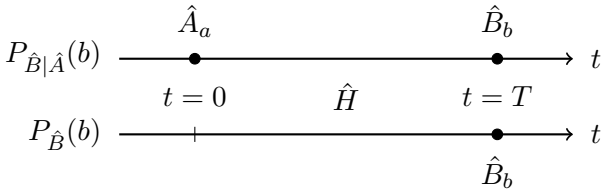

Figure 1.4: A system evolves from $t = 0$ to $t = T$ under Hamiltonian $\hat{H}$. In the first setup measurements $\hat{A}_a^\dagger \hat{A}_a$ and $\hat{B}_b^\dagger \hat{B}_b$ are performed at $t = 0$ and $t = T$, respectively, and in the second setup only a final measurement $\hat{B}_b^\dagger \hat{B}_b$ is performed.

1.6.1 Without time evolution

Let us start by considering the case $T = 0$ (NSIT$_{(0)0}$), i.e. the final measurement is performed immediately after the test measurement. In this setup, NSIT can be regarded as a case of joint measurability, a condition previously discussed in the context of compatibility of quantum measurements [146–153]. To rewrite eq. (1.27) we use that $\int \mathrm{d}a\ A_a^\dagger \hat{A}_a = 1$. This yields

$$P_{\hat{B}|\hat{A}}(b) - P_{\hat{B}}(b) = \int \mathrm{d}a\ \ \mathrm{tr}[(\hat{A}_a^\dagger \hat{B}_b^\dagger \hat{B}_b \hat{A}_a - \hat{B}_b^\dagger \hat{A}_a^\dagger \hat{A}_a \hat{B}_b)\hat{\rho}_0]. \tag{1.28}$$

The trace in the above equation can be interpreted as the expectation value of the Hermitian operator $\int \mathrm{d}a\,(\hat{A}_a^\dagger \hat{B}_b^\dagger \hat{B}_b \hat{A}_a - \hat{B}_b^\dagger \hat{A}_a^\dagger \hat{A}_a \hat{B}_b)$. For NSIT$_{(0)0}$ to be universally valid, we require that it is zero for *all* initial states $\hat{\rho}_0$. Thus, the operator itself has to be zero,

$$\begin{aligned} &\forall \hat{\rho}_0 \colon \mathrm{NSIT}_{(0)0} \\ &\quad \Leftrightarrow\ \forall b \colon \int \mathrm{d}a\ (\hat{A}_a^\dagger \hat{B}_b^\dagger \hat{B}_b \hat{A}_a - \hat{B}_b^\dagger \hat{A}_a^\dagger \hat{A}_a \hat{B}_b) = 0. \end{aligned} \tag{1.29}$$

This equation can be further simplified to $\int \mathrm{d}a\ \hat{A}_a^\dagger \hat{B}_b^\dagger \hat{B}_b \hat{A}_a = \hat{B}_b^\dagger \hat{B}_b$. Note that for Hermitian operators $\hat{A}_a = \hat{A}_a^\dagger$, $\hat{B}_b = \hat{B}_b^\dagger$ we can rewrite (1.29) using the commutator

$$\forall \hat{\rho}_0 \colon \mathrm{NSIT}_{(0)0}\ \Leftrightarrow\ \forall b \colon \int \mathrm{d}a\ [\hat{A}_a \hat{B}_b, \hat{B}_b \hat{A}_a] = 0. \tag{1.30}$$

Furthermore, we have as sufficient conditions the vanishing commutators

$$\forall a, b \colon [\hat{A}_a \hat{B}_b, \hat{B}_b \hat{A}_a] = 0 \Rightarrow\ \forall \hat{\rho}_0 \colon \mathrm{NSIT}_{(0)0}, \tag{1.31}$$

and, consequently,

$$\forall a, b \colon [\hat{A}_a, \hat{B}_b] = 0 \Rightarrow\ \forall \hat{\rho}_0 \colon \mathrm{NSIT}_{(0)0}. \tag{1.32}$$

It is interesting to note that both of these commutator conditions are, generally, only *sufficient* but *not necessary* for $\text{NSIT}_{(0)0}$. In fact, a formulation of $\text{NSIT}_{(0)0}$ must inherently have an asymmetry [152] between the test and final measurements, but both (1.31) and (1.32) are symmetric under exchange of $\hat{A}$ and $\hat{B}$[7].

We can, however, show that vanishing commutators in (1.31) and (1.32), are sufficient and necessary when $\hat{A}_a, \hat{B}_b$ are von Neumann projective measurements ($\hat{A}_a^2 = \hat{A}_a, \hat{B}_b^2 = \hat{B}_b$). Let us start by rewriting the equality in (1.29) using $\hat{A}_a = |a\rangle\langle a|$ and $\hat{B}_b = |b\rangle\langle b|$:

$$\int \mathrm{d}a \ |\langle a|b\rangle|^2 |a\rangle\langle a| = |b\rangle\langle b|. \tag{1.33}$$

Since $|b\rangle\langle b|$ is a projector, squaring the integral on the left-hand side must leave it unchanged. Using the fact that in order to sum up to identity, the $\hat{A}_a$ must be orthogonal projectors, and therefore $\langle a|a'\rangle = \delta(a - a')$, we obtain

$$\left[\int \mathrm{d}a \ |\langle a|b\rangle|^2 |a\rangle\langle a|\right]^2 = \int \mathrm{d}a \ |\langle a|b\rangle|^4 |a\rangle\langle a|. \tag{1.34}$$

Comparing eq. (1.33) and eq. (1.34), we see that $|\langle a|b\rangle|^2 = |\langle a|b\rangle|^4$ can only be fulfilled if it is non-zero for exactly one a. Thus, $|b\rangle$ is an eigenstate of $\hat{A}_a$, and the commutator is $[\hat{A}_a, \hat{B}_b] = 0$. We have therefore demonstrated that for von Neumann measurements (but not for general POVMs), vanishing commutators in (1.31) and (1.32) are both sufficient and necessary for $\text{NSIT}_{(0)0}$.

1.6.2 With time evolution

Let us now consider $\text{NSIT}_{(0)T}$ with unitary time evolution $\hat{U} = e^{-i\hat{H}t}$. Analogous to the derivation of (1.29) and defining $\tilde{B}_b^T \equiv \hat{U}_T^\dagger \hat{B}_b \hat{U}_T$, we obtain

$$\begin{aligned} &\forall \hat{\rho}_0 : \text{NSIT}_{(0)T} \\ &\quad \Leftrightarrow \ \forall b : \int \mathrm{d}a \ (\hat{A}_a^\dagger (\tilde{B}_b^T)^\dagger \tilde{B}_b^T \hat{A}_a - (\tilde{B}_b^T)^\dagger \hat{A}_a^\dagger \hat{A}_a \tilde{B}_b^T) = 0, \end{aligned} \tag{1.35}$$

and, if $\hat{A}_a, \hat{B}_b$ are Hermitian operators,

$$\forall \hat{\rho}_0 : \text{NSIT}_{(0)T} \ \Leftrightarrow \ \forall b : \int \mathrm{d}a \ [\hat{A}_a \tilde{B}_b^T, \tilde{B}_b^T \hat{A}_a] = 0. \tag{1.36}$$

[7] A simple example for this are the Pauli matrices with $\hat{A} = \hat{\sigma}_x, \hat{B} = \hat{\sigma}_y$. Then, $[\hat{A}, \hat{B}] = 2i\hat{\sigma}_z$ and $[\hat{A}\hat{B}, \hat{B}\hat{A}] = 0$. Although the first commutator is non-zero, $\text{NSIT}_{(0)0}$ is trivially fulfilled. The physical interpretation of a $\hat{\sigma}_x$ measurement (or rather, its corresponding POVM element $\mathbb{1}$) is a single-qubit operation without a meaningful measurement outcome.

Comparing (1.29) and (1.35), we can apply the results for $\text{NSIT}_{(0)0}$ derived above, namely

$$\forall a, b\colon [\hat{A}_a \tilde{B}_b^T, \tilde{B}_b^T \hat{A}_a] = 0 \;\Rightarrow\; \forall \hat{\rho}_0\colon \text{NSIT}_{(0)T}, \tag{1.37}$$

and

$$\forall a, b\colon [\hat{A}_a, \tilde{B}_b^T] = 0 \;\Rightarrow\; \forall \hat{\rho}_0\colon \text{NSIT}_{(0)T}. \tag{1.38}$$

Furthermore, one obtains

$$\forall a, b\colon [\hat{A}_a, \hat{B}_b] = [\hat{A}_a, \hat{U}_T] = 0 \;\Rightarrow\; \forall \hat{\rho}_0\colon \text{NSIT}_{(0)T}. \tag{1.39}$$

If $\hat{A}_a, \hat{B}_b$ are von Neumann operators, we have $(\tilde{B}_b^T)^2 = \hat{U}_T^\dagger \hat{B}_b \hat{U}_T \hat{U}_T^\dagger \hat{B}_b \hat{U}_T = \hat{U}_T^\dagger \hat{B}_b \hat{U}_T = \tilde{B}_b^T$. Thus, the results from subsection 1.6.1 apply here too: For projectors (but not for general POVMs), vanishing commutators in (1.37) and (1.38) are sufficient and necessary for $\text{NSIT}_{(0)T}$.

The above results suggest that a non-classical "resource" is required for an experimental violation of NSIT, namely either highly non-classical states (equivalent to non-classical measurements used in their preparation) or non-classical Hamiltonians (usually requiring an extremely large experimental "control precision" as discussed in [105–107]).

In chapter 2, we will use the above results to define the "classicality" of measurement operators and Hamiltonians, and apply our definition to a number of example systems.

1.7 Conclusion and outlook

In contrast to the still widespread belief that non-invasive measurability is a natural corollary of macrorealism per se, we rather showed the opposite, namely that macrorealism per se is implied by a strong interpretation of non-invasive measurability. Moreover, no-signaling in time (NSIT), i.e. non-invasiveness on the statistical level, is in general a more reliable witness for the violation of macrorealism than the well-known Leggett-Garg inequalities, which are based on two-time correlation functions. In fact, we demonstrated that the right combination of various NSIT and AoT conditions serves not only as a necessary but also a sufficient condition for a macrorealistic model for measurements at the predefined time instants accessible in the experiment. We then derived operational criteria for the measurement operators and the system Hamiltonian, whose fulfillment guarantees that no violation of macrorealism can in principle be observed.

While our results suggest that an experimental demonstration of non-classicalities requires either very precise measurements or a complex time evolution, a general proof of this trade-off (in terms of experimental control parameters) is still missing. To provide some intuition on this topic, several examples for measurement operators and Hamiltonians are discussed in the following chapter 2.

Appendix

1.A Proof that $\text{NSIT}_{0(1)2}$ is sufficient for $\text{NIC}_{0(1)2}$

Let us use the short notation $P_i(\pm_i) \equiv P_i(Q_i = \pm)$. Then, the correlations in $\text{NIC}_{0(1)2}$ can be written as

$$\begin{aligned} C_{02} = &+ P_{02}(+_0, +_2) + P_{02}(-_0, -_2) \\ &- P_{02}(+_0, -_2) - P_{02}(-_0, +_2), \end{aligned} \tag{1.40}$$

and, for the variant with a measurement at t_1,

$$\begin{aligned} C_{02|1} = &+ P_{012}(+_0, +_2) + P_{012}(-_0, -_2) \\ &- P_{012}(+_0, -_2) - P_{012}(-_0, +_2). \end{aligned} \tag{1.41}$$

Using $\text{NSIT}_{0(1)2}$, i.e. $P_{02}(Q_0, Q_2) = P_{012}(Q_0, Q_2)$, we immediately see that $\text{NSIT}_{0(1)2}$ is sufficient for $C_{02} = C_{02|1}$, and therefore for $\text{NIC}_{0(1)2}$.

2 Macroscopic classical dynamics from microscopic quantum behavior

> *We demand rigidly defined areas of doubt and uncertainty.*
>
> **— Douglas Adams**
> *The Hitchhiker's Guide to the Galaxy* [74]

Abstract

The frontier between quantum mechanics and classical physics has long been a major area of investigation in both physics and philosophy. Quantum behavior observed on microscopic scales differs vastly from the classical dynamics of our everyday world: We never see macroscopic objects in superposition states, and we are in principle able to perform non-invasive measurements on macroscopic systems. How and why do physical systems stop to behave quantumly, and start to follow classical dynamics?

Orthogonal to the introduction of novel physical processes, e.g. in objective collapse theories briefly mentioned in chapter 0, recent works have investigated the process of measurement itself, as discussed in chapter 1. They found that, as system sizes increase, either sharp measurements or highly non-classical Hamiltonians are required to observe quantum dynamics [1, 38, 39, 77, 103]. The results discussed in chapter 1 further strengthen this intuition.

In this chapter, we discuss a definition of "classicality" based on the condition of no-signaling in time. After a brief recapitulation of the results from chapter 1 (**section 2.1**), we propose a definition of the classicality of measurements operators and Hamiltonians (**section 2.2**). We then proceed to apply this definition to several commonly used measurement operators (**section 2.3**) and several interesting Hamiltonians (**section 2.4**). Finally, with the example of a toy model implementation of a

Schrödinger's cat setup, we show that the concept of classicality can be non-intuitive (**section 2.5**).

This chapter is based on and uses parts of refs. [1, 2]:

- L. Clemente and J. Kofler, 'Necessary and sufficient conditions for macroscopic realism from quantum mechanics', Phys. Rev. A **91**, 062103 (2015)
- L. Clemente and J. Kofler, 'The emergence of macroscopic classical dynamics from microscopic quantum behavior', (in preparation)

2.1 Quantifying violations of classicality

Historically, Leggett-Garg inequalities [72, 75] were used to witness quantum violations of macrorealism and thus classicality. However, a relatively novel condition called no-signaling in time (NSIT) [1, 73, 78] was recently found to be more suitable for such tests [3] (c.f. chapters 1 and 3). In this chapter, we will therefore only consider violations of NSIT.

The condition of NSIT can be seen as a statistical formulation of the requirement of non-invasive measurability. Consider an experiment where a system S evolves under a Hamiltonian $\hat{H}$. A positive-operator valued measurement (POVM) with Kraus operators $\hat{A}_a$ with outcomes a may be performed on the initial state $\hat{\rho}_0$. The system then undergoes unitary time evolution for time t, and is measured again, this time with Kraus operators $\hat{B}_b$ with outcomes b. NSIT can be written as

$$P_{\hat{B}}(b) = \sum_a P_{\hat{B}|\hat{A}}(b|a) \equiv \bar{P}_{\hat{B}|\hat{A}}(b), \tag{2.1}$$

where the subscript of the outcomes denotes the times of the measurements.

In section 1.6 it was shown that the condition of NSIT can generally be written as

$$\forall b\colon \mathrm{tr}(\hat{A}_b \hat{U} \hat{\rho}_0 \hat{U}^\dagger \hat{A}_b^\dagger) = \sum_a \mathrm{tr}(\hat{A}_b \hat{U} \hat{A}_a \hat{\rho}_0 \hat{A}_a^\dagger \hat{U}^\dagger \hat{A}_b^\dagger), \tag{2.2}$$

where $\hat{U} = \exp(-\mathrm{i}\hat{H}t/\hbar)$. Quite naturally, the magnitude of the violation of NSIT depends on the initial state of the system. Note that here we do not explicitly consider mixed initial states, since they can simply be treated as a combination of pure states.

To measure the overlap of the undisturbed and the disturbed probability distributions in eq. (2.2), we make use of the Bhattacharyya coefficient [154], as defined by

$$V = \int \mathrm{d}b \, \sqrt{P_{\hat{B}}(b) \bar{P}_{\hat{B}|\hat{A}}(b)} \in [0, 1]. \tag{2.3}$$

The extreme cases of $V = 0$ and $V = 1$ correspond to orthogonal and identical probability distributions, respectively.

In appendix 2.A we demonstrate that the overlap (2.3) of the Husimi distribution [155] can serve as a witness for the macroscopic distinctness of the states in a quantum superposition, and use it to expose microscopic distinctness of macroscopic states in a recent experiment.

2.2 A definition of classicality

As we have indicated before, the coarse-graining of "sharp" quantum measurement operators into "fuzzy" classical measurements, plays a crucial role in the transition from quantum mechanics to classical physics [38]. However, not every coarse-grained operator can be called classical. As an example, the parity operator (e.g. for large spins or photonic states) only differentiates two macrostates, but is in fact highly non-classical. Generally speaking, a suitable coarse-graining should "lump" together neighboring eigenvalues, independent of a (quantum) experiment's Hamiltonian. However, Hilbert spaces in quantum mechanics possess no inherent measure for the distance between orthogonal states. Such a measure must thus arise solely out of spontaneously realized Hamiltonians. Effectively, any definition of classicality must therefore depend on Hamiltonians spontaneously realized by nature, which define a natural order and closeness of states. This concept is discussed in more detail in section 2.5. In the following, the closeness of states is established with an *a priori* choice of suitable reference operators. With this reference set, we can write a definition for *classical operators* and *classical Hamiltonians*:

(I) A measurement operator is called *classical* with respect to a reference set iff it fulfills[1] the equality in (2.2) (with $t = 0$) pairwise with every member of the set.

(II) A Hamiltonian is called *classical* with respect to a reference set iff the equality in (2.2) is fulfilled for each combination of measurement operators from the set.

A natural choice for the reference set are coarse-grained versions of quantum operators in phase space. Phase space inherently involves the necessary definition of closeness in a suitable and intuitive way. Several exemplary candidates for different experiments are discussed in the next section.

2.3 Classicality of quantum measurements

In the following, we will apply our results from chapter 1 to a number of physical systems. In this section, we will focus on the classicality of operators—condition (I) from the previous section—and always assume either an immediate test measurement, or free time evolution in between.

[1] As mentioned in section 1.6, approximate fulfillment of eq. (2.2) is sufficient in practice.

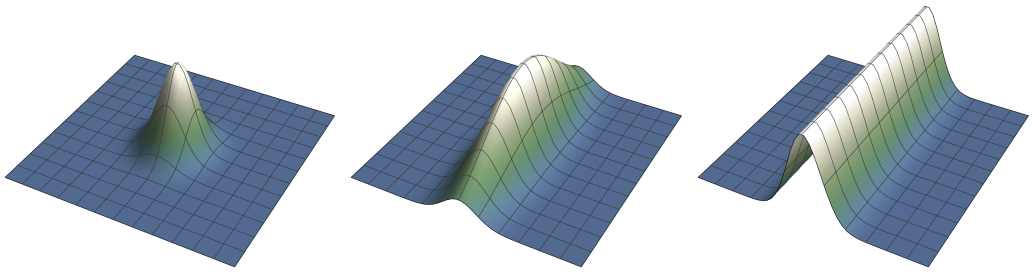

$\delta^2 = 1$ $\delta^2 = 0.03$ $\delta^2 = 0.0001$

$V \approx 0.990$ $V \approx 0.671$ $V \approx 0.168$

Figure 2.1: Husimi distribution in the complex plane (mesh with interval 1), immediately after a quadrature measurement with decreasing unsharpness δ. Sharp measurements (small δ) completely destroy the initial state, while unsharp measurements (large δ) keep it intact.

2.3.1 Quadrature measurements

Let us start with quadrature measurements on pure coherent initial states $\hat{\rho} = |\gamma\rangle\langle\gamma|$. We investigate coarse-grained measurements with unsharpness δ in the X-quadrature, and unsharpness κ in the P-quadrature, as described by the (dimensionless) operators

$$\hat{X}_x^\delta = \frac{1}{(\delta^2\pi)^{1/4}} \exp\left(-\frac{1}{2\delta^2}(x - \hat{X})^2\right), \tag{2.4}$$

$$\hat{P}_p^\kappa = \frac{1}{(\kappa^2\pi)^{1/4}} \exp\left(-\frac{1}{2\kappa^2}(p - \hat{P})^2\right). \tag{2.5}$$

Note that for $\hat{B}_\beta = \pi^{-1}|\beta\rangle\langle\beta|$, we recover the well-known Husimi Q-distribution [155], since $P_{\hat{B}}(\beta) = \pi^{-2}\,\mathrm{tr}(|\beta\rangle\langle\beta|\hat{\rho}_0|\beta\rangle\langle\beta|) = \pi^{-1}\,\langle\beta|\hat{\rho}_0|\beta\rangle = Q(\beta)$. As an example, choosing $\hat{A} = \hat{X}^\delta$ and $\hat{B}_\beta = \pi^{-1}|\beta\rangle\langle\beta|$, the Husimi distribution $P_{\hat{B}|\hat{A}}$ is shown in fig. 2.1 for several values of δ.

The behaviors for different combinations of $\hat{A}, \hat{B} \in \{\hat{X}^\delta, \hat{P}^\kappa\}$ are printed in table 2.1, and detailed analytic values for the overlaps are listed in appendix 2.B.

The importance of selecting a complete set of classical reference operators becomes clear when looking at different combinations of coarse-grained $\hat{X}^\delta, \hat{P}^\kappa$. In particular, even a sharp X measurement is revealed by a second (coarse-grained) X measurement only after time evolution. Therefore, $\hat{P}^\kappa$ has to be a member of the reference set. On the other hand, a sharp measurement in P can never be detected by another measurement in P under free time evolution $\hat{H} = \hat{P}^2/(2m)$. Therefore, $\hat{X}^\delta$ needs

	$\hat{A} = \hat{X}^\delta$	$\hat{A} = \hat{P}^\kappa$
$\hat{B} = \hat{X}^\delta$	$V(0) = 1$ $V(T \to \infty) < 1$	$V(0) < 1$ $V(T \to \infty) = 1$
$\hat{B} = \hat{P}^\kappa$	$V(t) = \text{const} < 1$	$V(t) = 1$

Table 2.1: Overlaps (2.3) between the invaded and the non-invaded probability distributions with different combinations of coarse-grained phase space quadrature measurements. For final measurements in the momentum quadrature, $\hat{B} = \hat{P}^\kappa$, the overlap of the system stays constant, since $\hat{P}^\kappa$ commutes with the free Hamiltonian. For analytical values and detailed discussion see appendix 2.B.

to be a member of the set. For $\hat{X}^\delta$ and $\hat{P}^\kappa$ to fulfill the consistency condition, we further require sufficiently large $\delta \gg 1$ and $\kappa \gg 1$, such that $[\hat{X}^\delta, \hat{P}^\kappa] \approx 0$.

Using the notation $\hat{X}_{\text{c.g.}}$ ($\hat{P}_{\text{c.g.}}$) for a sufficiently coarse-grained X (P) measurement, and $\hat{X}_{\text{sh.}}$ ($\hat{P}_{\text{sh.}}$) for a sharp, invasive measurement, we can write some candidate reference sets:

- $\{\hat{X}_{\text{c.g.}}\}$ and $\{\hat{X}_{\text{sh.}}\}$ do not constitute reference sets, since they cannot detect the invasiveness of a $\hat{X}_{\text{sh.}}$ measurement.
- $\{\hat{X}_{\text{sh.}}, \hat{P}_{\text{c.g.}}\}$ is not a reference set, since the operators do not fulfill (2.2).
- $\{\hat{X}_{\text{c.g.}}, \hat{P}_{\text{c.g.}}\}$ is a possible reference set.

For further discussion about the joint measurability and coexistence of coarse-grained phase space operators we refer the reader to references [156–158].

2.3.2 Coherent state measurements

As another example, let us now consider coarse-grained operators in coherent state space,

$$\hat{A}_a = \frac{1}{\pi} \int \mathrm{d}\alpha \; f_a(\alpha) \, |\alpha\rangle\langle\alpha|, \tag{2.6}$$

where $f_a(\alpha)$ are some real and positive envelope functions that define the coarse-grained regions. Again, we consider coherent initial states $\hat{\rho} = |\gamma\rangle\langle\gamma|$ and final measurements $\hat{B}_\beta = \pi^{-1}|\beta\rangle\langle\beta|$. An analytical result can be obtained for a measure-

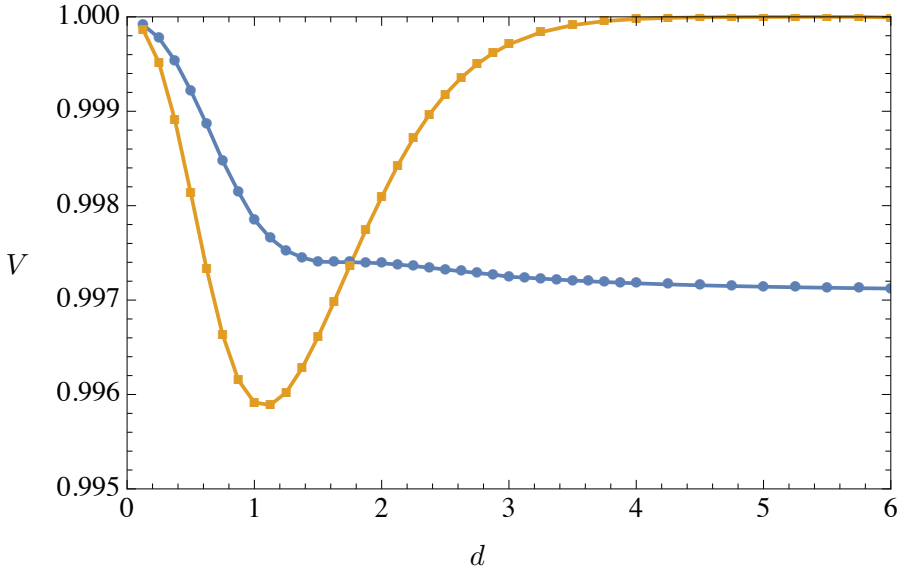

Figure 2.2: Overlap V vs coarse-graining ring width d. For coherent initial states in the center of the second region $|\gamma = 3d/2\rangle$ the overlap approaches unity as more of the state's probability distribution lies in the region. For initial states located on a border $|\gamma = d\rangle$ the overlap approaches a value close to 0.997. This is due to the artificial sharp boundary between the coarse-grained regions.

ment $f_a(\alpha) = \delta(a - \alpha)$ for $a \in \mathbb{C}$, yielding $\hat{A}_\alpha = \pi^{-1}|\alpha\rangle\langle\alpha|$. We can now calculate the overlap for $T = 0$:

$$\begin{aligned} V &= \frac{1}{\pi}\int \mathrm{d}\beta \ \left[|\langle\beta|\gamma\rangle|^2 \int \mathrm{d}\alpha \ |\langle\beta|\alpha\rangle\langle\alpha|\gamma\rangle|^2\right]^{\frac{1}{2}} \\ &= \frac{2\sqrt{2}}{3} \approx 0.943. \end{aligned} \tag{2.7}$$

This overlap provides us with a lower bound, that applies to all coarse-grained measurements based on coherent states. As an example, numerically evaluated overlaps for a ring-like coarse-graining ($f_a(r)$ is non-zero for $ad \leq r < (a+1)d$, with $a \in \mathbb{N}_0$ and d the ring width) are plotted in fig. 2.2.

A choice of reference set, alternative to the previously discussed $\{\hat{X}_{\text{c.g.}}, \hat{P}_{\text{c.g.}}\}$, can be made using the coarse-grained coherent state measurements from eq. (2.6), i.e. $\{\hat{A}_a\}$ with suitable envelope functions f_a such that $[\hat{A}_a, \hat{A}_{a'}] \approx 0$.

2.3.3 Fock state measurements

Instructive examples for observing the effect of coarse-graining are different combinations of Fock-measurements on coherent initial states. We look at coarse-grained

von Neumann measurement operators defined by different border functions $g(m)$:

$$\hat{A}_m = \sum_k \begin{cases} |k\rangle\langle k| & \text{if } g(m) \leq k < g(m+1), \\ 0 & \text{else.} \end{cases} \tag{2.8}$$

For quadratic dependence $g(m) = cm^2$ with $c > 0$, the region corresponding to each operator is constant-sized in the coherent state space, since the average photon number is $\bar{n} = |\alpha|^2$. For sufficiently large c the measurement is therefore sufficiently coarse-grained. Measurements with constant-sized regions in Fock space, $g(m) = cm$, correspond to increasingly sharp measurements in coherent state space. The resulting overlap for different choices of $g(m)$ can be calculated numerically and is discussed in fig. 2.3. The different degrees of invasiveness are illustrated in fig. 2.4.

2.4 Classicality of Hamiltonians

The formalism derived in section 1.6 also allows us to judge the classicality of Hamiltonians, as defined in section 2.2.

To simplify calculations, we now consider the setup printed in fig. 2.5. Since we are interested in the non-classicalities of Hamiltonians, we consider identical test and final measurements described by the POVM elements $\{\hat{A}_m^\dagger \hat{A}_m\}_m$. We denote the operator corresponding to the outcome of the test measurement as $\hat{A}_a$, and of the final measurement as $\hat{A}_b$. Furthermore, in an experiment, the preparation of the system in a specific initial state is usually achieved by performing a projective measurement. It is generally not reasonable to assume that the initial state should be more non-classical (e.g. sharp) than the measurement operators. In the following, we will therefore use an initial state obtained directly from the measurement operator $\hat{A}_i$ with outcome i,

$$\hat{\rho}_{0,i} = \frac{\hat{U}\hat{A}_i\hat{A}_i^\dagger\hat{U}^\dagger}{\mathrm{tr}(\hat{A}_i\hat{A}_i^\dagger)}. \tag{2.9}$$

We have added an additional time evolution from the state after the measurement (at time $-t$) to the initial state (at time 0). Without this step, the test measurement at time 0 could sometimes wrongly be judged as non-invasive (e.g. for projective measurements).

We now analyze the non-classicalities of several exemplary Hamiltonians. In this section, we consider as quantum system a large spin j with z-eigenstates $|-j\rangle \ldots |j\rangle$. As we are solely interested in non-classicalities resulting from the choice of Hamiltonian,

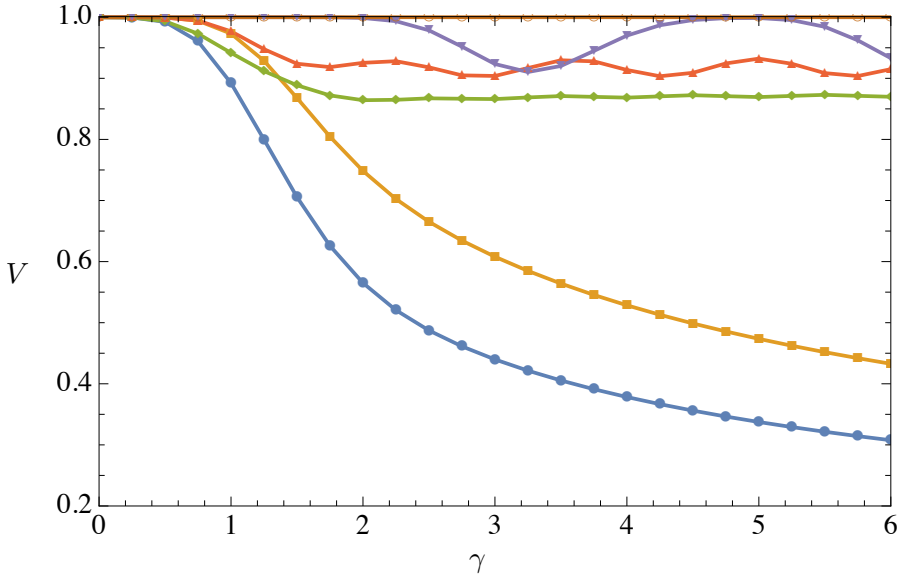

Figure 2.3: Overlap V (cf. eq. (2.3)) vs initial state $|\gamma\rangle$ for coarse-grained Fock measurements (2.8) with different border functions $g(m)$, from top: $100m^2, 10m^2, 2m^2, m^2, 2m, m$. Quadratic border functions are coarse in the coherent state space and therefore not as invasive. Linear border functions lead to increasingly sharp measurements. The oscillations are caused by the fact that the presented type of coarse-graining works better when the initial state is located in the center of a bin. Dips in the overlap occur when the initial state sits at the border between two bins.

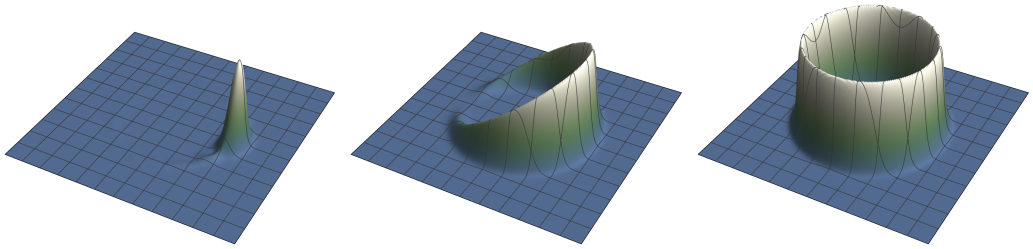

$g(m) = m^2$ $g(m) = 2m$ $g(m) = m$

Figure 2.4: The Husimi distribution after performing various Fock measurements on an initial state $|\gamma = 8\rangle$. While a coarse-grained measurement with m states per bin leaves the initial state mostly unchanged (left plot), a sharper measurement with 2 states per bin is invasive (center plot), or even projective with 1 state per bin (right plot).

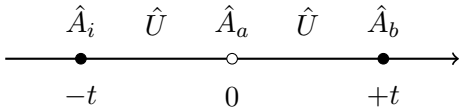

Figure 2.5: The setup discussed in section 2.4. An initial, preparatory measurement with measurement operator $\hat{A}_i$ is performed at time $-t$. The system then undergoes time evolution with unitary $\hat{U}$. At time 0, it may or may not be measured with operator $\hat{A}_a$. The final measurement, $\hat{A}_b$, is performed at time t, after the system evolved again according to unitary $\hat{U}$.

we choose a maximally coarse-grained which-hemisphere measurement, described by the operators

$$\hat{A}_\uparrow = \sum_{m>0} |m\rangle\langle m|, \tag{2.10}$$

and $\hat{A}_\downarrow = \mathbb{1} - \hat{A}_\uparrow$.

2.4.1 Rotation Hamiltonian

As first example Hamiltonian, we consider a simple Hamiltonian corresponding to a rotation around the x-axis,

$$\hat{H} = \omega \hat{J}_x, \tag{2.11}$$

where

$$(\hat{J}_x)_{ab} = \frac{\hbar}{2}(\delta_{a,b+1} + \delta_{a+1,b})\sqrt{(s+1)(a+b-1) - ab}. \tag{2.12}$$

As an example, for $j = 5/2$, we have

$$\hat{J}_x = \frac{\hbar\omega}{2}\begin{pmatrix} 0 & \sqrt{5} & 0 & 0 & 0 & 0 \\ \sqrt{5} & 0 & 2\sqrt{2} & 0 & 0 & 0 \\ 0 & 2\sqrt{2} & 0 & 3 & 0 & 0 \\ 0 & 0 & 3 & 0 & 2\sqrt{2} & 0 \\ 0 & 0 & 0 & 2\sqrt{2} & 0 & \sqrt{5} \\ 0 & 0 & 0 & 0 & \sqrt{5} & 0 \end{pmatrix}. \tag{2.13}$$

Taking again the Bhattacharyya coefficient, eq. (2.3), and setting $\omega = 1$ and $i = \uparrow$, we obtain the results plotted in fig. 2.6.

With the chosen Hamiltonian, the maximum violation of no-signaling in time (i.e. the smallest value of the overlap V) is obtained at $t = \pi/2$. The dependence of the maximum violation of j (i.e. the minimum $V_{\text{min}} = \min_t V(t)$) is plotted in fig. 2.7.

We observe that with increasing spin size, the system becomes more and more classical. Hence, $\hat{J}_x$ is a *classical* Hamiltonian.

2.4.2 Squeezing Hamiltonian

Next, we consider the spin squeezing Hamiltonian [159]

$$\hat{H} = \chi \hat{J}_x^2. \tag{2.14}$$

As an example, for $j = 5/2$, we have

$$\hat{J}_x^2 = \frac{\hbar^2\chi^2}{4} \begin{pmatrix} 5 & 0 & 2\sqrt{10} & 0 & 0 & 0 \\ 0 & 13 & 0 & 6\sqrt{2} & 0 & 0 \\ 2\sqrt{10} & 0 & 17 & 0 & 6\sqrt{2} & 0 \\ 0 & 6\sqrt{2} & 0 & 17 & 0 & 2\sqrt{10} \\ 0 & 0 & 6\sqrt{2} & 0 & 13 & 0 \\ 0 & 0 & 0 & 2\sqrt{10} & 0 & 5 \end{pmatrix}. \tag{2.15}$$

Setting $\chi = 1$, the time evolution of the overlap is plotted in fig. 2.8. Interestingly, the maximum violation of NSIT increases with the system size, and approaches a constant value (see fig. 2.9), which confirms the intuition that squeezing is a *non-classical* operation.

2.4.3 A Schrödinger's cat toy model

Finally, we consider a Hamiltonian that directly builds superpositions between both hemispheres,

$$(\hat{H}_d)_{ab} = \begin{cases} \frac{1}{2} & \text{if } a = n - b + 1 \text{ and } (a - 1 < d \text{ or } n - a < d), \\ 0 & \text{else,} \end{cases} \tag{2.16}$$

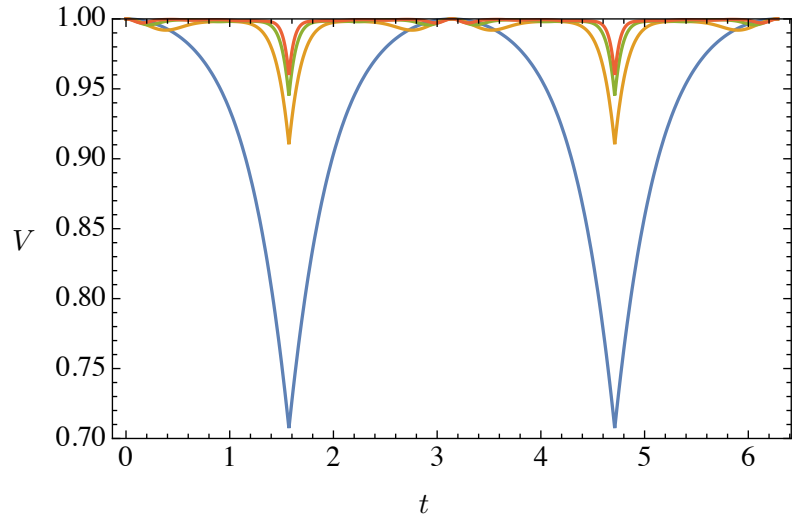

Figure 2.6: The overlap (2.3) as a function of time for spin sizes $1/2$ (blue), $5/2$ (orange), $9/2$ (green) and $13/2$ (red), with a $\hat{J}_x$ rotation Hamiltonian (2.11). A maximal violation of NSIT is reached at $t = \pi/2$; the magnitude of the violation decreases with increasing spin size (c.f. fig. 2.7).

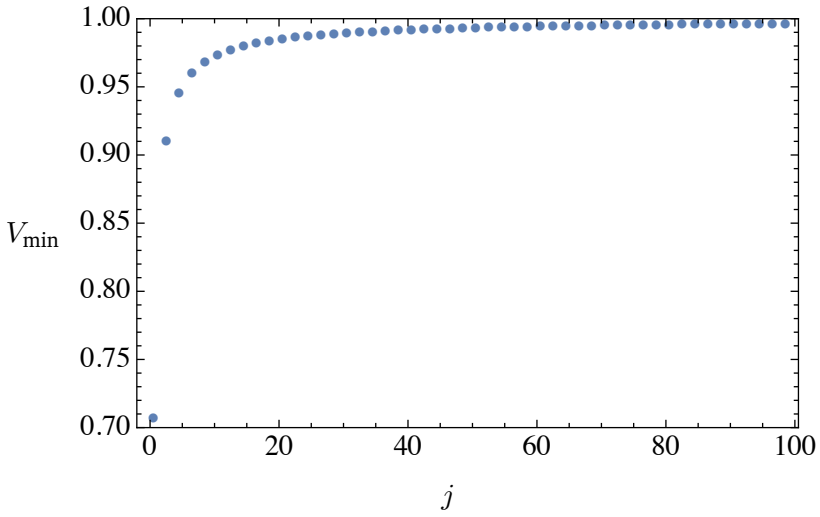

Figure 2.7: The minimum with respect to time t of the overlap as a function of the spin size j, with a $\hat{J}_x$ rotation Hamiltonian (2.11). Plotted here are values of $j = 1/2 + 2n$ with $n \in \mathbb{N}$, to avoid issues with an even or odd number of states per hemisphere. It can readily be seen that the overlap approaches unity as the system becomes increasingly macroscopic.

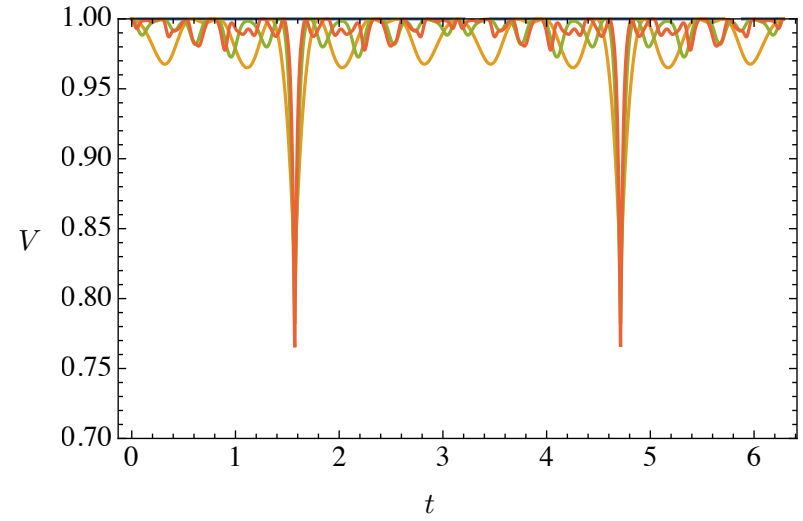

Figure 2.8: The overlap (2.3) as a function of time for spin sizes $1/2$ (blue, barely visible as it is equal to 1), $5/2$ (orange), $9/2$ (green) and $13/2$ (red), with a squeezing $\hat{J}_x^2$ Hamiltonian (2.14). A maximal violation of NSIT is reached at $t = \pi/2$; the magnitude of the violation approaches a constant value smaller than 1 with increasing spin size (c.f. fig. 2.9).

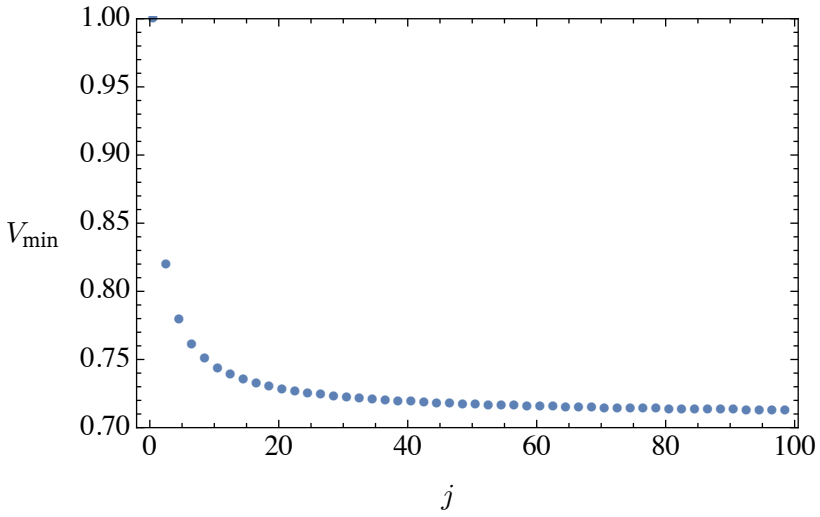

Figure 2.9: The minimum with respect to time t of the overlap as a function of the spin size j, with a squeezing $\hat{J}_x^2$ Hamiltonian (2.14). Again, plotted here are values of $j = 1/2 + 2n$ with $n \in \mathbb{N}$. In contrast to the $\hat{J}_x$ Hamiltonian (c.f. fig. 2.7), the violation of NSIT approaches a constant value smaller than 1 with increasing system size.

where $n = 2j + 1$ is the dimension of the system. Intuitively, $\hat{H}_d$ is zero for all entries off the anti-diagonal, and only has $2d$ entries on the anti-diagonal that are non-zero, extending from the edges of the matrix. As an example, for $j = 5/2$ ($n = 6$),

$$\hat{H}_{d=0} = \frac{1}{2}\begin{pmatrix} 0 & 0 & 0 & 0 & 0 & 0 \\ 0 & 0 & 0 & 0 & 0 & 0 \\ 0 & 0 & 0 & 0 & 0 & 0 \\ 0 & 0 & 0 & 0 & 0 & 0 \\ 0 & 0 & 0 & 0 & 0 & 0 \\ 0 & 0 & 0 & 0 & 0 & 0 \end{pmatrix}, \quad \hat{H}_{d=1} = \frac{1}{2}\begin{pmatrix} 0 & 0 & 0 & 0 & 0 & \mathbf{1} \\ 0 & 0 & 0 & 0 & 0 & 0 \\ 0 & 0 & 0 & 0 & 0 & 0 \\ 0 & 0 & 0 & 0 & 0 & 0 \\ 0 & 0 & 0 & 0 & 0 & 0 \\ \mathbf{1} & 0 & 0 & 0 & 0 & 0 \end{pmatrix}, \tag{2.17}$$

$$\hat{H}_{d=2} = \frac{1}{2}\begin{pmatrix} 0 & 0 & 0 & 0 & 0 & \mathbf{1} \\ 0 & 0 & 0 & 0 & \mathbf{1} & 0 \\ 0 & 0 & 0 & 0 & 0 & 0 \\ 0 & 0 & 0 & 0 & 0 & 0 \\ 0 & \mathbf{1} & 0 & 0 & 0 & 0 \\ \mathbf{1} & 0 & 0 & 0 & 0 & 0 \end{pmatrix}, \quad \hat{H}_{d=3} = \frac{1}{2}\begin{pmatrix} 0 & 0 & 0 & 0 & 0 & \mathbf{1} \\ 0 & 0 & 0 & 0 & \mathbf{1} & 0 \\ 0 & 0 & 0 & \mathbf{1} & 0 & 0 \\ 0 & 0 & \mathbf{1} & 0 & 0 & 0 \\ 0 & \mathbf{1} & 0 & 0 & 0 & 0 \\ \mathbf{1} & 0 & 0 & 0 & 0 & 0 \end{pmatrix}. \tag{2.18}$$

The time evolution of the NSIT violation is plotted in fig. 2.10; its minimum value as a function of d is plotted in fig. 2.11.

For macroscopically large j (e.g. of the order of 10^{23}), the Hamiltonian (2.16) establishes "long-range interactions" already for very small values of $d \sim 1$. However, as there are many more states in the coarse-grained measurement operator, the resulting time evolution remains approximately classical.

2.5 Spontaneously realized Hamiltonians

In the definition of classicality from section 2.2, we have omitted a discussion of the Hamiltonians that are spontaneously realized by nature. In fact, we will now argue that the Hamiltonians that give rise to classical dynamics are not as limited as one might think.

Let us start by recalling that, as orthogonal vectors in a Hilbert space, states that span a basis in quantum mechanics possess no inherent measure of closeness. Without any physical intuition, it is therefore not clear whether the spin state $|m = 1/2\rangle$ is closer to $|m = 3/2\rangle$ or to $|m = 99/2\rangle$. Our *classical* intuition of closeness stems from

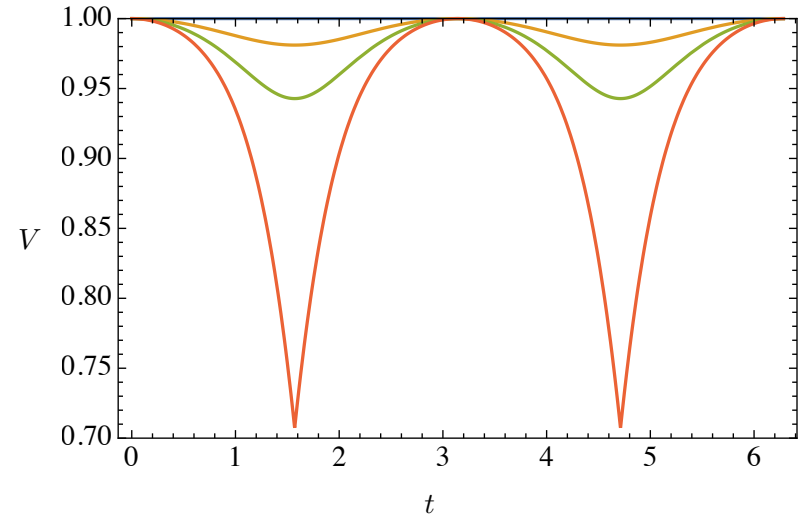

Figure 2.10: The overlap (2.3) as a function of time for $d = 0$ (blue), $d = 1$ (orange), $d = 2$ (green) and $d = 3$ (red), with the Hamiltonian (2.16) for $j = 5/2$. A maximal violation of NSIT is reached at $t = \pi/2$; the magnitude of the violation increases with d (c.f. fig. 2.11).

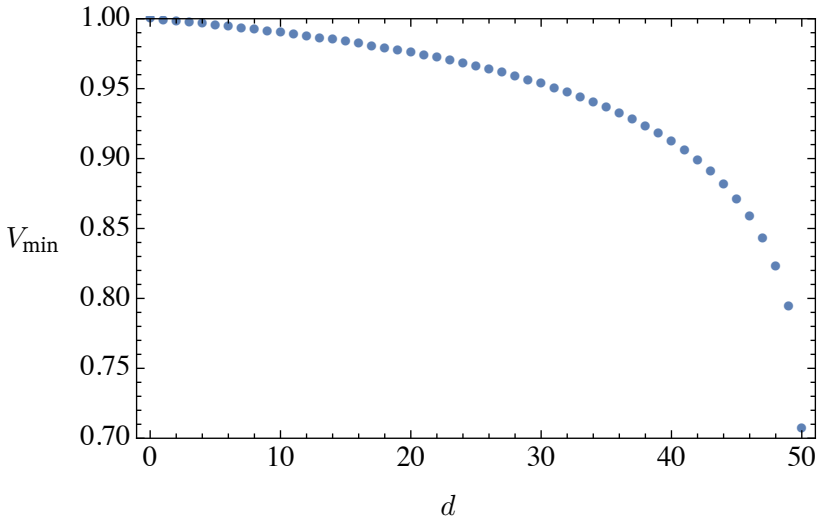

Figure 2.11: The minimum with respect to time t of the overlap as a function of the parameter d in the Hamiltonian (2.16), with $j = 99/2$. With increasing d, the NSIT violation also increases.

the Hamiltonians that are spontaneously realized by nature, in our case e.g. $\hat{J}_x$-like Hamiltonians.

However, imagine an "exotic" region of space (e.g. a box), where instead the Schrödinger's cat toy model Hamiltonian (2.16) from subsection 2.4.3 is spontaneously realized. An inhabitant of this box might have a completely different intuition of closeness of states, taking states $|\pm m\rangle$ to be neighboring. With this reordering[2] of the basis states, the Hamiltonian (2.16) becomes diagonal, and looses its long-range interactions. Thus, after coarse-graining, from the inhabitant's perspective, the world would behave completely classical, perhaps even indistinguishable from our observation of the world outside of the box. However, when we look inside the box, we would see an "exotic" world, with spontaneously realized Schrödinger cats.

This example shows that the conditions for classicality to arise from quantum behavior are not as intuitive as previously thought. In fact, to judge whether a Hamiltonian gives rise to classical behavior, eq. (2.2) should be tested with coarse-grainings in all possible reorderings of the basis states.

2.6 Conclusions and outlook

In this chapter, we have used the results from ref. [1] and chapter 1 to define the "classicality" of measurements, and by extension, of Hamiltonians. We have then applied this definition to a number of exemplary measurements, and found that it is fulfilled when measurements are suitable coarse-grained. Next, we tested several Hamiltonians for non-classicalities. Finally, we discussed the possibility of obtaining "exotic" classical behavior from Hamiltonians that are very non-classical in our intuitive notion.

It is left for future work to investigate conditions for obtaining classical behavior from spontaneously realized Hamiltonians, as outlined in section 2.5. Especially a condition of no long-range interactions in a rearranged basis might be investigated. A more operational formulation of the emergence of classical phase space out of microscopic quantum behavior would certainly be interesting.

[2] Interestingly, when we consider the Hamiltonian (or the resulting unitary) to be the adjacency matrix of a weighted graph, this problem is generally equivalent to graph partitioning, a well-known NP-complete problem in computer science [160–162].

Appendix

2.A The Husimi distribution as measure of distinctness of quantum states

In this appendix we illustrate how the Husimi distribution [155] can be used to witness distinctness of quantum states. Recall the definition of the distribution,

$$Q(\alpha, \hat{\rho}) = \mathcal{N} \langle \alpha | \hat{\rho} | \alpha \rangle \,, \tag{2.19}$$

where $\mathcal{N}$ is some normalization parameter, $|\alpha\rangle$ is a coherent state, and $\hat{\rho}$ is the quantum state. We can compare the Husimi distributions for two quantum states, $\hat{\rho}$ and $\hat{\rho}'$, using the Bhattacharyya coefficient [154],

$$V = \int \mathrm{d}\alpha \sqrt{Q(\alpha, \hat{\rho}) Q(\alpha, \hat{\rho}')} \in [0, 1]. \tag{2.20}$$

Note that the use of coherent states in a measure for distinctness is motivated by their similarity to classical states.

We can now apply this measure exemplary to quantum states used by two recent experiments. Let us start with an experiment by De Martini *et. al.* [163]. In a slightly simplified model, they produced a superposition of the states

$$\begin{aligned} |+\rangle &\propto \sum_{k=0}^{\infty} |2k\rangle\langle 2k|\beta\rangle, \\ |-\rangle &\propto \sum_{k=0}^{\infty} |2k+1\rangle\langle 2k+1|\beta\rangle. \end{aligned} \tag{2.21}$$

Although their states are completely orthogonal, $\langle +|-\rangle = 0$, the Q-distributions are very similar, despite the large number of photons ($|\beta|^2 \sim 10^4$) involved in their experiment. In fact, we have $V \approx 1$, as visualized in fig. 2.12.

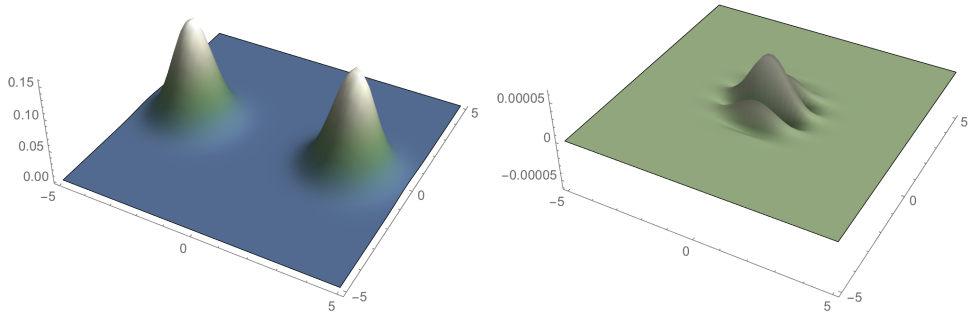

Figure 2.12: Left: Plot of $|+\rangle$ (and $|-\rangle$, which is in fact indistinguishable to the naked eye) for $\beta = 3$, as described in the main text of appendix 2.A. Right: Plot of $Q(\alpha, |+\rangle\langle+|) - Q(\alpha, |-\rangle\langle-|)$. Note that the difference is around four orders of magnitude smaller than the Q-distributions.

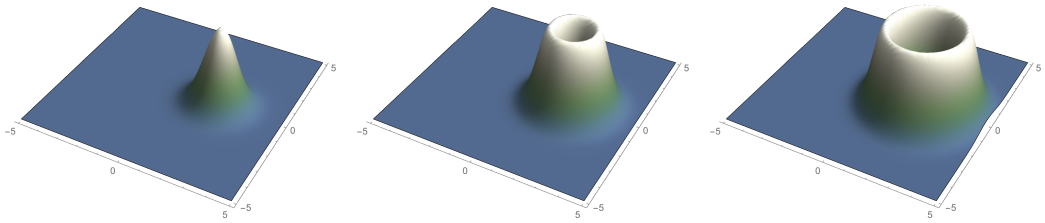

Figure 2.13: The Q-distributions for $|\psi_0\rangle$, $|\psi_1\rangle$, and $|\psi_3\rangle$, for $\beta = 2$, as described in appendix 2.A. With increasing k, the states become more and more distinct.

On the other hand, a recent experiment by Lvovsky *et. al.* [120] realized a superposition of displaced Fock states,

$$\begin{aligned} |\psi_0\rangle &= \hat{D}(\beta)\,|0\rangle = |\beta\rangle \\ |\psi_k\rangle &= \hat{D}(\beta)\,|k\rangle\,, \end{aligned} \tag{2.22}$$

where $\hat{D}(\beta) = \exp(\beta\hat{a}^\dagger - \beta^*\hat{a})$ is the displacement operator. Using our analysis outlined above, we find the states to be moderately distinct, with V decreasing with increasing k:

$$V_{k=0} = 1,\ V_{k=1} \approx 0.89,\ V_{k=2} \approx 0.71,\ V_{k=3} \approx 0.54. \tag{2.23}$$

Three exemplary Q-distributions are printed in fig. 2.13.

2.B Overlaps for quadrature measurements

In the following we will give analytical values for the overlap for different combinations of coarse-grained $\hat{X}^\delta$ and $\hat{P}^\kappa$ measures, as defined by eq. (2.4) and eq. (2.5), acting on a particle with initial state $\langle x|\psi\rangle = \pi^{-1/4}\sigma^{-1/2}\exp(-x^2/(2\sigma^2))$. In between the measurements we apply a unitary generated by a free Hamiltonian $\hat{U}_T = \exp(-it\hat{p}^2/2m)$. There are four combinations:

- $\hat{A} = \hat{X}^\delta, \hat{B} = \hat{X}^\delta$. Here the overlap starts at $V(0) = 1$, but approaches the value
$$\lim_{t\to\infty} V(t) = \frac{4\delta^2(\delta^2+\sigma^2)}{(2\delta^2+\sigma^2)^2}. \tag{2.24}$$
The effect of the measurement only becomes apparent with time evolution.

- $\hat{A} = \hat{P}^\kappa, \hat{B} = \hat{X}^\delta$. The overlap starts at
$$V(0) = \frac{4\kappa^2(\delta^2+\sigma^2)[\kappa^2(\delta^2+\sigma^2)+1]}{[2\kappa^2(\delta^2+\sigma^2)+1]^2}, \tag{2.25}$$
and approaches 1 for $t \to \infty$. The momentum measurement changes the spatial distribution once, but with wave packet expansion the impact becomes less apparent.

- $\hat{A} = \hat{X}^\delta, \hat{B} = \hat{P}^\kappa$. The overlap is constant in time at the value
$$V = \frac{4\delta^2(\kappa^2\sigma^2+1)[\delta^2(\kappa^2\sigma^2+1)+\sigma^2]}{[2\delta^2(\kappa^2\sigma^2+1)+\sigma^2]^2}, \tag{2.26}$$
since $[\hat{P}^\kappa, \hat{H}] = 0$.

- $\hat{A} = \hat{P}^\kappa, \hat{B} = \hat{P}^\kappa$. The overlap is constant at 1, and a measurement in $\hat{P}$ cannot be detected by a second $\hat{P}$ measurement, as again, $[\hat{P}^\kappa, \hat{H}] = 0$.

These examples reaffirm the importance of the selection of multiple final measurements.

3

The local realism and macrorealism polytopes

> *[. . .] the conception of chance enters into the very first steps of scientific activity, in virtue of the fact that no observation is absolutely correct. I think chance is a more fundamental conception than causality; for whether in a concrete case a cause-effect relation holds or not can only be judged by applying the laws of chance to the observations.*
>
> **— Max Born**
> *Natural Philosophy of Cause and Chance* [164]

Abstract

Tests of local realism (c.f. section 0.2) and macrorealism (c.f. chapter 1) have historically been discussed in very similar terms: Leggett-Garg inequalities follow Bell inequalities as necessary conditions for classical behavior. However, some discrepancies in this analogy have recently become apparent. While the concept of no-signaling applies generally in all reasonable physical theories, its temporal analogue, no-signaling in time, is readily violated by quantum physics [73].

Here, we analyze further differences between local realism and macrorealism. We compare the probability polytopes spanned by all measurable probability distributions for both scenarios, and show that their structure differs strongly between spatially and temporally separated measurements. We arrive at the conclusion that, in contrast to tests of local realism, where Bell inequalities form a necessary and sufficient set of conditions, no set of inequalities can ever be necessary and sufficient for a macrorealistic description. Fine's famous proof, that Bell inequalities are necessary and sufficient for the existence of a local realistic model, can therefore not be transferred to macrorealism. A recently proposed condition, no-signaling in time, fulfills this criterion, and we show why it is better suited for future experimental

tests and theoretical studies of macrorealism. Our work thereby identifies a major difference between the mathematical structure of local realism and macrorealism.

After a brief introduction (**section 3.1**), we start our discussion with a review of the probability space spanned by local realistic theories (**section 3.2**). We then derive the structure of the comparable macrorealism polytope (**section 3.3**), and discuss the structure of quantum mechanics in tests of macrorealism (**section 3.4**). Finally, we compare local realism and macrorealism, and reach some conclusions about the Leggett-Garg inequality (**section 3.5**).

This chapter is based on and uses parts of ref. [3]:

- L. Clemente and J. Kofler, 'No Fine theorem for macrorealism: Retiring the Leggett-Garg inequality', (2015), arXiv:1509.00348 [quant-ph]

3.1 Introduction

The violation of classical world views, such as local realism [45] and macrorealism [72, 75], is one of the most interesting properties of quantum mechanics. Experiments performed over the past decades have shown violations of local realism in various systems [53, 55, 58], while violations of macrorealism are on the horizon [76, 110–119, 121, 122, 125–128]. The latter endeavors pave the way towards the experimental realization of Schrödinger's famous thought experiment [8]. In the future, they might offer insight into important foundational questions, such as the quantum measurement problem [11, 12], and allow experimental tests of (possibly gravitational) extensions of quantum mechanics [36].

Historically, the discussion of tests of macrorealism (MR) follows the discussion of tests of local realism (LR) closely: Leggett-Garg inequalities (LGIs) [72] are formulated similarly to Bell inequalities [45, 48, 50], and some concepts, e.g. quantum contextuality [165], are connected to both fields [166–170]. However, recently, a discrepancy between LR and MR has been identified: Whereas Bell *inequalities* are found to be both necessary and sufficient for LR [171], a combination of arrow of time (AoT) and no-signaling in time (NSIT) [73] *equalities* are necessary and sufficient for the existence of a macrorealistic description [1] (c.f. chapter 1). A previous study [1] also demonstrated that two-time LGIs are not sufficient for macrorealism, but did not rule out a potential sufficiency of other sets of LGIs, e.g. of the CH type [50, 172]. Moreover, cases have been identified where LGIs hide violations of macrorealism [166] that are detected by NSIT [1, 73]. These fundamental differences between tests of local realism and macrorealism seem connected to the peculiar definition of macrorealism [78, 79].

In this chapter, we analyze the reasons for and the consequences of this difference. We show that the probability space spanned by quantum mechanics (QM) is of a higher dimension in an MR test than in an LR test, and analyze the resulting structure of the probability polytope. We conclude that inequalities—excluding the pathological case of two inequalities merging into a single equality—are not suited as sufficient conditions for MR, and form only weak necessary conditions. Fine's theorem [171], which states that Bell inequalities are necessary and sufficient for a local realistic model, therefore cannot be transferred to macrorealism (unless one uses potentially negative quasi-probabilities [173]). Our study thus identifies a striking difference between the mathematical structures of LR and MR. While current experimental tests of macrorealism overwhelmingly use Leggett-Garg inequalities,

we argue that NSIT is better suited as a witness of non-classicality: Not only is it, in combination with AoT, *logically equivalent* to MR, but it is violated in a much larger range of parameters. In fact, our work shows that there is no compelling reason (other than history) to use LGIs in future theoretical and experimental studies.

3.2 The local realism polytope

Let us start with reviewing the structure of the LR polytope (LR), as described in refs. [13, 174, 175]. Consider an LR test between $n \geq 2$ parties $i \in \{1 \dots n\}$. Each party can perform a measurement in one of $m \geq 2$ settings $s_i \in \{1 \dots m\}$. Each setting has the same number $\Delta \geq 2$ of possible outcomes $q_i \in \{1 \dots \Delta\}$, and, to allow for all possible types of correlations, may measure a distinct property of the system. We can define probability distributions $p_{q_1 \dots q_n | s_1 \dots s_n}$ for obtaining outcomes $q_1 \dots q_n$, given the measurement settings $s_1 \dots s_n$. If a party i chooses to not perform a measurement, the corresponding "setting" is labeled $s_i = 0$, and there is only one "outcome" labeled $q_i = 0$ (e.g. $p_{q_1,0|s_1,0}$ when only the first party performs a measurement). We leave out final zeroes, e.g. $p_{q_1 \dots q_i,0 \dots 0|s_1 \dots s_i,0 \dots 0} = p_{q_1 \dots q_i|s_1 \dots s_i}$. Note that this convention differs from the literature for LR tests, where the case of no measurement is often left out [13, 174], but simplifies the comparison between LR and MR tests. Each experiment is then completely described by $(m\Delta + 1)^n$ probability distributions; it can be seen as a point in a probability space $\mathbb{R}^{(m\Delta+1)^n}$.

We now require normalization of the probabilities. There are $(m + 1)^n$ linearly independent normalization conditions, as each probability only appears once:

$$\forall s_1 \dots s_n : \sum_{q_1 \dots q_n} p_{q_1 \dots q_n | s_1 \dots s_n} = 1. \tag{3.1}$$

Due to the special case of no measurements ($s_i = 0$), here (and in the following equations) we have abbreviated the notation of the summation: the possible values of q_i in fact depend on s_i. The normalization conditions reduce the dimension of the probability space to

$$(m\Delta + 1)^n - (m + 1)^n. \tag{3.2}$$

Furthermore, the positivity conditions

$$\forall s_1 \dots s_n, q_1 \dots q_n : p_{q_1 \dots q_n | s_1 \dots s_n} \geq 0 \tag{3.3}$$

restrict the reachable space to a subspace with the same dimension, but delimited by flat hyperplanes. The resulting subspace is called the *probability polytope* P.

In an LR test with space-like separated parties, special relativity prohibits signaling from every party to any other,

$$\begin{aligned} &\forall i, q_1 \dots q_{i-1}, q_{i+1} \dots q_n, s_1 \dots s_n, s_i \neq 0: \\ &p_{q_1 \dots q_{i-1},0,q_{i+1} \dots q_n | s_1 \dots s_{i-1},0,s_{i+1} \dots s_n} = \sum_{q_i=1}^{\Delta} p_{q_1 \dots q_n | s_1 \dots s_n}. \end{aligned} \tag{3.4}$$

These *no-signaling* (NS) conditions restrict the probability polytope to a NS polytope (NS) of lower dimension. Taking their linear dependence, both amongst each other and with the normalization conditions, into account, we arrive at dimension [174]

$$\dim \mathsf{NS} = [m(\Delta - 1) + 1]^n - 1. \tag{3.5}$$

Since quantum mechanics obeys NS, and due to Tsirelson bounds [176], the space of probability distributions from spatially separated experiments implementable in quantum mechanics, $\mathsf{QM_S}$, is located strictly within the NS polytope. Furthermore, the space of local realistic probability distributions, LR, is a strict subspace of $\mathsf{QM_S}$. It is delimited by Bell inequalities (e.g. the CH/CHSH inequalities for $n = m = \Delta = 2$) and positivity conditions, and therefore forms a polytope within $\mathsf{QM_S}$ [171, 174]. In summary, we have $\mathsf{P} \supset \mathsf{NS} \supset \mathsf{QM_S} \supset \mathsf{LR}$, with $\dim \mathsf{P} > \dim \mathsf{NS} = \dim \mathsf{QM_S} = \dim \mathsf{LR}$. The structure of the NS, $\mathsf{QM_S}$ and LR spaces is sketched on the left of fig. 3.1.

3.3 The macrorealism polytope

In a test of MR, temporal correlations take the role of an LR test's spatial correlations. Instead of spatially separated measurements on n systems by different observers, a single observer performs n sequential (macroscopically distinct) measurements on one and the same system. Again, each measurement is either skipped ("0") or performed in one of $m \geq 1$[1] settings, with Δ possible outcomes each. With this one-to-one correspondence, the resulting probability polytope P in the space $\mathbb{R}^{(m\Delta+1)^n-(m+1)^n}$ is identical to the one in the Bell scenario. However, without further physical assumptions, no-signaling in temporally separated experiments is only a requirement in one direction: While past measurements can affect the future,

[1] In contrast to LR tests, where $m \geq 2$ is required to observe quantum violations, $m = 1$ allows for violations of MR, and is in fact the most considered case in the literature.

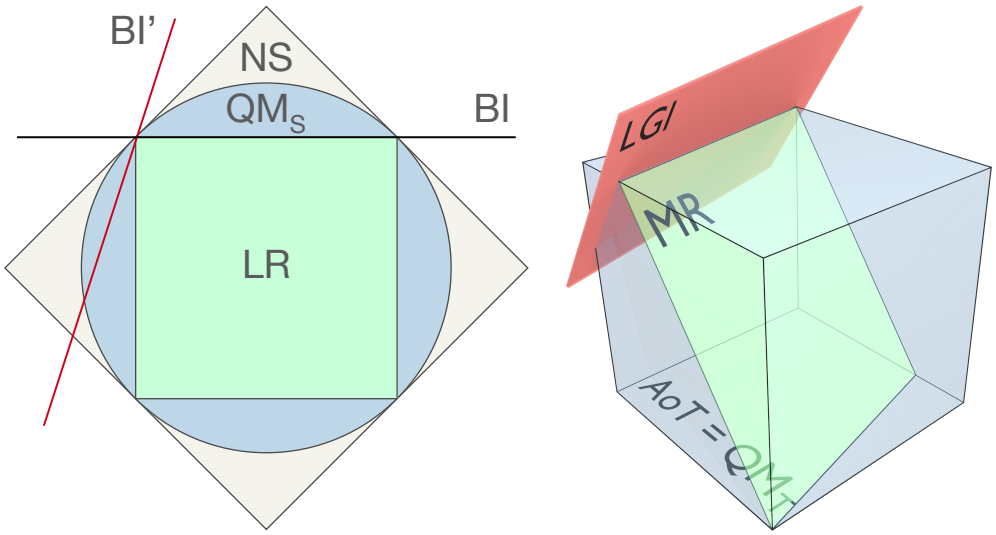

Figure 3.1: Left: A sketch of subspaces in an LR test [13]. The no-signaling polytope (NS) contains the space of probability distributions realizable from spatially separated experiments in quantum mechanics (QM_S), which contains the local realism polytope (LR). LR is delimited by Bell inequalities and the positivity conditions. NS, QM_S, and LR have the same dimension. A Bell inequality (BI) is also sketched, delimiting LR. Another tight Bell inequality (BI') is less suited as a witness of non-LR behavior, and illustrates the role of Leggett-Garg inequalities in macrorealism tests.
Right: A sketch of polytopes in an MR test. The arrow of time polytope (AoT) is equal to the space of probability distributions realizable from temporally separated experiments in quantum mechanics (QM_T), which contains the macrorealism polytope (MR). MR is a polytope of lower dimension, located fully within the QM_T subspace and solely delimited by positivity constraints. Since each probability can easily be minimized or maximized individually, MR reaches all facets of AoT. A Leggett-Garg inequality (LGI) is also sketched; it is a hyperplane of dimension $\dim \mathsf{QM}_\mathsf{T} - 1$, which, in general, is much larger than $\dim \mathsf{MR}$. Note that the LGI can only touch MR (i.e. be tight) at the boundary of the positivity constraints.

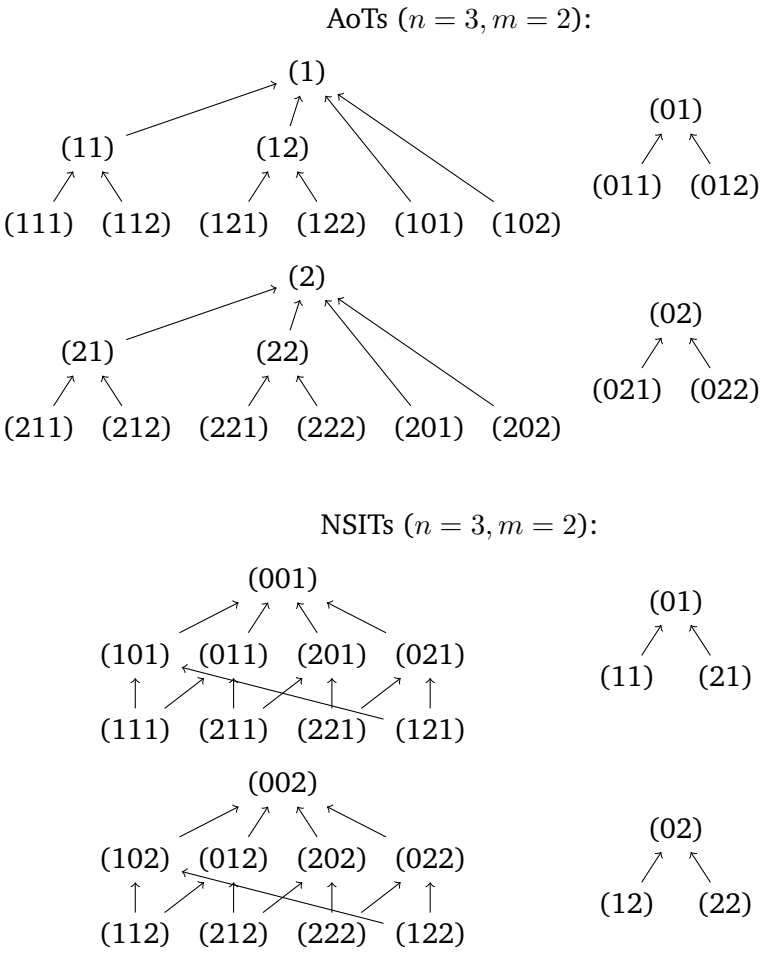

Figure 3.2: Arrow of time (AoT) and no-signaling in time (NSIT) conditions relating different outcome probability distributions for the case $n = 3$ measurement times and $m = 2$ possible settings. The notation (xyz) refers to distributions with settings $s_1 = x, s_2 = y, s_3 = z$. The arrows denote the process of marginalization: e.g. the AoT condition $p_{q_1|s_1=x} = \sum_{q_2} p_{q_1,q_2|s_1=x,s_2=y}$ is denoted by $(x) \leftarrow (xy)$, and the NSIT condition $p_{q_2|s_2=y} = \sum_{q_1} p_{q_1,q_2|s_1=x,s_2=y}$ is denoted by $(y) \leftarrow (xy)$. It can easily be seen that the AoT conditions are linearly independent, since they cannot form loops. Adding more measurement times (adding further rows), or adding more settings (broadening the trees) does not change their independence. In contrast, the NSIT conditions are not linearly independent, and thus form loops. Note that marginalizing only over a single measurement is sufficient, as simultaneous marginalizations follow from individual ones, and hence are always linearly dependent.

causality demands that future measurements cannot affect the past. This assumption is captured by the *arrow of time* (AoT) conditions:

$$\begin{aligned}&\forall i \geq 2 \colon \forall q_1 \dots q_{i-1}, s_1 \dots s_{i-1} \text{ with } \Sigma_{j=1}^{i-1} s_j \neq 0, s_i \neq 0 \colon \\ &p_{q_1 \dots q_{i-1}|s_1 \dots s_{i-1}} = \sum_{q_i=1}^{\Delta} p_{q_1 \dots q_i|s_1 \dots s_i}.\end{aligned} \tag{3.6}$$

Counting the number of equalities in eq. (3.6) shows that their number is

$$\sum_{i=2}^{n} [(m\Delta+1)^{i-1} - 1]m = \frac{(m\Delta+1)^n - nm\Delta - 1}{\Delta}, \tag{3.7}$$

where the first factor in the sum counts the setting and outcome combinations for times $1 \dots i-1$, excluding the choice of all $s_i = 0$, and the second factor the number of settings at time i. All listed conditions are linearly independent due to their hierarchical construction, see fig. 3.2. However, a number of the normalization conditions for the marginal distributions, already subtracted in eq. (3.2), are not linearly independent from AoT, and thus become obsolete. Their number is obtained by counting the different settings in eq. (3.6):

$$\sum_{i=2}^{n} [(m+1)^{i-1} - 1]m = (m+1)^n - nm - 1. \tag{3.8}$$

The remaining normalization conditions are the ones for probability distributions with just one measurement and for the "0-distribution"; there are $nm+1$ such distributions. Taking eq. (3.2), subtracting eq. (3.7) and adding eq. (3.8), we conclude that the AoT conditions restrict the probability polytope to an AoT polytope (AoT) of dimension

$$\dim \mathsf{AoT} = \frac{[(m\Delta+1)^n - 1](\Delta - 1)}{\Delta}. \tag{3.9}$$

As shown in [1] (c.f. chapter 1), the set of all *no-signaling in time* (NSIT) conditions,

$$\begin{aligned}&\forall i < n, q_1 \dots q_{i-1}, q_{i+1} \dots q_n, s_1 \dots s_n, \Sigma_{j>i} s_j \neq 0, s_i \neq 0 \colon \\ &p_{q_1 \dots q_{i-1}, 0, q_{i+1} \dots q_n|s_1 \dots s_{i-1}, 0, s_{i+1} \dots s_n} = \sum_{q_i=1}^{\Delta} p_{q_1 \dots q_n|s_1 \dots s_n},\end{aligned} \tag{3.10}$$

is, together with AoT, necessary and sufficient for macrorealism. To get from AoT to the macrorealism polytope, MR, we therefore require a linearly independent subset these conditions. However, since the AoT conditions from eq. (3.6) plus the NSIT

	LR test	MR test
number of unnormalized distributions	$(m\Delta+1)^n$	
$\dim \mathsf{P}$	$(m\Delta+1)^n-(m+1)^n$	
$\dim \mathsf{QM_S}/\dim \mathsf{QM_T}$	$[m(\Delta-1)+1]^n-1$	$<\quad[(m\Delta+1)^n-1](\Delta-1)/\Delta$
$\dim \mathsf{LR}/\dim \mathsf{MR}$	$[m(\Delta-1)+1]^n-1$	

Table 3.1: Dimensions of the probability space P and its subspaces reachable by spatially separated ($\mathsf{QM_S}$) / temporally separated ($\mathsf{QM_T}$) experiments in quantum mechanics, local realism (LR), and macrorealism (MR). There are n spatially / temporally separated measurements with m settings and Δ outcomes each.

conditions from eq. (3.10) are equivalent to the NS conditions from eq. (3.4), we arrive at MR with the same dimension as the LR polytope:

$$\dim \mathsf{MR} = \dim \mathsf{LR} = [m(\Delta-1)+1]^n - 1. \tag{3.11}$$

3.4 Quantum mechanics in macrorealism tests

We are left with the question of how the space of probability distributions realizable from temporally separated experiments in quantum mechanics, $\mathsf{QM_T}$, relates to AoT. Fritz has shown in ref. [177] that $\mathsf{QM_T} = \mathsf{AoT}$ for $n = m = \Delta = 2$, if we allow for positive-operator valued measurements (POVMs). Let us now generalize his proof to arbitrary n, m, Δ. We do so by constructing a quantum experiment that produces all possible probability distributions which are allowed by AoT.

Consider a quantum system of dimension $(m\Delta+1)^n$, with states enumerated as $|q_1 \dots q_n; s_1 \dots s_n\rangle$. As with the probability distributions, final zeros may be omitted. The initial state of the system is $|0 \dots 0; 0 \dots 0\rangle$. Now, n POVMs are performed on the system. The measurements are chosen such that depending on their setting and outcome they take the system to the corresponding state: Performing a measurement on a system in state $|q_1 \dots q_{i-1}; s_1 \dots s_{i-1}\rangle$ with setting s_i and obtaining outcome q_i

should leave the system in state $|q_1 \dots q_i; s_1 \dots s_i\rangle$. This is accomplished by choosing Kraus operators for the i-th measurement in basis s_i for outcome q_i as

$$\begin{aligned} K^{(i)}_{s_i,q_i} = & \sum_{s_1 \dots s_{i-1}, q_1 \dots q_{i-1}} \sqrt{r_{q_i|q_1 \dots q_{i-1}, s_1 \dots s_i}} \\ & \times |q_1 \dots q_i; s_1 \dots s_i\rangle\langle q_1 \dots q_{i-1}; s_1 \dots s_{i-1}| \\ + & \sum_{\substack{s_1 \dots s_n \\ q_1 \dots q_n \\ \Sigma_{j=i}^n s_j \neq 0}} \frac{1}{\sqrt{\Delta}} |q_1 \dots q_n; s_1 \dots s_n\rangle\langle q_1 \dots q_n; s_1 \dots s_n|. \end{aligned} \tag{3.12}$$

For $i = 1$, the first sum in eq. (3.12) reduces to the single term $\sqrt{p_{q_1|s_1}}|q_1; s_1\rangle\langle 0 \dots 0; 0 \dots 0|$, while the second sum remains unchanged. The second sum in eq. (3.12) is necessary for the completeness relation $\sum_{q_i} (K^{(i)}_{s_i,q_i})^\dagger K^{(i)}_{s_i,q_i} = \mathbb{1}$. The above definitions also work for $s_i = 0$, where $r_{q_i=0|q_1 \dots q_{i-1}, s_1 \dots s_{i-1}, s_i=0} = 1$, and $(K^{(i)}_{s_i,q_i})^\dagger K^{(i)}_{s_i,q_i} = \mathbb{1}$. The conditional probabilities r in eq. (3.12) can be obtained from the probabilities p using the assumption of AoT:

$$r_{q_i|q_1 \dots q_{i-1}, s_1 \dots s_i} = \frac{p_{q_1 \dots q_i|s_1 \dots s_i}}{p_{q_1 \dots q_{i-1}|s_1 \dots s_{i-1}}}. \tag{3.13}$$

This construction gives a recipe to obtain any point in the AoT probability space in a quantum experiment. We have therefore shown that $\mathsf{AoT} = \mathsf{QM}_\mathsf{T}$ for any choice of n, m, Δ.

Note that the probability distributions constructed above can also be achieved by a purely classical stochastic model, albeit with invasive measurements. Such an experiment would therefore not convince a macrorealist to give up their world view. For that to happen, an experiment needs to properly address the clumsiness loophole [72, 101, 178].

Since AoT is a polytope, QM_T with POVMs is also a polytope, and no non-trivial Tsirelson-like bounds exist. If, on the other hand, we only allowed projective measurements, we would have $\mathsf{QM}_\mathsf{T} \subset \mathsf{AoT}$ with non-trivial Tsirelson-like bounds, as shown in ref. [177]. In this case, QM_T would not be a polytope. It is easy to see that QM with projectors is unable to reproduce some probability distributions: $n = 2, m = 1, \Delta = 2$, $p_{11|11} = 1, p_{01|01} = 0$ fulfills AoT but cannot be constructed in projective quantum mechanics, since the initial state must be an eigenstate of the first measurement. Here we consider the general case of POVMs.

In summary, we have

$$\begin{array}{ccccccc} \mathsf{P} & \supset & \mathsf{NS} & \supset & \mathsf{QM_S} & \supset & \mathsf{LR} \\ \| & & \cap & & \cap & & \cap\,, \\ \mathsf{P} & \supset & \mathsf{AoT} & = & \mathsf{QM_T} & \supset & \mathsf{MR} \end{array} \tag{3.14}$$

with $\mathsf{NS} = \mathsf{MR}$, and dimensions

$$\begin{array}{ccccccc} \dim \mathsf{P} & > & \dim \mathsf{NS} & = & \dim \mathsf{QM_S} & = & \dim \mathsf{LR} \\ \| & & \wedge & & \wedge & & \| \quad . \\ \dim \mathsf{P} & > & \dim \mathsf{AoT} & = & \dim \mathsf{QM_T} & > & \dim \mathsf{MR} \end{array} \tag{3.15}$$

The structure of AoT, $\mathsf{QM_T}$ and MR within P is sketched on the right of fig. 3.1, the dimensions of all mentioned subspaces are printed in table 3.1.

3.5 Comparing local realism and macrorealism

Finally, let us compare the characteristics of quantum mechanics in LR and MR tests. Trivially, QM fulfills NS between spatially separated measurements, and AoT between temporally separated measurements. While $\mathsf{QM_S}$ and LR have the same dimension and are separated by Bell inequalities, $\mathsf{QM_T}$ and MR span subspaces with different dimensions. Inequalities can never reduce the dimension of the probability space, since they act as a hyperplane separating the fulfilling from the violating volume of probability distributions. We conclude that no combination of (Leggett-Garg) inequalities can be sufficient for macrorealism.

The observation that inequalities cannot be sufficient for macrorealism, and the differences in the structure of the probability space shown above, present fundamental discrepancies between LR and MR. Fine's observation [171] that Bell inequalities are necessary and sufficient for LR can therefore not be transferred to the case of LGIs and MR. More precisely, Fine's proof uses the implicit assumption of NS, which is obeyed by all reasonable physical theories, including QM. However, the temporal analogue to NS is the conjunction of AoT and NSIT, where AoT is obeyed by all reasonable physical theories, while NSIT is violated in QM. Therefore,

$$\text{BIs} \overset{\Leftarrow}{\not\Rightarrow} \text{LR} \;\Leftrightarrow \text{NS} \wedge \text{BIs} \tag{3.16}$$

$$\text{LGIs} \overset{\Leftarrow}{\not\Rightarrow} \text{MR} \Leftrightarrow \text{AoT} \wedge \text{NSIT} \overset{\not\Leftarrow}{\Rightarrow} \text{AoT} \wedge \text{LGIs}, \tag{3.17}$$

where “BIs” and “LGIs” denote the sets of all Bell and Leggett-Garg inequalities, respectively. In appendix 3.A we explicitly construct a counter-example for AoT $\wedge$ CH-LGIs $\Rightarrow$ MR.

Moreover, since MR is a polytope with smaller dimension than QM_T, LGIs can only touch MR (i.e. be *tight*) at one facet, i.e. a positivity constraint, as sketched in fig. 3.1 on the right. A comparable Bell inequality, sketched in fig. 3.1 on the left as BI', clearly illustrates the limitations resulting from this requirement. In fact, for each facet, there is an infinite number of such LGIs, compared to a single NSIT condition. In an experimental test of MR, using a LGI therefore needlessly restricts the parameter space where violations can be found. Note also the mathematical simplicity of NSIT conditions when compared to the LGI, which can facilitate further theoretical studies. In summary, engineering future experiments for violations of NSIT conditions instead of LGIs appears to be better motivated by the underlying theory.

Appendix

3.A A counter-example for LGIs as sufficient conditions

In the following, we will demonstrate that CH-type Leggett-Garg inequalities [172] are not sufficient for macrorealism, and therefore Fine's theorem does not apply to macrorealism. Consider the experimental setup from fig. 3.3: A combination of Mach-Zehnder interferometers with 50/50 beamsplitters is set up as sketched. At times t_0, t_1, t_2, and t_3, which-path measurements may be performed; the outcomes are denoted as $|+\rangle$ and $|-\rangle$. The initial state at t_0 is $|+\rangle$.

We obtain the following probabilities:

$$\begin{array}{lll} p_{01}(+,+) = \frac{1}{2} & p_{02}(+,+) = 0 & p_{03}(+,+) = \frac{1}{2} \\ p_{12}(+,+) = \frac{1}{4} & p_{13}(+,+) = 0 & p_{0}(+) = 1 \\ p_{1}(+) = \frac{1}{2} & p_{2}(+) = 0 & p_{3}(+) = \frac{1}{2} \\ p_{12}(-,+) = \frac{1}{4} & p_{012}(+,+,+) = \frac{1}{4} & p_{012}(+,-,+) = \frac{1}{4}. \end{array} \tag{3.18}$$

We now evaluate a standard LGI, the CH-type LGIs and various NSIT conditions. The standard LGI is easily fulfilled:

$$\text{LGI}: C_{01} + C_{12} + C_{23} - C_{03} = 0 \leq 2. \tag{3.19}$$

The CH-type LGIs, taken from ref. [171] with the replacement rules[2] from ref. [73], are also fulfilled,

$$\begin{aligned}
-1 \leq p_{01}(+,+) + p_{03}(+,+) + p_{23}(+,+) - p_{12}(+,+) - p_0(+) - p_3(+) = -\frac{3}{4} \leq 0,\\
-1 \leq p_{12}(+,+) + p_{23}(+,+) + p_{03}(+,+) - p_{01}(+,+) - p_2(+) - p_3(+) = -\frac{1}{4} \leq 0,\\
-1 \leq p_{03}(+,+) + p_{01}(+,+) + p_{12}(+,+) - p_{23}(+,+) - p_0(+) - p_1(+) = -\frac{1}{4} \leq 0,\\
-1 \leq p_{23}(+,+) + p_{12}(+,+) + p_{01}(+,+) - p_{03}(+,+) - p_2(+) - p_1(+) = -\frac{1}{4} \leq 0.
\end{aligned} \tag{3.20}$$

On the other hand, various NSIT conditions are easily violated:

$$\begin{aligned}
&\text{NSIT}_{(1)2}: p_2(+) = 0 \neq p_{12}(+,+) + p_{12}(-,+) = \frac{1}{2},\\
&\text{NSIT}_{0(1)2}: p_{02}(+,+) = 0 \neq p_{012}(+,+,+) + p_{012}(+,-,+) = \frac{1}{2}.
\end{aligned} \tag{3.21}$$

We conclude that the CH-type LGIs are only necessary but not sufficient for macrorealism:

$$\text{AoT} \wedge \text{CH-LGIs} \nLeftrightarrow \text{AoT} \wedge \text{NSIT} \Leftrightarrow \text{MR}. \tag{3.22}$$

Obviously, the setup satisfies AoT.

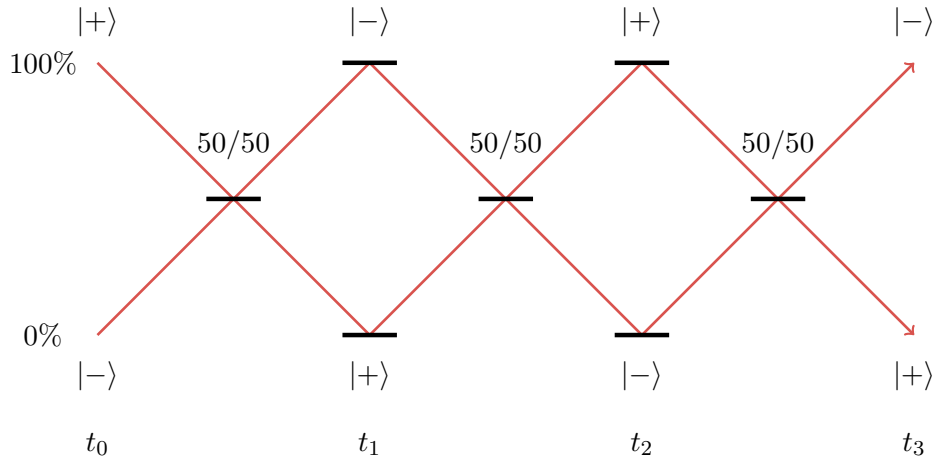

Figure 3.3: A setup of Mach-Zehnder interferometers, with which-path measurements at four times. The beamsplitters are perfect 50/50 half-mirrors, and the initial state is $|+\rangle$.

[2]We replace $A \leftrightarrow t_0, A' \leftrightarrow t_2, B \leftrightarrow t_1, B' \leftrightarrow t_3$, where $A, A', (B, B')$ are the settings for Alice (Bob) in ref. [171].

4 Quantum magnetomechanics

> *Yeah [beep], magnets!*
>
> — **Jesse Pinkman**
> *Breaking Bad*, Season 5, Episode 1

Abstract

Tests of quantum mechanical predictions for the behavior of macroscopic quantities are of high interest for various extensions of quantum mechanics and quantum gravity, as outlined in chapter 0 and section 1.1. In recent years, various setups with nano- and micro-mechanical resonators in the quantum regime have therefore been theorized and experimentally investigated. Such experiments are however typically hindered by strong coupling to the environment, often simply from mechanical connections. Recent proposals attempt to mitigate these issues by mechanically disconnecting a test mass through optical levitation. They thereby trade decoherence from a mechanical connection for decoherence from the increased heating and scattering of laser light.

In this chapter, we propose a novel kind of setup, where quasi-magnetostatic fields take the role of conventional optical tools. Our setup consists of a levitating superconducting sphere in the Meißner state. The variation of its expelled field with the center-of-mass motion leads to a resonant coupling to a superconducting quantum circuit. We show that this interaction can be tuned to the sideband cooling regime, where ground state cooling is experimentally feasible. We also calculate the most common sources of decoherence for the mechanical resonator, and show that they are extremely low when compared to the cooling rate. Our proposal therefore enables quantum experiments with micrometer-sized, massive objects.

After motivating a novel experimental design (**section 4.1**), we start with a detailed discussion of our proposed experiment (**section 4.2**). We then calculate the cooling rate and final occupation number for sideband cooling (**section 4.3**), and analyze the

most common sources of decoherence of the superconducting sphere (**section 4.4**). Finally, we discuss a protocol to build spatial superposition states (**section 4.5**), and give exemplary experimental parameters (**section 4.6**).

This chapter is based on and uses parts of ref. [4]:

- O. Romero-Isart, L. Clemente, C. Navau, A. Sanchez, and J. I. Cirac, 'Quantum Magnetomechanics with Levitating Superconducting Microspheres', Phys. Rev. Lett. **109**, 147205 (2012)

An initial discussion of mechanical levitation for quantum experiments can be found in ref. [179]. In parallel to our work, a similar proposal was reported by Cirio, Brennen and Twamley [180]. Additionally, a *News and Views* article [181] was published in *Nature Physics* on both works.

4.1 Introduction and motivation

The experimental realization of macroscopic quantum behavior presents a multitude of interesting applications, ranging from answers to fundamental questions of quantum theory [11, 12], over improved detection efficiencies of gravitational waves [182] to experimental tests of quantum gravity [36]. Over the past decade, various experimental setups with nano- and micromechanical resonators of ever increasing size have been theorized, and many experiments have been performed. An important milestone on the way to quantum behavior is the cooling of a macroscopic degree of freedom to the quantum ground state, a spectacular feat that has been demonstrated in multiple different setups [136, 183–185], some of them using sideband cooling techniques [186–188]. For an extensive overview of the field of mechanical resonators in the quantum regime see refs. [189–194].

The experiments discussed above share a common construction: A macroscopic mechanical degree of freedom (e.g. the center-of-mass motion) is coupled to a well-understood quantum device. This coupling is then exploited for both active and passive cooling techniques, and finally to manipulate and measure the quantum state of the macroscopic object.

However, when constructing quantum experiments, the experimenter is often faced with a difficult tradeoff: The system has to be well-enough isolated from the surrounding environment to allow the observation of quantum behavior, but it must still be precisely controllable and measurable when required by experimental protocols. With mechanical resonators in particular, the former presents a major challenge on the way to ground state cooling: The mechanical connection of the resonator to the environment is a strong source of heating and decoherence, the so-called *clamping losses*. For this reason, it was recently proposed to use setups where the mechanical resonator is optically levitated, and therefore completely mechanically disconnected from the environment [195–199]. This *optomechanical* setup is sketched in fig. 4.1. Additionally, novel protocols for building quantum superpositions are theoretically feasible in the parameter ranges admitted by these setups [36, 200]. Notably, the possibility of performing such experiments in space, in order to improve isolation, has been discussed in refs. [201, 202].

While experiments using light to trap and cool mechanical resonators eliminate mechanical coupling to the environment, they share two common problems: Photons are scattered by the object, producing position-localization decoherence [195, 196, 199, 200], and photons are absorbed, heating the object and increasing decoherence

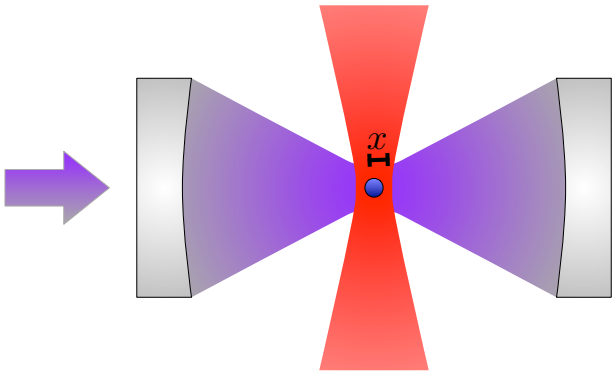

Figure 4.1: The optomechanical setup discussed in refs. [195–199]. A dielectric micro-sphere is levitated and trapped by optical tweezers (red), and positioned inside of an optical cavity (purple). When a suitable driving field is applied (here from the left), the motion of the object's center-of-mass position x can in theory be cooled to the quantum ground state.

due to the emission of black body radiation [36, 195, 196, 199, 200]. These issues make an experimental realization more challenging, and limit the maximum size of the object to tens or hundreds of nanometers.

In this chapter, we propose a novel kind of system that eliminates these problems by relying solely on magnetic fields for both trapping and the coupling to a quantum device. Since cooling of the mechanical motion to low energies is an important first step in realizing many interesting macroscopic quantum states, we will focus our discussion on ground-state cooling.

Our proposed setup consists of a type-I superconducting micro-sphere (e.g. made of lead), levitated and trapped by a strong external magnetic field. Due to the Meißner effect [203], the superconductor expels the magnetic field from inside the material, as sketched in fig. 4.2. To pick up this expelled field, a pickup coil is placed close to the sphere. It is connected to a superconducting quantum circuit, e.g. an LC resonator or a flux qubit[1]. Then, the center-of-mass position of the sphere couples to the quantum circuit through the pickup coil.

In the following, we show that with sideband cooling techniques [186–188], the motion of the sphere can be cooled the quantum ground state. We start by looking at the details of the setup, and calculate the magnetomechanical coupling.

[1] See refs. [204–208] for reviews on the topic of superconducting quantum circuits.

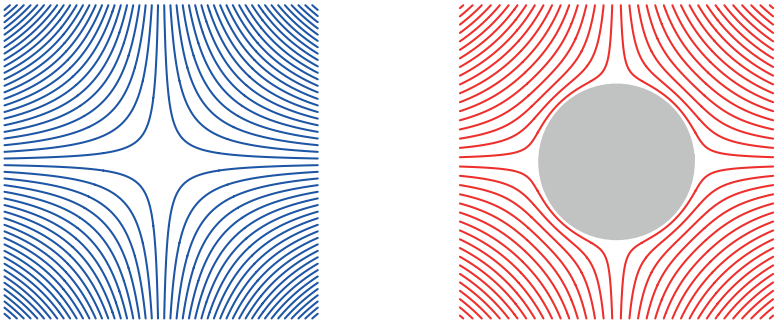

Figure 4.2: Left: Sketch of the magnetic field lines at the center of the trap. The magnetic field minimum used for levitation and trapping is clearly visible.
Right: Same setup with the superconducting sphere present. The Meißner effect [203] is apparent, as the superconductor expels the magnetic field.

4.2 The magnetomechanical setup

We consider the setup depicted in fig. 4.3: A superconducting sphere of radius R and mass M is cooled to a temperature T below its critical temperature T_C. We choose the material and the radius such that both the penetration length λ of the field inside the superconductor and the coherence length ξ of Cooper pairs inside the superconductor are much smaller than the radius of the sphere, $\lambda, \xi \ll R$. (Exemplary experimental parameters are printed in table 4.1 in section 4.6.) We can then assume that the magnetic field penetration into the sphere is negligible, and the sphere has zero total magnetic field inside, $\boldsymbol{B} = 0$. The sphere is trapped at the center of the harmonic potential generated by a magnetic trap [209], more concretely a pair of circular coils of radius l in an anti-Helmholtz configuration, i.e. positioned coaxially with distance l from each and with opposing currents $\pm I$ inside the coils. As shown in appendix 4.A, the resulting trapping potential is harmonic in all three dimensions, and of the form

$$\hat{V}_{\text{trap}} = \frac{M}{2}[\omega_t^2 \hat{x}^2 + \omega_\perp^2(\hat{y}^2 + \hat{z}^2)], \tag{4.1}$$

where the x-axis is placed along the axis of the coils. Following the derivation in appendix 4.A, we arrive at trapping frequencies

$$\omega_t \approx 1.49\sqrt{\frac{\mu_0}{\rho}\frac{I}{l^2}}, \tag{4.2}$$

and

$$\omega_\perp \approx 0.74\sqrt{\frac{\mu_0}{l^4\rho}}, \tag{4.3}$$

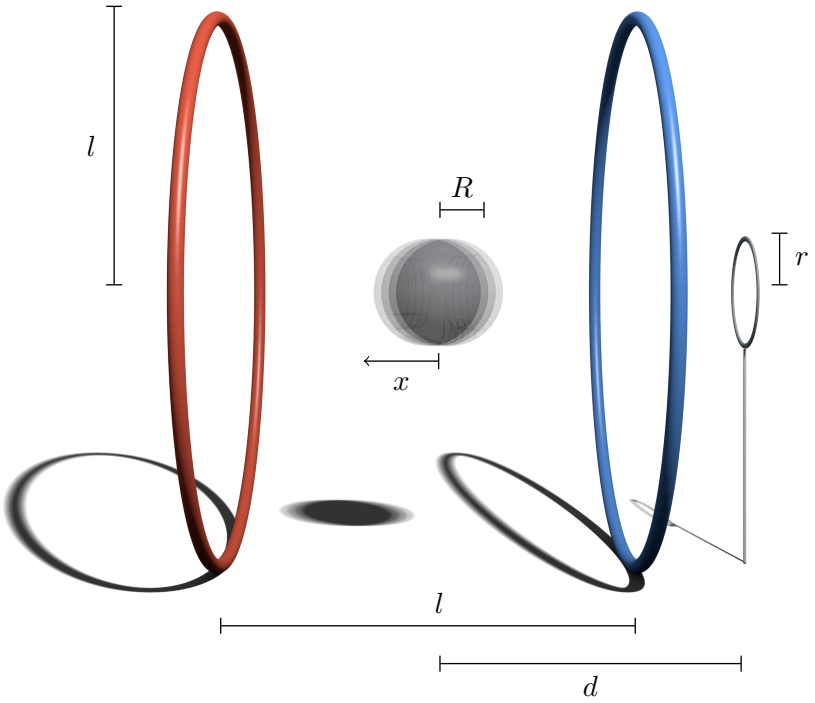

Figure 4.3: The magnetomechanical setup described in this chapter. A pair of coils in the anti-Helmholtz configuration (opposing directions of current, with equal radius and positioned coaxially in distance l) creates a static magnetic field to trap the superconducting sphere (radius R). A pickup coil of radius r, connected to a superconducting qubit, is placed coaxially to the coils at distance d. It serves to couple the center-of-mass position $\hat{x}$ of the sphere to the qubit.

where μ_0 is the vacuum permeability, and ρ is the density of the sphere.

For the material of the sphere to stay superconducting during the experiment, it is important that the magnetic field at the surface of the sphere never exceeds the material's critical field B_C. This restriction results in an upper bound on the radius of the sphere,

$$R \ll R_{\text{max}} \approx 1.15 \frac{B_C}{\omega_t \sqrt{\mu_0 \rho}}. \tag{4.4}$$

See appendix 4.B for derivation of this value.

At distance d from the center of the trap, a pickup coil of radius r is placed coaxially with the anti-Helmholtz coils. We require $d > l/2$, such that the pickup coil is placed outside of the anti-Helmholtz setup. The pickup coil is then connected either to an LC resonator, or to a superconducting flux qubit, so that it transmits the sphere's expelled magnetic field to the quantum circuit. As we will see below, the

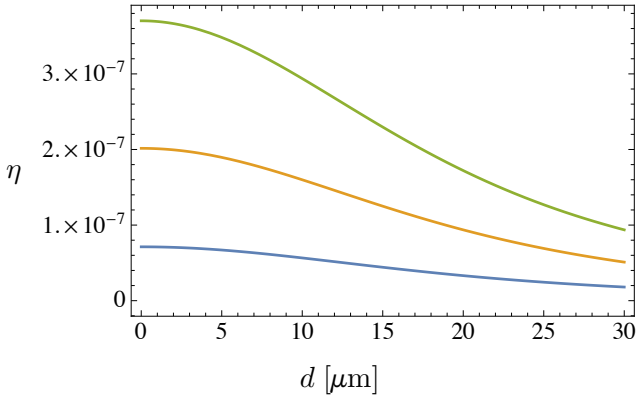

Figure 4.4: The dimensionless magnetomechanical coupling parameter η due to the magnetic flux expelled by the superconducting sphere at the pickup coil, plotted as a function of the distance d of the pickup coil, for the experimental parameters printed in table 4.1 in section 4.6. The blue line corresponds to sphere radius $R = 1\,\mu\mathrm{m}$, the orange line to $R = 2\,\mu\mathrm{m}$, and the green line to $R = 3\,\mu\mathrm{m}$.

magnetomechanical sphere-circuit coupling depends on a dimensionless parameter

$$\eta \equiv x_{\mathrm{zp}} \frac{\Phi'_{\mathrm{ext}}}{\Phi_0}, \tag{4.5}$$

where $x_{\mathrm{zp}} = \sqrt{\hbar/(2M\omega_t)}$ is the mechanical zero point motion (also referred to as *ground state size*), $\Phi_0 = \pi\hbar/e$ is the magnetic flux quantum, and $\Phi'_{\mathrm{ext}} = \frac{\mathrm{d}\Phi_{\mathrm{ext}}(d+x)}{\mathrm{d}x}|_{x=0}$ is the derivative of the magnetic field expelled by the sphere with respect to the sphere's position, evaluated at the location of the pickup coil, assuming the sphere is at the center of the trap. In appendix 4.C we show that, assuming $l, r \gg R$,

$$\Phi'_{\mathrm{ext}} \approx 2.70\mu_0 \frac{I}{l^2} \frac{R^3 r^2}{(d^2+r^2)^{3/2}}. \tag{4.6}$$

The dimensionless parameter η as a function of the distance d is sketched in fig. 4.4 for different radii of the sphere.

4.3 Calculation of the cooling rate

4.3.1 The initial master equation

Let us now write the system Hamiltonian, starting with an LC resonator with inductance L and capacity C. Its Hamiltonian is

$$\hat{H}_{\mathrm{LC}} = \frac{[\hat{\Phi} - \Phi_{\mathrm{ext}}(\hat{x})]^2}{2L} + \frac{\hat{Q}^2}{2C}, \tag{4.7}$$

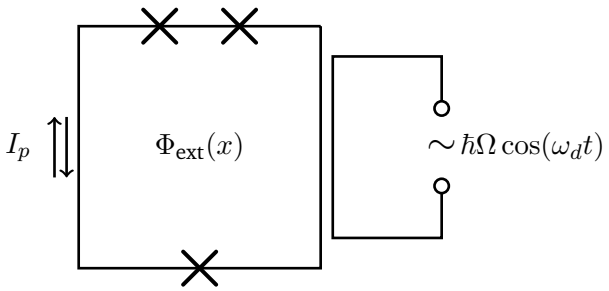

Figure 4.5: A flux qubit [204] with three Josephson junctions (denoted by crosses). The two qubit states $|\uparrow\rangle$ and $|\downarrow\rangle$ correspond to a current I_p flowing clockwise or counterclockwise, respectively. The external magnetic flux $\Phi_{\text{ex}}(x)$ threads the pickup coil, and therefore effectively the flux qubit connected to it. An external driving field with frequency ω_d and amplitude Ω is applied.

with $[\hat{\Phi}, \hat{Q}] = \mathrm{i}\hbar$, where $\hat{\Phi}$ is the magnetic flux in the inductance, and $\hat{Q}$ the charge in the capacitor. Since the expectation value of the sphere's position operator, $\hat{x}$, is usually small, we expand $\Phi_{\text{ext}}(\hat{x})$ linearly. We furthermore replace $\hat{x} = x_{\text{zp}}(\hat{b}^\dagger + \hat{b})$ and $\hat{\Phi} = \Phi_{\text{zp}}(\hat{a}^\dagger + \hat{a})$ with the zero-point flux $\Phi_{\text{zp}} = \sqrt{\hbar/(2C\omega_{LC})}$ and the resonator frequency $\omega_{LC} = 1/\sqrt{LC}$. Additionally, we define $g_{LC} = \epsilon_{LC}\eta$. We thus obtain the Hamiltonian

$$\hat{H}_{\text{LC}}/\hbar = \omega_{LC}\hat{a}^\dagger\hat{a} + g_{LC}(\hat{a}^\dagger + \hat{a})(\hat{b}^\dagger + \hat{b}). \tag{4.8}$$

Next, let us turn to the option of a superconducting flux qubit [205–208]. We consider a qubit with three Josephson junctions [204], as shown in fig. 4.5. We assume that the external flux is tuned so that the qubit is near its degeneracy point, i.e. $f(\Phi_{\text{ext}}) = \Phi_{\text{ext}}/\Phi_0 - 1/2 \approx 0$. In this case, the qubit Hamiltonian reads

$$\hat{H}_s/\hbar = -\frac{\tilde{\epsilon}}{2}\hat{\sigma}_z - \frac{\Delta}{2}\hat{\sigma}_x, \tag{4.9}$$

where we have introduced the bias of the qubit $\tilde{\epsilon} = \nu f(\Phi_{\text{ext}})$ with $\nu = 2\Phi_0 I_p/\hbar$, the tunneling amplitude Δ, and the persistent current in the qubit I_p. As before, $\hat{\sigma}_x$, $\hat{\sigma}_y$ and $\hat{\sigma}_z$ are the Pauli matrices. Again, we expand $\tilde{\epsilon}(\hat{x})$ linearly to obtain $\tilde{\epsilon}(\hat{x}) \approx \tilde{\epsilon}(0) + \tilde{\epsilon}'(0)\hat{x}$. Including the Hamiltonian for the mechanical resonator, we arrive at the total magnetomechanical Hamiltonian

$$\hat{H}_{\text{MM}}/\hbar = \omega_t\hat{b}^\dagger\hat{b} - \frac{\epsilon}{2}\hat{\sigma}_z - \frac{\Delta}{2}\hat{\sigma}_x - g_0\hat{\sigma}_z(\hat{b}^\dagger + \hat{b}). \tag{4.10}$$

We have introduced $\epsilon = \tilde{\epsilon}(0)$ and the magnetomechanical coupling $g_0 = \nu\eta$.

With experimentally feasible numbers (c.f. table 4.1 in section 4.6), the coupling to the qubit g_0 is significantly smaller than the coupling to the LC resonator g_{LC}. While the linear LC resonator is therefore better-suited for ground state cooling or other Gaussian dynamics, the qubit presents a much more interesting and diverse addition to the experimenter's toolbox due to its non-linearity. We will therefore continue our calculations for the qubit. More detailed calculations for the LC resonator can be found in ref. [4].

In order to resonantly couple the qubit (with a frequency of a few GHz) to the mechanical resonator (with a frequency in the kHz or low MHz regime), we need to apply a suitable driving field to the flux qubit. Its Hamiltonian reads

$$\hat{H}_{\text{drive}}/\hbar = \Omega\cos(\omega_d t)\hat{\sigma}_z, \tag{4.11}$$

where Ω is the amplitude and ω_d the frequency of the driving field, a setup that has been studied in refs. [210–214]. The total Hamiltonian of the system can now be written as

$$\begin{aligned}\hat{H}/\hbar &= \hat{H}_{\text{MM}}/\hbar + \hat{H}_{\text{drive}}/\hbar \\ &= \omega_t\hat{b}^\dagger\hat{b} - \frac{\epsilon}{2}\hat{\sigma}_z - \frac{\Delta}{2}\hat{\sigma}_x + \Omega\cos(\omega_d t)\hat{\sigma}_z - g_0\hat{\sigma}_z(\hat{b}^\dagger + \hat{b}).\end{aligned} \tag{4.12}$$

Let us first write this Hamiltonian in the eigenbasis of the qubit. Diagonalization yields[2]

$$\hat{H}/\hbar = \omega_t\hat{b}^\dagger\hat{b} - \frac{\omega_s}{2}\hat{\sigma}_z + \Omega\cos(\omega_d t)(\hat{\sigma}_z\cos\alpha + \hat{\sigma}_x\sin\alpha) - g_0(\hat{\sigma}_z\cos\alpha + \hat{\sigma}_x\sin\alpha)(\hat{b}^\dagger + \hat{b}). \tag{4.13}$$

Here, we have defined $\omega_s = \sqrt{\epsilon^2 + \Delta^2}$ and $\tan\alpha = \Delta/\epsilon$.

To obtain the cooling rate, we also need to consider sources of decoherence for both the superconducting sphere and the qubit. The former, decoherence of the sphere, will later (section 4.4) be shown to be negligible, and is therefore not included in the following discussion. On the other hand, decoherence of the qubit consists of spontaneous decay to the lower energy state with rate Γ_0, and pure dephasing with rate Γ_φ [205–208]. We model these processes with Lindblad terms in the master equation

$$\dot{\hat{\rho}} = -\frac{\mathrm{i}}{\hbar}[\hat{H}, \hat{\rho}] + \mathcal{L}_0[\hat{\rho}] + \mathcal{L}_\varphi[\hat{\rho}], \tag{4.14}$$

[2] Here and in the following, for simplicity, we omit stylistic changes to the symbol of the Hamiltonian, and keep using $\hat{H}$, even as the Hamiltonian undergoes various transformations.

where

$$\mathcal{L}_0[\hat{\rho}] = \frac{\Gamma_0}{2}(2\hat{\sigma}_-\hat{\rho}\hat{\sigma}_+ - \hat{\rho}\hat{\sigma}_+\hat{\sigma}_- - \hat{\sigma}_+\hat{\sigma}_-\hat{\rho}) \tag{4.15}$$

describes the spontaneous decay, and

$$\mathcal{L}_\varphi[\hat{\rho}] = \frac{\Gamma_\varphi}{2}(\hat{\sigma}_z\hat{\rho}\hat{\sigma}_z - \hat{\rho}) \tag{4.16}$$

describes the pure dephasing. We have introduced the creation and annihilation operators for the qubit, $\hat{\sigma}_+ = (\hat{\sigma}_x + \mathrm{i}\hat{\sigma}_y)/2$ and $\hat{\sigma}_- = (\hat{\sigma}_x - \mathrm{i}\hat{\sigma}_y)/2$.

4.3.2 The master equation in the interaction picture

Let us now move to a frame rotating with the drive frequency ω_d. We apply the transformation $\hat{\rho} \to \hat{U}_R\hat{\rho}\hat{U}_R^\dagger$ where

$$\hat{U}_R = \exp(\mathrm{i}\hat{\sigma}_z\omega_d t/2) = \cos(\omega_d t/2)\mathbb{1} + \mathrm{i}\sin(\omega_d t/2)\hat{\sigma}_z. \tag{4.17}$$

This results in a transformation to the Hamiltonian $\hat{H} \to \hat{U}_R\hat{H}\hat{U}_R^\dagger - \mathrm{i}\dot{\hat{U}}_R\hat{U}_R^\dagger$, which yields

$$\begin{aligned}\hat{H}/\hbar = \omega_t\hat{b}^\dagger\hat{b} + \frac{\delta\omega}{2}\sigma_z \\ + \frac{\Omega}{2}\left[\cos\alpha\left(e^{-\mathrm{i}\omega_d t} + e^{\mathrm{i}\omega_d t}\right)\hat{\sigma}_z + \sin\alpha[\hat{\sigma}_x + \cos(2\omega_d t)\hat{\sigma}_x - \sin(2\omega_d t)\hat{\sigma}_y]\right] \\ - g_0\left[\cos\alpha\hat{\sigma}_z + \sin\alpha[\cos(\omega_d t)\hat{\sigma}_x - \sin(\omega_d t)\hat{\sigma}_y]\right](\hat{b}^\dagger + \hat{b}),\end{aligned} \tag{4.18}$$

where $\delta\omega = \omega_d - \omega_s$. Note that the Lindblad terms are unaffected by this transformation.

Now we perform a rotating-wave approximation, i.e. we drop all rapidly oscillating terms, since their contribution averages out to zero. This is valid provided the rotation frequency is much larger than the other significant frequencies: $\omega_d \gg \omega_t, \delta\omega, g_0$. We then arrive at the Hamiltonian

$$\hat{H}/\hbar = \omega_t\hat{b}^\dagger\hat{b} + \frac{\delta\omega}{2}\sigma_z + \frac{\tilde{\Omega}}{2}\hat{\sigma}_x - g\hat{\sigma}_z(\hat{b}^\dagger + \hat{b}), \tag{4.19}$$

where we introduced $\tilde{\Omega} = \Omega\sin\alpha$ and $g = g_0\cos\alpha$.

Next, we again diagonalize the qubit. We obtain the Hamiltonian

$$\hat{H}/\hbar = \omega_t\hat{b}^\dagger\hat{b} + \frac{\tilde{\omega}_s}{2}\hat{\sigma}_z - g(\cos\beta\hat{\sigma}_z + \sin\beta\hat{\sigma}_x)(\hat{b}^\dagger + \hat{b}), \tag{4.20}$$

where $\tilde{\omega}_s = \sqrt{\delta\omega^2 + \tilde{\Omega}^2}$, and $\tan\beta = \tilde{\Omega}/\delta\omega$. Using the unitary $\hat{U} = \exp[\mathrm{i}(\omega_t \hat{b}^\dagger \hat{b} + \tilde{\omega}_s \hat{\sigma}_z/2)t]$, we can now bring the Hamiltonian to the interaction picture. We thus arrive at

$$\hat{H}_I/\hbar = -g\left(\cos\beta\hat{\sigma}_z + \sin\beta e^{\mathrm{i}\tilde{\omega}_s t}\hat{\sigma}_+ + \sin\beta e^{-\mathrm{i}\tilde{\omega}_s t}\hat{\sigma}_-\right)\left(e^{\mathrm{i}\omega_t t}\hat{b}^\dagger + e^{-\mathrm{i}\omega_t t}\hat{b}\right). \tag{4.21}$$

Setting $\tilde{\omega}_s = \omega_t$ and assuming $\omega_t \gg g_0$, we can perform another rotating-wave approximation, yielding the final Hamiltonian in the interaction picture,

$$\hat{H}_I/\hbar = -\tilde{g}(\hat{\sigma}_-\hat{b}^\dagger + \hat{\sigma}_+\hat{b}), \tag{4.22}$$

where we have introduced $\tilde{g} = g\sin\beta$.

We now need to apply the diagonalization and the transformation to the interaction picture to the dissipative terms. After diagonalization, and a subsequent rotating-wave approximation, similar to the one outlined above (valid provided that $\omega_t \gg \Gamma_0, \Gamma_\varphi$), we obtain

$$\begin{aligned}\mathcal{L}_0[\hat{\rho}] = &\frac{\Gamma_\varphi^*}{2}(\hat{\sigma}_z\hat{\rho}\hat{\sigma}_z - \hat{\rho}) \\ &+ \frac{\Gamma_\downarrow}{2}(2\hat{\sigma}_-\hat{\rho}\hat{\sigma}_+ - \hat{\rho}\hat{\sigma}_+\hat{\sigma}_- - \hat{\sigma}_+\hat{\sigma}_-\hat{\rho}) \\ &+ \frac{\Gamma_\uparrow}{2}(2\hat{\sigma}_+\hat{\rho}\hat{\sigma}_- - \hat{\rho}\hat{\sigma}_-\hat{\sigma}_+ - \hat{\sigma}_-\hat{\sigma}_+\hat{\rho}).\end{aligned} \tag{4.23}$$

Note that due to the diagonalization, a term describing spontaneous excitation in the qubit with rate $\Gamma_\uparrow$ has appeared. We have defined

$$\Gamma_\varphi^* = \Gamma_\varphi\cos^2\beta + \frac{\Gamma_0}{2}\sin^2\beta, \tag{4.24}$$

$$\Gamma_\downarrow = \frac{\Gamma_\varphi}{2}\sin^2\beta + \frac{\Gamma_0}{4}(1+\cos\beta)^2, \tag{4.25}$$

$$\Gamma_\uparrow = \frac{\Gamma_\varphi}{2}\sin^2\beta + \frac{\Gamma_0}{4}(1-\cos\beta)^2. \tag{4.26}$$

In summary, we have the master equation in the interaction picture,

$$\dot{\hat{\rho}} = \mathcal{L}_0[\hat{\rho}] + \mathcal{L}_I[\hat{\rho}], \tag{4.27}$$

where $\mathcal{L}_I[\hat{\rho}] = -\mathrm{i}[\hat{H}_I, \hat{\rho}]/\hbar$.

With Hamiltonian (4.22) and the spontaneous decay described by the master equation (4.27), the system is in the sideband cooling regime. An intuitive interpretation

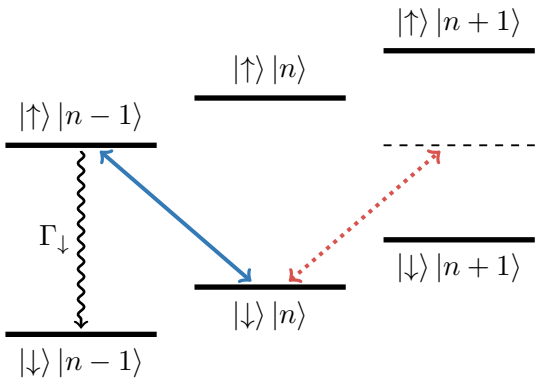

Figure 4.6: The sideband cooling scheme discussed in this chapter. The columns correspond to different energy levels in the mechanical resonator, the vertical levels are the two states of the qubit. The Hamiltonian (4.22) leads to a resonant coupling, depicted by the blue arrow. Note that the transition corresponding to the dotted red arrow is prohibited due to the choice of detuning $\delta\omega$. In combination with the decay of the qubit with rate $\Gamma_\downarrow$, this setup leads to a cooling of the mechanical motion.

of Hamiltonian (4.22) and the resulting cooling of the system is sketched and explained in fig. 4.6.

4.3.3 Adiabatic elimination

With the experimental parameters chosen below (table 4.1 in section 4.6), the coupling strength is much smaller than the decoherence rates, $\tilde{g} \ll \Gamma_\varphi^*, \Gamma_\downarrow, \Gamma_\uparrow$. Looking at the master equation (4.27), we realize that in this case we can treat the hermitian part, $\mathcal{L}_I[\hat{\rho}]$, as a perturbation. In the following, we perform an *adiabatic elimination* [215, 216] of the qubit, following the calculation in ref. [217].

Consider the subspace of eigenvectors of $\mathcal{L}_0$ with eigenvalue $\lambda = 0$. These states can be written as

$$\mathcal{L}_0\left(|n\rangle\langle n| \otimes \hat{\rho}_{\text{ss}}\right) = 0, \tag{4.28}$$

where $|n\rangle$ with $n = 0, 1, \ldots$ are the eigenstates of the mechanical resonator, and $\hat{\rho}_{\text{ss}}$ is the steady-state of the qubit. Let $\mathcal{P}$ be a projector onto that subspace; it can be written as

$$\mathcal{P}\hat{\rho} = \text{tr}_\text{s}(\hat{\rho}) \otimes \hat{\rho}_{\text{ss}}, \tag{4.29}$$

where tr_s is the trace over the qubit degrees of freedom. Applying perturbation theory, eq. (4.27) can be written as

$$\frac{\text{d}}{\text{d}t}\mathcal{P}\hat{\rho} = [\mathcal{P}\mathcal{L}_I\mathcal{P} - \mathcal{P}\mathcal{L}_I(\mathbb{1} - \mathcal{P})\mathcal{L}_0^{-1}(\mathbb{1} - \mathcal{P})\mathcal{L}_I\mathcal{P}]\hat{\rho}. \tag{4.30}$$

For the cooling process we are just interested in the evolution of the mechanical state,

$$\dot{\hat{\rho}}_m = \mathrm{tr_s}(\mathcal{P}\dot{\hat{\rho}}) = \mathrm{tr_s}\left([\mathcal{P}\mathcal{L}_I\mathcal{P} - \mathcal{P}\mathcal{L}_I(\mathbb{1}-\mathcal{P})\mathcal{L}_0^{-1}(\mathbb{1}-\mathcal{P})\mathcal{L}_I\mathcal{P}]\hat{\rho}\right). \tag{4.31}$$

The first term is zero:

$$\mathrm{tr_s}(\mathcal{P}\mathcal{L}_I\mathcal{P}\hat{\rho}) = \mathrm{i}\tilde{g}[\langle\hat{\sigma}_-\rangle_{\mathrm{ss}}\,\hat{b}^\dagger + \langle\hat{\sigma}_+\rangle_{\mathrm{ss}}\,\hat{b}, \hat{\rho}_m] = 0. \tag{4.32}$$

Using the fluctuation-dissipation theorem, the second term can be evaluated as (c.f. ref. [217])

$$\begin{aligned} &-\mathrm{tr_s}[\mathcal{P}\mathcal{L}_I(\mathbb{1}-\mathcal{P})\mathcal{L}_0^{-1}(\mathbb{1}-\mathcal{P})\mathcal{L}_I\mathcal{P}\hat{\rho}] = \\ &\frac{A_+}{2}\left(2\hat{b}^\dagger\hat{\rho}_m\hat{b} - \hat{b}\hat{b}^\dagger\hat{\rho}_m - \hat{\rho}_m\hat{b}^\dagger\hat{b}\right) + \frac{A_-}{2}\left(2\hat{b}\hat{\rho}_m\hat{b}^\dagger - \hat{b}^\dagger\hat{b}\hat{\rho}_m - \hat{\rho}_m\hat{b}\hat{b}^\dagger\right), \end{aligned} \tag{4.33}$$

where the excitation rate is

$$\begin{aligned} A_+ &= 2\tilde{g}^2\int_0^\infty \mathrm{d}\tau\ \langle\hat{\sigma}_+(\tau)\hat{\sigma}_-(0)\rangle_{\mathrm{ss}} = 2\tilde{g}^2\int_0^\infty \mathrm{d}\tau\, e^{M_1\tau}\,\langle\hat{\sigma}_+\hat{\sigma}_-\rangle_{\mathrm{ss}} \\ &= \frac{\tilde{g}^2}{\left(\Gamma_\varphi^* + \frac{\Gamma_\uparrow+\Gamma_\downarrow}{2}\right)}\left(1 - \frac{\Gamma_\downarrow - \Gamma_\uparrow}{\Gamma_\downarrow + \Gamma_\uparrow}\right), \end{aligned} \tag{4.34}$$

and the decay rate is

$$\begin{aligned} A_- &= 2\tilde{g}^2\int_0^\infty \mathrm{d}\tau\ \langle\hat{\sigma}_-(\tau)\hat{\sigma}_+(0)\rangle_{\mathrm{ss}} = 2\tilde{g}^2\int_0^\infty \mathrm{d}\tau\, e^{M_2\tau}\,\langle\hat{\sigma}_-\hat{\sigma}_+\rangle_{\mathrm{ss}} \\ &= \frac{\tilde{g}^2}{\left(\Gamma_\varphi^* + \frac{\Gamma_\uparrow+\Gamma_\downarrow}{2}\right)}\left(1 + \frac{\Gamma_\downarrow - \Gamma_\uparrow}{\Gamma_\downarrow + \Gamma_\uparrow}\right). \end{aligned} \tag{4.35}$$

Here, the parameters $M_1 = M_2 = -[\Gamma_\varphi^* + (\Gamma_\uparrow + \Gamma_\downarrow)/2]$ are the first two elements of the diagonal matrix in the Bloch equations

$$\begin{pmatrix} \langle\dot{\hat{\sigma}}_+\rangle \\ \langle\dot{\hat{\sigma}}_-\rangle \\ \langle\dot{\hat{\sigma}}_z\rangle \end{pmatrix} = \begin{pmatrix} M_1 & 0 & 0 \\ 0 & M_2 & 0 \\ 0 & 0 & -(\Gamma_\uparrow+\Gamma_\downarrow) \end{pmatrix}\begin{pmatrix} \langle\hat{\sigma}_+\rangle \\ \langle\hat{\sigma}_-\rangle \\ \langle\hat{\sigma}_z\rangle \end{pmatrix} + \begin{pmatrix} 0 \\ 0 \\ -(\Gamma_\downarrow - \Gamma_\uparrow) \end{pmatrix}. \tag{4.36}$$

We arrive at the master equation of the mechanical resonator,

$$\dot{\hat{\rho}}_m = \frac{A_+}{2}\left(2\hat{b}^\dagger\hat{\rho}_m\hat{b} - \hat{b}\hat{b}^\dagger\hat{\rho}_m - \hat{\rho}_m\hat{b}^\dagger\hat{b}\right) + \frac{A_-}{2}\left(2\hat{b}\hat{\rho}_m\hat{b}^\dagger - \hat{b}^\dagger\hat{b}\hat{\rho}_m - \hat{\rho}_m\hat{b}\hat{b}^\dagger\right). \tag{4.37}$$

From this, we obtain a simple differential equation for the occupation number operator $\hat{n} = \hat{b}^\dagger \hat{b}$:

$$\langle \dot{\hat{n}} \rangle = -\Gamma \langle \hat{n} \rangle + A_+, \tag{4.38}$$

with $\Gamma = A_- - A_+$. We finally obtain the cooling rate

$$\begin{aligned} \Gamma &= \frac{2\tilde{g}^2}{\left(\Gamma_\varphi^* + \frac{\Gamma_\uparrow + \Gamma_\downarrow}{2}\right)} \frac{\Gamma_\downarrow - \Gamma_\uparrow}{\Gamma_\downarrow + \Gamma_\uparrow} \\ &= -32 \frac{g_0^2 \Gamma_0 \cos^2\alpha \cos\beta \sin^2\beta}{[\cos(2\beta)(\Gamma_0 - 2\Gamma_\varphi) - 5\Gamma_0 - 6\Gamma_\varphi](\Gamma_0 + \Gamma_0 \cos^2\beta + 2\Gamma_\varphi \sin^2\beta)}, \end{aligned} \tag{4.39}$$

and the occupation number in the steady state,

$$\langle \hat{n} \rangle_{\text{ss}} = \frac{A_+}{\Gamma} = \frac{1}{2}\left(\frac{\Gamma_\downarrow + \Gamma_\uparrow}{\Gamma_\downarrow - \Gamma_\uparrow} - 1\right) = \frac{\Gamma_0(\sec\beta + \cos\beta - 2) + 2\Gamma_\varphi \sin\beta \tan\beta}{4\Gamma_0}. \tag{4.40}$$

The occupation numbers and cooling rates for different values of β are plotted in fig. 4.7.

4.4 Sources of decoherence

As mentioned in subsection 4.3.1, we have thus far assumed the absence of decoherence acting directly on the superconducting sphere. In this section, we will justify this assumption by explicitly calculating the rates for a variety of possible sources of decoherence. The resulting decoherence rates are printed in table 4.1 in section 4.6.

4.4.1 Imperfect vacuum

If the experiment is performed in an imperfect vacuum, air molecules hitting the sphere cause position localization decoherence. The rate can be estimated from geometric considerations and was calculated before in refs. [179, 195]. It is

$$\Gamma_{\text{air}} = \frac{16P}{\pi R \rho \bar{v}}, \tag{4.41}$$

where $\bar{v} = \sqrt{3kT/m}$ is the mean velocity of air molecules of average mass $m = 28.3\,\text{u}$ in the vacuum chamber, T is the temperature and P the pressure.

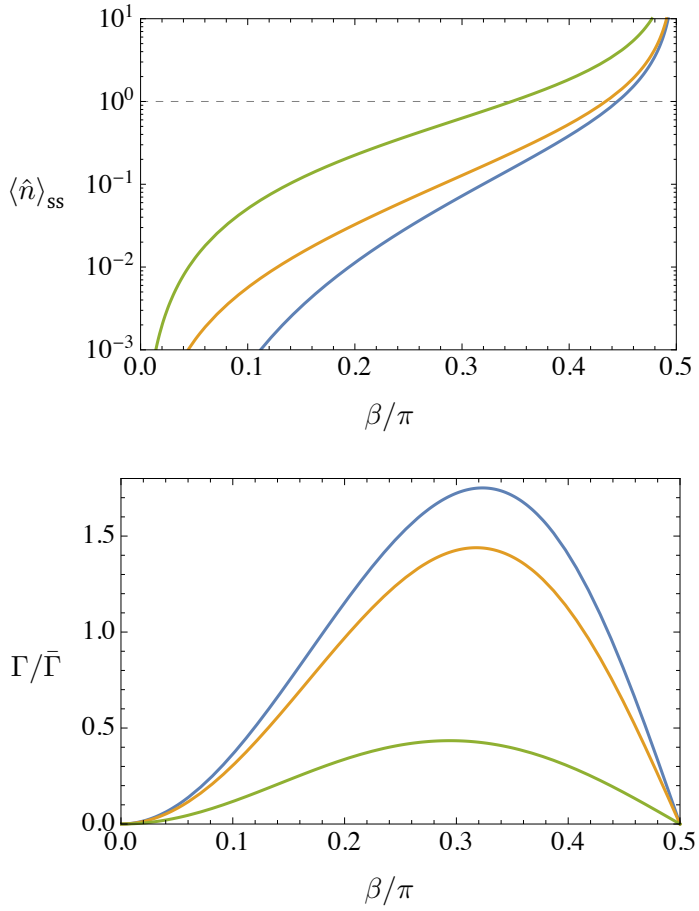

Figure 4.7: Top: The steady-state occupation number of the mechanical resonator, $\langle\hat{n}\rangle_{ss}$, as a function of β, plotted for three cases: $\Gamma_\varphi = 0$ in blue, $\Gamma_\varphi = \Gamma_0/10$ in orange, and $\Gamma_\varphi = \Gamma_0$ in green. Ground state cooling can be achieved if $\langle\hat{n}\rangle_{ss} < 1$.
Bottom: The cooling rate Γ in units of $\bar{\Gamma} = \tilde{g}^2/(\Gamma_0 \sin^2\beta)$ as a function of β. The values of Γ_φ/Γ_0 are the same in the top plot.

4.4.2 Fluctuations of the trap frequency and center

Next, we calculate the decoherence rate from fluctuations in the trap. As was shown in ref. [218], fluctuations $\xi_\omega(t)$ of the form

$$\hat{H}(t) = \frac{\hat{p}^2}{2M} + \frac{M\omega_t}{2}[1 + \xi_\omega(t)]\hat{x}^2 \tag{4.42}$$

result in two-level transitions with rate

$$R^\omega_{n\to n\pm2} = \frac{\pi\omega_t^2}{16} S_\omega(2\omega_t)(n+1\pm1)(n\pm1). \tag{4.43}$$

Here, $S_\omega(\omega)$ is the one-sided power spectrum of the fractional fluctuation in the resonance frequency,

$$S_\omega(\omega) = \frac{2}{\pi}\int_0^\infty \mathrm{d}\tau\, \cos(\omega\tau)\, \langle \xi_\omega(t)\xi_\omega(t+\tau)\rangle\,, \tag{4.44}$$

where

$$\langle \xi_\omega(t)\xi_\omega(t+\tau)\rangle = \frac{1}{T}\int_0^T \mathrm{d}t\, \xi(t)\xi(t+\tau). \tag{4.45}$$

We obtain the decoherence rate

$$\Gamma_\omega = R^\omega_{0\to 2} = \frac{\pi\omega_t^2}{8} S_\omega(2\omega_t). \tag{4.46}$$

Similarly, we can follow ref. [218] to calculate the decoherence rate for position fluctuations $\xi_x(t)$ modeled by

$$\hat{H}(t) = \frac{\hat{p}^2}{2M} + \frac{M\omega_t}{2}[\hat{x} - \xi_x(t)]^2. \tag{4.47}$$

We find

$$\Gamma_x = R_{0\to 1} = \frac{\pi\omega_t^2}{4}\frac{S_x(\omega_t)}{x_{\mathrm{zp}}^2}, \tag{4.48}$$

where

$$S_x(\omega) = \frac{2}{\pi}\int_0^\infty \mathrm{d}\tau\, \cos(\omega\tau)\, \langle \xi_x(t)\xi_x(t+\tau)\rangle\,. \tag{4.49}$$

4.4.3 Hysteresis in the trapping coils

The oscillating magnetic moment of the sphere induces currents in both the trap coils and the pickup coil. In a type-II superconductor (as required for the coils due to the high currents), this is a dissipative process due to flux vortex pinning. In this subsection, we will approximate the decoherence rates from this effect. As a simplification, we replace the coil by a thin cylinder. Furthermore, we consider a uniform magnetic field over the whole cylinder, with the magnitude of the expelled field on the x-axis in distance d from the sphere.

We start by presenting the phenomenology of rapidly changing magnetic fields applied to thin type-II superconducting disks [219]. Consider a thin disk in zero external field, where we slowly apply a weak magnetic field. Screening currents are induced at the surface of the material, counteracting the external magnetic field. If the applied field exceeds the lower critical field for the superconductor, flux vortices (see fig. 4.8 for explanation) appear at the edges of the disk. With increasing

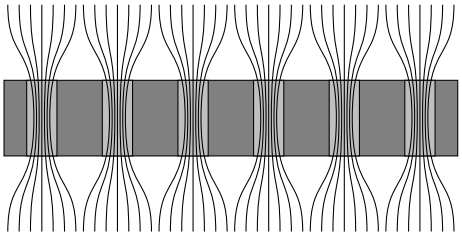

Figure 4.8: A type-II superconductor under an external magnetic field stronger than its lower critical field. The magnetic field lines penetrate the material only through *flux vortices*. Their movement through the superconductor is not frictionless, and therefore dissipates energy.

magnetic field, these vortices permeate towards the center of the disk. Depending on the strength of pinning of these vortices in the material, energy is dissipated as they move. We consider hard type-II superconductors, where the vortices are strongly pinned and can be described by the *critical-state model* [220].

The critical-state model asserts that vortices penetrate only so far into the material as to reduce the local current density $|\boldsymbol{J}|$ to the critical current density J_c. This results in an outer critical region with $|\boldsymbol{J}| = J_c$, and an inner flux-free region. With increasing external magnetic field, the critical region expands towards the center of the material. On the other hand, reversing the external field results in vortices of the opposite flux direction forming at the surface, and moving into the material. Therefore, the flux at the edges is first neutralized, later the flux pinned near the center. It is clear that this process of delayed magnetization is not reversible, and gives rise to hysteresis losses.

With an oscillating external field, the magnetization in x-direction, M_x, versus applied field in x-direction, H_x, runs in closed loops with area A given by

$$A = \oint \mathrm{d}M_x \, H_a = \frac{W_V}{\mu_0}, \tag{4.50}$$

where we have introduced the energy dissipation per cycle per unit volume, W_V. This energy dissipation has been calculated for many geometries, e.g. thin long strips [221]. Here we use the result for the rate of energy dissipation P_h from ref. [219], for thin disks of radius r, thickness t, critical current J_C and applied field H_x:

$$P_h = \frac{16\mu_0}{3\pi} \frac{\omega_t r^3}{J_c^2 t^2} H_x^4. \tag{4.51}$$

Note that the H_x^4 dependence is valid only for thin disks, $t \ll r$. For geometries where $t \sim r$ it changes to a H_0^3 scaling, c.f. refs. [222–225]. Equation (4.51) has

been confirmed to high precision by experiments, e.g. the ones performed in ref. [226].

We use eq. (4.67) from appendix 4.C for the applied magnetic field generated by the dipole, and eq. (4.60) from appendix 4.A for the magnetic moment. We thus have an external field

$$H_x = \frac{2m_x}{4\pi d^3}, \tag{4.52}$$

and arrive at the energy dissipation rate

$$P_x \approx 1.37 \frac{I^4 r^3 \bar{x}^4 \mu_0}{J_c^2 t^2 l^8} \left(\frac{R}{d}\right)^{12}, \tag{4.53}$$

where $\bar{x}$ is the amplitude of the oscillation of the sphere. Due to the dependence on $(R/d)^{12}$ we only consider the trap coils, and neglect the pickup coil, which is placed farther away. We therefore set $d = l/2$ and $r = l$. Using $P_h/\Gamma_h = \hbar\omega_t$ and choosing $\bar{x} = x_{\text{zp}}$, we obtain the rate of decoherence due to hysteresis,

$$\Gamma_h \approx 24.3 \frac{\hbar I^2 R^6}{J_c^2 l^1 3 t^2 \rho}. \tag{4.54}$$

4.4.4 Miscellaneous sources

Here, we do not explicitly consider a number of other decoherence sources, which we assume to be negligible:

- The internal vibrational modes of the sphere are sufficiently decoupled from its center-of-mass motion, as shown in ref. [198], and are assumed to not significantly contribute to decoherence.

- The superconductor reacts quickly to changes in the external field, since its energy splitting (of the order of tens of GHz) is much larger than the trapping frequencies (of the order of tens of kHz).

- Blackbody radiation of the sphere is negligible due to the cryogenic temperatures of $\sim 100\,\text{mK}$. In refs. [196, 200, 227], it was shown that the blackbody decoherence rate scales as T^6. Note that in optically levitated setups, blackbody radiation due to heating from the lasers presents a significant challenge for ground state cooling, which is by construction absent from our system.

We remark that the coupling to the flux qubit can easily be switched off by changing the drive frequency to be off-resonant. In this case, the sphere's center-of-mass motion is effectively completely decoupled from the environment.

4.5 Spatial superposition states

Let us now discuss a protocol for building spatial superpositions. Note that we can rewrite the Hamiltonian (4.10) in the form

$$\hat{H}_{\mathrm{MM}}/\hbar = \frac{\omega_s}{2}\hat{\sigma}_z + \hat{T}^\dagger(\chi\hat{\sigma}_z)\omega_t\hat{a}^\dagger\hat{a}\hat{T}(\chi\hat{\sigma}_z), \tag{4.55}$$

where $\hat{T}(\zeta) = \exp(-i\hat{p}\zeta x_{\mathrm{zp}}/\hbar)$ is the translation operator, and $\chi = 2g/\omega_t$ is a dimensionless parameter. From this form, we observe that the center of the magnetic trap depends on the qubit state. We can then prepare the qubit in an initial state

$$|\psi_0\rangle = \frac{1}{\sqrt{2}}(|\uparrow\rangle_s + |\downarrow\rangle_s), \tag{4.56}$$

and the mechanical oscillator in state $|0\rangle_m$, such that, after time π/ω_t has elapsed, the system is in the joint state

$$|\psi\rangle = \frac{1}{\sqrt{2}}(|\uparrow\rangle_s |x_-\rangle_m + |\downarrow\rangle_s |x_+\rangle_m), . \tag{4.57}$$

where $|x_-\rangle_m = \hat{T}(-2\chi)|0\rangle_m$ and $|x_+\rangle_m = \hat{T}(2\chi)|0\rangle_m$ are the displaced vacuum states of the mechanical oscillator. After performing a measurement in the superposition basis of the qubit, the sphere is thus left in a spatial superposition state, albeit only with microscopic distinctness (on the order of femtometers). Note that squeezing the position state of the sphere before the start of the protocol is necessary in some parameter regimes.

We also refer the reader to refs. [36, 200], where an alternative protocol to perform a quasi-double-slit experiment was discussed in detail for optically levitated nanospheres. This protocol requires quickly turning off the trap (realized there by letting a dieletric nano-sphere fall through an optical cavity), and might benefit from the ease of tuning the trapping frequency in the presented magnetomechanical setup.

4.6 Experimental parameters and outlook

Above, we have shown that sideband cooling of a mechanical resonator can be implemented in a magnetomechanical system. We have also calculated the major decoherence sources. Table 4.1 shows an exemplary choice of parameters, and the most important derived characteristics of our setup. Due to the extremely low decoherence rates in the mechanical resonator (on the order of few Hz), ground state cooling is feasible if the drive amplitude Ω and the detuning of the qubit $f(0)$ (c.f. subsection 4.3.1) are chosen properly, as shown in fig. 4.7.

A number of experiments testing parts of our proposal have been performed [228–230], and some theoretical works have built on the concepts discussed here [231–233]. Furthermore, new proposals have been put forward to use superconducting vortex lattices in ultracold atom experiments [234]. The experimental toolbox of magnetic building blocks is also rapidly increasing with novel magnetic configurations [235, 236].

The unique combination of levitation, large masses ($\sim 2 \times 10^{14}\,\mathrm{u}$), low bulk temperatures and very weak coupling to the environment make our proposal a candidate for future experiments investigating the boundary of macroscopic quantum physics [36]. Maybe even superpositions of living organisms may be finally realized [195, 237, 238].

Parameter	Symbol	Value	Comment
Qubit splitting	ν	$2\pi \times 10\,\mathrm{GHz}$	c.f. [204–208]
Qubit amplitude	Δ	$2\pi \times 10\,\mathrm{GHz}$	c.f. [204–208]
Qubit decay rate	Γ_0	$2\pi \times 16\,\mathrm{kHz}$	c.f. [204–208]
Qubit decay rate	Γ_φ	$2\pi \times 8\,\mathrm{kHz}$	c.f. [204–208]
LC inductance	L	$0.1\,\mathrm{nH}$	c.f. [204–208]
LC capacitance	C	$1\,\mathrm{pF}$	c.f. [204–208]
Sphere radius	R	$2\,\mu\mathrm{m}$	
Sphere density	ρ	$11\,340\,\mathrm{kg\,m^{-3}}$	
Coherence length	ξ	$96\,\mathrm{nm}$	c.f. [239]
Penetration depth	λ	$30.5\,\mathrm{nm}$	c.f. [239]
Critical magnetic field	B_C	$0.08\,\mathrm{T}$	c.f. [240]
Trap coils radius	l	$25\,\mu\mathrm{m}$	
Trap coils crit. current	J_c	$7 \times 10^{11}\,\mathrm{A\,m^{-2}}$	c.f. [241]
Trap coils current	I	$10\,\mathrm{A}$	$I/(t^2\pi) < J_c$
Trap coils thickness	t	$2.5\,\mu\mathrm{m}$	
Pickup coil distance	d	$17.5\,\mu\mathrm{m}$	
Pickup coil radius	r	$24.5\,\mu\mathrm{m}$	
Temperature	T	$100\,\mathrm{mK}$	
Critical temperature	T_C	$7.2\,\mathrm{K}$	c.f. [239]
Pressure	P	$1 \times 10^{-8}\,\mathrm{Pa}$	
Trap freq. fluct.	$S_\omega(2\omega_t)$	$1 \times 10^{-10}\,\mathrm{Hz^{-1}}$	
Trap pos. fluct.	$S_x(\omega_t)/x_{\mathrm{zp}}^2$	$1 \times 10^{-10}\,\mathrm{Hz^{-1}}$	
Sphere mass	M	$2 \times 10^{14}\,\mathrm{u}$	
Max radius	R_{max}	$3.1\,\mu\mathrm{m}$	
Trap frequency	ω_t	$2\pi \times 40\,\mathrm{kHz}$	
Coupling	g_0	$2\pi \times 1.1\,\mathrm{kHz}$	
Coupling to LC	g_{LC}	$2\pi \times 78\,\mathrm{kHz}$	
Dec. from air	Γ_{air}	$0.32\,\mu\mathrm{Hz}$	
Dec. from freq. fluct.	Γ_ω	$2\,\mathrm{Hz}$	
Dec. from pos. fluct.	Γ_x	$5\,\mathrm{Hz}$	
Dec. from hysteresis	Γ_h	$3.2 \times 10^{-22}\,\mathrm{Hz}$	

Table 4.1: An exemplary choice of experimental parameters for a sphere made of lead, allowing ground state cooling. The most important derived values are printed after the vertical space.

Appendix

4.A Trapping frequency

In this section, we calculate the frequency of the magnetic trap described in section 4.2. The magnetic field close to the center of the the pair of anti-Helmholtz coils (of equal radius and distance l) is

$$\boldsymbol{B_a} = \mu_0 \frac{24}{25\sqrt{5}} \frac{I}{l^2} (2x, -y, -z)^T. \tag{4.58}$$

When a superconducting sphere is placed inside this setup, the external magnetic field induces currents inside of the material. The currents in turn produce the magnetic field used for both trapping and the interaction with the pickup coil (the latter is calculated in appendix 4.C). Assuming that the external magnetic field does not penetrate into the sphere (i.e. $\lambda \ll R$), we can assume that the internal field $\boldsymbol{H}$ is equal to the negative magnetization, $\boldsymbol{M} = -\boldsymbol{H}$. For spheres, the internal (demagnetizing) field is

$$\boldsymbol{H} = \frac{3}{2}\boldsymbol{H_a} = \frac{3}{2}\frac{\boldsymbol{B_a}}{\mu_0}, \tag{4.59}$$

where the factor of $3/2$ originates from the spherical geometry [242]. Assuming $R \ll l$, we can approximate the induced currents by replacing the sphere with a magnetic dipole with moment

$$\boldsymbol{m} = \boldsymbol{M}\frac{4}{3}R^3\pi = -\frac{2\boldsymbol{B_a}}{\mu_0}R^3\pi. \tag{4.60}$$

Since the potential energy of the moment $\boldsymbol{m}$ in an external field is given by $V = -\boldsymbol{m}\boldsymbol{B_a}$, we arrive at the harmonic trapping potential

$$V = \frac{2304}{3125}\frac{\mu_0 \pi I^2 R^3}{l^4}(4x^2 + y^2 + z^2), \tag{4.61}$$

and therefore at trapping frequencies

$$\omega_t = \frac{48\sqrt{3}}{25\sqrt{5}}\sqrt{\frac{\mu_0}{\rho}}\frac{I}{l^2} \approx 1.49\sqrt{\frac{\mu_0}{\rho}}\frac{I}{l^2} \tag{4.62}$$

and

$$\omega_\perp = \frac{24\sqrt{3}}{25\sqrt{5}}\sqrt{\frac{\mu_0}{\rho}}\frac{I}{l^2} \approx 0.74\sqrt{\frac{\mu_0}{\rho}}\frac{I}{l^2}. \tag{4.63}$$

The same results can be obtained using the image method of ref. [243].

4.B Maximum radius of the sphere

Since the sphere is placed in a field minimum, the maximum magnetic field will appear at its surface. However, when evaluating the field at the surface, the above dipole approximation slightly overestimates the magnitude of the field. For our purposes, the accuracy is sufficient; an exact calculation using the image method [243] can be found in the supplementary material of ref. [4]. With the simplified calculation, we find the field at the surface to be

$$|\boldsymbol{B}| = \frac{72}{25\sqrt{5}}\frac{\mu_0 I R}{l^2} \approx 1.29\frac{\mu_0 I R}{l^2}. \tag{4.64}$$

Given a critical field B_C, this restricts the radius of the sphere to

$$R_{\text{max}} = \frac{25\sqrt{5}}{72}\frac{B_C l^2}{I\mu_0}, \tag{4.65}$$

or, using ω_t from appendix 4.A,

$$R_{\text{max}} = \frac{2}{\sqrt{3}}\frac{B_C}{\sqrt{\mu_0\rho}}\frac{1}{\omega_t} \approx 1.15\frac{B_C}{\sqrt{\mu_0\rho}}\frac{1}{\omega_t}. \tag{4.66}$$

4.C Magnetomechanical coupling to the pickup coil

In this section, we will calculate the effect of the expelled magnetic field on the pickup coil of radius r, placed in distance $d + x$ from the center of the trap. The x-component of the field of a magnetic dipole with $\boldsymbol{m} = (m, 0, 0)^T$ in spherical coordinates (radius a, inclination θ) can be written as

$$B_x = \left[\frac{\mu_0}{4\pi}\left(\frac{3\boldsymbol{a}(\boldsymbol{m}\cdot\boldsymbol{a})}{a^5} - \frac{\boldsymbol{m}}{r^3}\right)\right]_x = \frac{\mu_0}{4\pi}\left(\frac{3ma_x^2}{a^5} - \frac{m}{a^3}\right) = \frac{\mu_0}{4\pi}\frac{3m\cos^2\theta - m}{a^3}. \tag{4.67}$$

We can now calculate the flux Φ_{ext} through the pickup coil using cylindrical coordinates

$$\Phi_{\text{ext}} = \int_S \mathrm{d}S\, B_x = \int_0^{2\pi} \int_0^r \mathrm{d}\varphi\, \mathrm{d}r'\, r' B_x(r'). \tag{4.68}$$

Using the magnetic moment from eq. (4.60) and, for the coordinates, $\tan\theta = r'/(d+x)$ and $a^2 = (x+d)^2 + (r')^2$, we obtain

$$\Phi_{\text{ext}} = -\frac{48}{25\sqrt{5}} \frac{I\mu_0 \pi r^2 R^3 x}{l^2 [r^2 + (d+x)^2]^{\frac{3}{2}}}. \tag{4.69}$$

Taking the derivative with respect to x yields

$$\Phi'_{\text{ext}}(0) = -\frac{48}{25\sqrt{5}} \frac{I\mu_0 \pi r^2 R^3}{l^2 (r^2 + d^2)^{\frac{3}{2}}} \approx -2.70 \frac{I\mu_0 r^2 R^3}{l^2 (r^2 + d^2)^{\frac{3}{2}}}. \tag{4.70}$$

5 Conclusions and outlook

Over the course of this thesis, we have looked at two major concepts used to define the border between quantum mechanics and classical physics, the world views of local realism and macrorealism. In **chapter 1** we gave an introduction to macrorealism, and discussed some of its main properties. We then turned to experimentally testable conditions for macrorealism and found that a set of no-signaling in time and arrow of time conditions is both necessary and sufficient for macrorealism. This led us to derive some operational conditions for macrorealistic behavior in an experiment in terms of measurement operators and Hamiltonians.

Next, we have used our results to define the "classicality" of measurement operators and Hamiltonians in **chapter 2**. We investigated coarse-grained measurements and various Hamiltonians in several exemplary systems to confirm our intuition, and discussed the role of spontaneously realized Hamiltonians in a definition of classical behavior.

In **chapter 3**, we compared the probability polytope of local realistic and macrorealistic theories. We identified some fundamental differences between the two, which led us to conclude that (Leggett-Garg) inequalities can never form sufficient conditions for macrorealism. Our work shows that Fine's theorem cannot be transferred from local realism to macrorealism, and motivates the "retirement" of the Leggett-Garg inequalities in favor of no-signaling in time for future experimental and theoretical studies.

Finally, in **chapter 4**, we proposed a novel type of experimental system for the realization of macroscopic quantum experiments. The use of magnetostatics for trapping a superconducting micro-sphere and coupling it to a superconducting quantum circuit establishes an extremely clean and isolated setup. Ground-state cooling of the sphere's center-of-mass motion, an important ingredient for many types of experiments, appears feasible in the studied parameter regime.

The conditions and experimental setups discussed in this thesis are integral for many proposed experiments studying quantum foundations. Although extremely challenging, their experimental realization will likely bring many new fundamental

insights into the inner workings of the quantum-to-classical transition, and may even allow the study of more exotic theories, such as objective collapse models and quantum gravity.

It is quite astonishing how far into the macroscopic domain quantum experiments have come in recent decades. While initial experiments focused on interference patterns of single particles such as photons and electrons, today, quantum states of objects with masses of as much as 10^{13} u are experimentally feasible [183]. It will be exciting to see over the next few decades whether fundamental (or technological) limits to the upper size of quantum systems emerge. Perhaps even Schrödinger's cat will finally cease to be a mere thought experiment.

Bibliography

[1] L. Clemente and J. Kofler, 'Necessary and sufficient conditions for macroscopic realism from quantum mechanics', Phys. Rev. A **91**, 062103 (2015).

[2] L. Clemente and J. Kofler, 'The emergence of macroscopic classical dynamics from microscopic quantum behavior', (in preparation).

[3] L. Clemente and J. Kofler, 'No Fine theorem for macrorealism: Retiring the Leggett-Garg inequality', (2015), arXiv:1509.00348 [quant-ph].

[4] O. Romero-Isart, L. Clemente, C. Navau, A. Sanchez, and J. I. Cirac, 'Quantum Magnetomechanics with Levitating Superconducting Microspheres', Phys. Rev. Lett. **109**, 147205 (2012).

[5] W. Assmann, R. Becker, H. Otto, M. Bader, L. Clemente, S. Reinhardt, C. Schäfer, J. Schirra, S. Uschold, A. Welzmüller, and R. Sroka, '32P-haltige Folien als Implantate für die LDR-Brachytherapie gutartiger Stenosen in der Urologie und Gastroenterologie', Zeit. Med. Phys. **23**, 21 (2013).

[6] F. Pastawski, L. Clemente, and J. I. Cirac, 'Quantum memories based on engineered dissipation', Phys. Rev. A **83**, 012304 (2011).

[7] C. Hoeschen, H. Schlattl, M. Zankl, T. Seggebrock, L. Clemente, and F. Grüner, 'Simulating Mammographic Absorption Imaging and Its Radiation Protection Properties', in *World Congress on Medical Physics and Biomedical Engineering, September 7 - 12, 2009, Munich, Germany* (Springer Berlin Heidelberg, Berlin, Heidelberg, 2009), pp. 355–358.

[8] E. Schrödinger, 'Die gegenwärtige Situation in der Quantenmechanik', Naturwissenschaften **23**, 807 (1935).

[9] J. D. Timmer, 'The present situation in quantum mechanics', Proc. Am. Philos. Soc. **124**, 323 (1980).

[10] R. Bouchendira, P. Cladé, S. Guellati-Khélifa, F. Nez, and F. Biraben, 'New Determination of the Fine Structure Constant and Test of the Quantum Electrodynamics', Phys. Rev. Lett. **106**, 080801 (2011).

[11] M. Schlosshauer, 'Decoherence, the measurement problem, and interpretations of quantum mechanics', Rev. Mod. Phys. **76**, 1267 (2005).

[12] A. J. Leggett, 'The Quantum Measurement Problem', Science **307**, 871 (2005).

[13] N. Brunner, D. Cavalcanti, S. Pironio, V. Scarani, and S. Wehner, 'Bell nonlocality', Rev. Mod. Phys. **86**, 419 (2014).

[14] M. Schlosshauer, J. Kofler, and A. Zeilinger, 'A snapshot of foundational attitudes toward quantum mechanics', Stud. Hist. Phil. Mod. Phys. **44**, 222 (2013).

[15] C. Sommer, 'Another Survey of Foundational Attitudes Towards Quantum Mechanics', (2013), arXiv:1303.2719 [quant-ph].

[16] T. Norsen and S. Nelson, 'Yet Another Snapshot of Foundational Attitudes Toward Quantum Mechanics', (2013), arXiv:1306.4646 [quant-ph].

[17] C. J. Davisson, 'The Diffraction of Electrons by a Crystal of Nickel', Bell System Technical Journal **7**, 90 (1928).

[18] M. Arndt, O. Nairz, J. Vos-Andreae, C. Keller, G. van der Zouw, and A. Zeilinger, 'Wave–particle duality of C60 molecules', Nature **401**, 680 (1999).

[19] S. Gerlich, S. Eibenberger, M. Tomandl, S. Nimmrichter, K. Hornberger, P. J. Fagan, J. Tüxen, M. Mayor, and M. Arndt, 'Quantum interference of large organic molecules', Nat. Commun. **2**, 263 (2011).

[20] H. D. Zeh, 'On the interpretation of measurement in quantum theory', Found. Phys. **1**, 69 (1970).

[21] W. H. Zurek, 'Pointer basis of quantum apparatus: Into what mixture does the wave packet collapse?', Phys. Rev. D **24**, 1516 (1981).

[22] W. H. Zurek, 'Environment-induced superselection rules', Phys. Rev. D **26**, 1862 (1982).

[23] W. H. Zurek, 'Decoherence, einselection, and the quantum origins of the classical', Rev. Mod. Phys. **75**, 715 (2003).

[24] W. H. Zurek, 'Quantum Darwinism, classical reality, and the randomness of quantum jumps', Phys. Today **67**, 44 (2014).

[25] G. C. Ghirardi, A. Rimini, and T. Weber, 'Unified dynamics for microscopic and macroscopic systems', Phys. Rev. D **34**, 470 (1986).

[26] P. Pearle, 'Combining stochastic dynamical state-vector reduction with spontaneous localization', Phys. Rev. A **39**, 2277 (1989).

[27] G. C. Ghirardi, P. Pearle, and A. Rimini, 'Markov processes in Hilbert space and continuous spontaneous localization of systems of identical particles', Phys. Rev. A **42**, 78 (1990).

[28] A. Bassi and G. Ghirardi, 'Dynamical reduction models', Phys. Rep. **379**, 257 (2003).

[29] R. Penrose, 'On Gravity's role in Quantum State Reduction', Gen. Relat. Gravit. **28**, 581 (1996).

[30] L. Diósi, 'Gravitation and quantum-mechanical localization of macro-objects', Phys. Lett. A **105**, 199 (1984).

[31] L. Diósi, 'A universal master equation for the gravitational violation of quantum mechanics', Phys. Lett. A **120**, 377 (1987).

[32] L. Diósi, 'Models for universal reduction of macroscopic quantum fluctuations', Phys. Rev. A **40**, 1165 (1989).

[33] R. Penrose, *The Emperor's New Mind* (Oxford University Press, Oxford, 1989).

[34] J. Ellis, S. Mohanty, and D. V. Nanopoulos, 'Quantum gravity and the collapse of the wavefunction', Phys. Lett. B **221**, 113 (1989).

[35] J. Ellis, N. E. Mavromatos, and D. V. Nanopoulos, 'String theory modifies quantum mechanics', Phys. Lett. B **293**, 37 (1992).

[36] O. Romero-Isart, 'Quantum superposition of massive objects and collapse models', Phys. Rev. A **84**, 052121 (2011).

[37] M. Inman, *Cat's Schrödinger - The Oatmeal*, `http://theoatmeal.com/comics/cats_schrodinger` (visited on 10/02/2015).

[38] J. Kofler and Č. Brukner, 'Classical World Arising out of Quantum Physics under the Restriction of Coarse-Grained Measurements', Phys. Rev. Lett. **99**, 180403 (2007).

[39] J. Kofler and Č. Brukner, 'Conditions for Quantum Violation of Macroscopic Realism', Phys. Rev. Lett. **101**, 090403 (2008).

[40] J. Kofler, 'Quantum violation of macroscopic realism and the transition to classical physics', PhD thesis (Universität Wien, June 2008).

[41] A. Einstein, B. Podolsky, and N. Rosen, 'Can Quantum-Mechanical Description of Physical Reality Be Considered Complete?', Phys. Rev. **47**, 777 (1935).

[42] M. Born and A. Einstein, *The Born-Einstein Letters*, edited by M. Born (Palgrave Macmillan, London, 1971).

[43] D. Bohm and Y. Aharonov, 'Discussion of Experimental Proof for the Paradox of Einstein, Rosen, and Podolsky', Phys. Rev. **108**, 1070 (1957).

[44] S. Aaronson, *Bell inequality violation finally done right*, `http://www.scottaaronson.com/blog/?p=2464` (visited on 09/24/2015).

[45] J. S. Bell, 'On the Einstein Podolsky Rosen paradox', Physics **1**, 195 (1964).

[46] R. Horodecki, P. Horodecki, M. Horodecki, and K. Horodecki, 'Quantum entanglement', Rev. Mod. Phys. **81**, 865 (2009).

[47] K. Popper, *Logik der Forschung* (Julius Springer, Vienna, 1934).

[48] J. F. Clauser, M. A. Horne, A. Shimony, and R. A. Holt, 'Proposed Experiment to Test Local Hidden-Variable Theories', Phys. Rev. Lett. **23**, 880 (1969).

[49] E. P. Wigner, 'On Hidden Variables and Quantum Mechanical Probabilities', Am. J. Phys. **38**, 1005 (1970).

[50] J. F. Clauser and M. A. Horne, 'Experimental consequences of objective local theories', Phys. Rev. D **10**, 526 (1974).

[51] P. H. Eberhard, 'Background level and counter efficiencies required for a loophole-free Einstein-Podolsky-Rosen experiment', Phys. Rev. A **47**, R747 (1993).

[52] A. Khrennikov, S. Ramelow, R. Ursin, B. Wittmann, J. Kofler, and I. Basieva, 'On the equivalence of the Clauser–Horne and Eberhard inequality based tests', Phys. Scr. **2014**, 014019 (2014).

[53] S. J. Freedman and J. F. Clauser, 'Experimental Test of Local Hidden-Variable Theories', Phys. Rev. Lett. **28**, 938 (1972).

[54] A. Aspect, P. Grangier, and G. Roger, 'Experimental Tests of Realistic Local Theories via Bell's Theorem', Phys. Rev. Lett. **47**, 460 (1981).

[55] A. Aspect, J. Dalibard, and G. Roger, 'Experimental Test of Bell's Inequalities Using Time- Varying Analyzers', Phys. Rev. Lett. **49**, 1804 (1982).

[56] A. Aspect, P. Grangier, and G. Roger, 'Experimental Realization of Einstein-Podolsky-Rosen-Bohm Gedankenexperiment: A New Violation of Bell's Inequalities', Phys. Rev. Lett. **49**, 91 (1982).

[57] W. Tittel, J. Brendel, H. Zbinden, and N. Gisin, 'Violation of Bell Inequalities by Photons More Than 10 km Apart', Phys. Rev. Lett. **81**, 3563 (1998).

[58] G. Weihs, T. Jennewein, C. Simon, H. Weinfurter, and A. Zeilinger, 'Violation of Bell's Inequality under Strict Einstein Locality Conditions', Phys. Rev. Lett. **81**, 5039 (1998).

[59] J.-W. Pan, D. Bouwmeester, M. Daniell, H. Weinfurter, and A. Zeilinger, 'Experimental test of quantum nonlocality in three-photon Greenberger–Horne–Zeilinger entanglement', Nature **403**, 515 (2000).

[60] M. A. Rowe, D. Kielpinski, V. Meyer, C. A. Sackett, W. M. Itano, C. Monroe, and D. J. Wineland, 'Experimental violation of a Bell's inequality with efficient detection', Nature **409**, 791 (2001).

[61] D. Salart, A. Baas, J. A. W. van Houwelingen, N. Gisin, and H. Zbinden, 'Spacelike Separation in a Bell Test Assuming Gravitationally Induced Collapses', Phys. Rev. Lett. **100**, 220404 (2008).

[62] M. Ansmann, H. Wang, R. C. Bialczak, M. Hofheinz, E. Lucero, M. Neeley, A. D. O'Connell, D. Sank, M. Weides, J. Wenner, A. N. Cleland, and J. M. Martinis, 'Violation of Bell's inequality in Josephson phase qubits', Nature **461**, 504 (2009).

[63] T. Scheidl, R. Ursin, J. Kofler, S. Ramelow, X.-S. Ma, T. Herbst, L. Ratschbacher, A. Fedrizzi, N. K. Langford, T. Jennewein, and A. Zeilinger, 'Violation of local realism with freedom of choice', Proc. Natl. Acad. Sci. U.S.A. **107**, 19708 (2010).

[64] M. Giustina, A. Mech, S. Ramelow, B. Wittmann, J. Kofler, J. Beyer, A. Lita, B. Calkins, T. Gerrits, S. W. Nam, R. Ursin, and A. Zeilinger, 'Bell violation using entangled photons without the fair-sampling assumption', Nature **497**, 227 (2013).

[65] B. Hensen, H. Bernien, A. E. Dréau, A. Reiserer, N. Kalb, M. S. Blok, J. Ruitenberg, R. F. L. Vermeulen, R. N. Schouten, C. Abellán, W. Amaya, V. Pruneri, M. W. Mitchell, M. Markham, D. J. Twitchen, D. Elkouss, S. Wehner, T. H. Taminiau, and R. Hanson, 'Loophole-free Bell inequality violation using electron spins separated by 1.3 kilometres', Nature **526**, 682 (2015).

[66] M. Giustina, M. A. M. Versteegh, S. Wengerowsky, J. Handsteiner, A. Hochrainer, K. Phelan, F. Steinlechner, J. Kofler, J.-Å. Larsson, C. Abellan, W. Amaya, V. Pruneri, M. W. Mitchell, J. Beyer, T. Gerrits, A. E. Lita, L. K. Shalm, S. W. Nam, T. Scheidl, R. Ursin, B. Wittmann, and A. Zeilinger, 'A significant-loophole-free test of Bell's theorem with entangled photons', (2015), arXiv:`1511.03190 [quant-ph]`.

[67] L. K. Shalm, E. Meyer-Scott, B. G. Christensen, P. Bierhorst, M. A. Wayne, M. J. Stevens, T. Gerrits, S. Glancy, D. R. Hamel, M. S. Allman, K. J. Coakley, S. D. Dyer, C. Hodge, A. E. Lita, V. B. Verma, C. Lambrocco, E. Tortorici, A. L. Migdall, Y. Zhang, D. R. Kumor, W. H. Farr, F. Marsili, M. D. Shaw, J. A. Stern, C. Abellan, W. Amaya, V. Pruneri, T. Jennewein, M. W. Mitchell, P. G. Kwiat, J. C. Bienfang, R. P. Mirin, E. Knill, and S. W. Nam, 'A strong loophole-free test of local realism', (2015), arXiv:1511.03189 [quant-ph].

[68] J. Kofler and M. Giustina, 'Requirements for a loophole-free Bell test using imperfect setting generators', (2014), arXiv:1411.4787 [quant-ph].

[69] J.-Å. Larsson, 'Loopholes in Bell inequality tests of local realism', J. Phys. A. **47**, 424003 (2014).

[70] R. Munroe, *xkcd: Bell's Theorem*, http://xkcd.com/1591/ (visited on 10/28/2015).

[71] N. Gisin, S. Tanzilli, and W. Tittel, 'Quantum teleportation and nonlocality: the puzzling predictions of entanglement are coming of age', (2015), arXiv:1508.05962 [quant-ph].

[72] A. J. Leggett and A. Garg, 'Quantum mechanics versus macroscopic realism: Is the flux there when nobody looks?', Phys. Rev. Lett. **54**, 857 (1985).

[73] J. Kofler and Č. Brukner, 'Condition for macroscopic realism beyond the Leggett-Garg inequalities', Phys. Rev. A **87**, 052115 (2013).

[74] D. Adams, *The Hitchhiker's Guide to the Galaxy* (Pan Books, 1979).

[75] A. J. Leggett, 'Testing the limits of quantum mechanics: motivation, state of play, prospects', J. Phys.: Condens. Matter **14**, R415 (2002).

[76] C. Emary, N. Lambert, and F. Nori, 'Leggett–Garg inequalities', Rep. Prog. Phys. **77**, 016001 (2014).

[77] D. Saha, S. Mal, P. K. Panigrahi, and D. Home, 'Wigner's form of the Leggett-Garg inequality, the no-signaling-in-time condition, and unsharp measurements', Phys. Rev. A **91**, 032117 (2015).

[78] O. J. E. Maroney and C. G. Timpson, 'Quantum- vs. Macro- Realism: What does the Leggett-Garg Inequality actually test?', (2014), arXiv:1412.6139 [quant-ph].

[79] G. Bacciagaluppi, 'Leggett-Garg Inequalities, Pilot Waves and Contextuality', Int. J. Quantum Found. **1**, 1 (2015).

[80] S. Lloyd, 'Pure state quantum statistical mechanics and black holes', (1988), arXiv:1307.0378 [quant-ph].

[81] N. Linden, S. Popescu, A. Short, and A. Winter, 'Quantum mechanical evolution towards thermal equilibrium', Phys. Rev. E **79**, 061103 (2009).

[82] L. Maccone, 'Quantum Solution to the Arrow-of-Time Dilemma', Phys. Rev. Lett. **103**, 080401 (2009).

[83] D. Jennings and T. Rudolph, 'Entanglement and the thermodynamic arrow of time', Phys. Rev. E **81**, 061130 (2010).

[84] Y. Shikano, K. Chisaki, E. Segawa, and N. Konno, 'Emergence of randomness and arrow of time in quantum walks', Phys. Rev. A **81**, 062129 (2010).

[85] C. Rovelli, 'Why do we remember the past and not the future? The 'time oriented coarse graining' hypothesis', (2014), arXiv:1407.3384 [hep-th].

[86] M. Noorbala, 'On the second law of thermodynamics: The significance of coarse-graining and the role of decoherence', Ann. Phys. **351**, 914 (2014).

[87] A. Peres, *Quantum Theory: Concepts and Methods* (Springer Netherlands, Dordrecht, 1993).

[88] W. Dür, C. Simon, and J. I. Cirac, 'Effective Size of Certain Macroscopic Quantum Superpositions', Phys. Rev. Lett. **89**, 210402 (2002).

[89] G. Björk and P. G. L. Mana, 'A size criterion for macroscopic superposition states', J. Opt. B: Quantum Semiclass. Opt. **6**, 429 (2004).

[90] J. I. Korsbakken, K. B. Whaley, J. Dubois, and J. I. Cirac, 'Measurement-based measure of the size of macroscopic quantum superpositions', Phys. Rev. A **75**, 042106 (2007).

[91] F. Marquardt, B. Abel, and J. von Delft, 'Measuring the size of a quantum superposition of many-body states', Phys. Rev. A **78**, 012109 (2008).

[92] C.-W. Lee and H. Jeong, 'Quantification of Macroscopic Quantum Superpositions within Phase Space', Phys. Rev. Lett. **106**, 220401 (2011).

[93] F. Fröwis and W. Dür, 'Measures of macroscopicity for quantum spin systems', New J. Phys. **14**, 093039 (2012).

[94] F. Fröwis and W. Dür, 'Are Cloned Quantum States Macroscopic?', Phys. Rev. Lett. **109**, 170401 (2012).

[95] S. Nimmrichter and K. Hornberger, 'Macroscopicity of Mechanical Quantum Superposition States', Phys. Rev. Lett. **110**, 160403 (2013).

[96] M. Mraz, J. Sperling, W. Vogel, and B. Hage, 'Witnessing the degree of nonclassicality of light', Phys. Rev. A **90**, 033812 (2014).

[97] H. Jeong, M. Kang, and H. Kwon, 'Characterizations and quantifications of macroscopic quantumness and its implementations using optical fields', Opt. Commun. **337**, 12 (2015).

[98] A. Laghaout, J. S. Neergaard-Nielsen, and U. L. Andersen, 'Assessments of macroscopicity for quantum optical states', Opt. Commun. **337**, 96 (2015).

[99] F. Fröwis, N. Sangouard, and N. Gisin, 'Linking measures for macroscopic quantum states via photon–spin mapping', Opt. Commun. **337**, 2 (2015).

[100] M. Kang, C.-W. Lee, J. Bang, S.-W. Lee, C.-Y. Park, and H. Jeong, 'Measure of Quantum Macroscopicity for Arbitrary Spin Systems and Quantum Phase Transition as a Genuine Macroscopic Quantum Phenomenon', (2015), arXiv:1510.02876 [quant-ph].

[101] M. M. Wilde and A. Mizel, 'Addressing the Clumsiness Loophole in a Leggett-Garg Test of Macrorealism', Found. Phys. **42**, 256 (2012).

[102] S. Raeisi, P. Sekatski, and C. Simon, 'Coarse Graining Makes It Hard to See Micro-Macro Entanglement', Phys. Rev. Lett. **107**, 250401 (2011).

[103] A. Reddy, J. Samuel, K. Shivam, and S. Sinha, 'Coarse Quantum Measurement : Stern-Gerlach Revisited', (2015), arXiv:1509.09024 [quant-ph].

[104] C. Budroni, G. Vitagliano, G. Colangelo, R. J. Sewell, O. Gühne, G. Tóth, and M. W. Mitchell, 'Quantum Nondemolition Measurement Enables Macroscopic Leggett-Garg Tests', Phys. Rev. Lett. **115**, 200403 (2015).

[105] T. Wang, R. Ghobadi, S. Raeisi, and C. Simon, 'Precision requirements for observing macroscopic quantum effects', Phys. Rev. A **88**, 062114 (2013).

[106] H. Jeong, Y. Lim, and M. S. Kim, 'Coarsening Measurement References and the Quantum-to-Classical Transition', Phys. Rev. Lett. **112**, 010402 (2014).

[107] P. Sekatski, N. Gisin, and N. Sangouard, 'How Difficult Is It to Prove the Quantumness of Macroscropic States?', Phys. Rev. Lett. **113**, 090403 (2014).

[108] J. R. Friedman, V. Patel, W. Chen, S. K. Tolpygo, and J. E. Lukens, 'Quantum superposition of distinct macroscopic states', Nature **406**, 43 (2000).

[109] B. Julsgaard, A. Kozhekin, and E. S. Polzik, 'Experimental long-lived entanglement of two macroscopic objects', Nature **413**, 400 (2001).

[110] A. Palacios-Laloy, F. Mallet, F. Nguyen, P. Bertet, D. Vion, D. Esteve, and A. N. Korotkov, 'Experimental violation of a Bell/'s inequality in time with weak measurement', Nat. Phys. **6**, 442 (2010).

[111] J. Dressel, C. J. Broadbent, J. C. Howell, and A. N. Jordan, 'Experimental Violation of Two-Party Leggett-Garg Inequalities with Semiweak Measurements', Phys. Rev. Lett. **106**, 040402 (2011).

[112] M. E. Goggin, M. P. Almeida, M. Barbieri, B. P. Lanyon, J. L. O'Brien, A. G. White, and G. J. Pryde, 'Violation of the Leggett-Garg inequality with weak measurements of photons', Proc. Natl. Acad. Sci. U.S.A. **108**, 1256 (2011).

[113] A. Fedrizzi, M. P. Almeida, M. A. Broome, A. G. White, and M. Barbieri, 'Hardy's Paradox and Violation of a State-Independent Bell Inequality in Time', Phys. Rev. Lett. **106**, 200402 (2011).

[114] G. Waldherr, P. Neumann, S. F. Huelga, F. Jelezko, and J. Wrachtrup, 'Violation of a Temporal Bell Inequality for Single Spins in a Diamond Defect Center', Phys. Rev. Lett. **107**, 090401 (2011).

[115] J.-S. Xu, C.-F. Li, X.-B. Zou, and G.-C. Guo, 'Experimental violation of the Leggett-Garg inequality under decoherence', Sci. Rep. **1**, 101 (2011).

[116] V. Athalye, S. S. Roy, and T. S. Mahesh, 'Investigation of the Leggett-Garg Inequality for Precessing Nuclear Spins', Phys. Rev. Lett. **107**, 130402 (2011).

[117] A. M. Souza, I. S. Oliveira, and R. S. Sarthour, 'A scattering quantum circuit for measuring Bell's time inequality: a nuclear magnetic resonance demonstration using maximally mixed states', New J. Phys. **13**, 053023 (2011).

[118] G. C. Knee, S. Simmons, E. M. Gauger, J. J. L. Morton, H. Riemann, N. V. Abrosimov, P. Becker, H.-J. Pohl, K. M. Itoh, M. L. W. Thewalt, G. A. D. Briggs, and S. C. Benjamin, 'Violation of a Leggett-Garg inequality with ideal non-invasive measurements', Nat. Commun. **3**, 606 (2012).

[119] Y. Suzuki, M. Iinuma, and H. F. Hofmann, 'Violation of Leggett–Garg inequalities in quantum measurements with variable resolution and back-action', New J. Phys. **14**, 103022 (2012).

[120] A. I. Lvovsky, R. Ghobadi, A. Chandra, A. S. Prasad, and C. Simon, 'Observation of micro–macro entanglement of light', Nat. Phys. **9**, 541 (2013).

[121] R. E. George, L. M. Robledo, O. J. E. Maroney, M. S. Blok, H. Bernien, M. L. Markham, D. J. Twitchen, J. J. L. Morton, G. A. D. Briggs, and R. Hanson, 'Opening up three quantum boxes causes classically undetectable wavefunction collapse', Proc. Natl. Acad. Sci. U.S.A. **110**, 3777 (2013).

[122] H. Katiyar, A. Shukla, K. R. K. Rao, and T. S. Mahesh, 'Violation of entropic Leggett-Garg inequality in nuclear spins', Phys. Rev. A **87**, 052102 (2013).

[123] P. Sekatski, M. Aspelmeyer, and N. Sangouard, 'Macroscopic Optomechanics from Displaced Single-Photon Entanglement', Phys. Rev. Lett. **112**, 080502 (2014).

[124] R. Ghobadi, S. Kumar, B. Pepper, D. Bouwmeester, A. I. Lvovsky, and C. Simon, 'Optomechanical Micro-Macro Entanglement', Phys. Rev. Lett. **112**, 080503 (2014).

[125] A. Asadian, Č. Brukner, and P. Rabl, 'Probing Macroscopic Realism via Ramsey Correlation Measurements', Phys. Rev. Lett. **112**, 190402 (2014).

[126] T. C. White, J. Y. Mutus, J. Dressel, J. Kelly, R. Barends, E. Jeffrey, D. Sank, A. Megrant, B. Campbell, Y. Chen, Z. Chen, B. Chiaro, A. Dunsworth, I. C. Hoi, C. Neill, P. J. J. O'Malley, P. Roushan, A. Vainsencher, J. Wenner, A. N. Korotkov, and J. M. Martinis, 'Violating the Bell-Leggett-Garg inequality with weak measurement of an entangled state', (2015), arXiv:1504.02707 [quant-ph].

[127] C. Robens, W. Alt, D. Meschede, C. Emary, and A. Alberti, 'Ideal Negative Measurements in Quantum Walks Disprove Theories Based on Classical Trajectories', Phys. Rev. X **5**, 011003 (2015).

[128] Z.-Q. Zhou, S. F. Huelga, C.-F. Li, and G.-C. Guo, 'Experimental Detection of Quantum Coherent Evolution through the Violation of Leggett-Garg-Type Inequalities', Phys. Rev. Lett. **115**, 113002 (2015).

[129] A. Tiranov, J. Lavoie, P. C. Strassmann, N. Sangouard, M. Afzelius, F. Bussières, and N. Gisin, 'Light-matter micro-macro entanglement', (2015), arXiv:1510.02665 [quant-ph].

[130] C. Monroe, D. M. Meekhof, B. E. King, and D. J. Wineland, 'A "Schrödinger Cat" Superposition State of an Atom', Science **272**, 1131 (1996).

[131] Z. Zhao, T. Yang, Y.-A. Chen, A.-N. Zhang, M. Żukowski, and J.-W. Pan, 'Experimental Violation of Local Realism by Four-Photon Greenberger-Horne-Zeilinger Entanglement', Phys. Rev. Lett. **91**, 180401 (2003).

[132] Z. Zhao, Y.-A. Chen, A.-N. Zhang, T. Yang, H. J. Briegel, and J.-W. Pan, 'Experimental demonstration of five-photon entanglement and open-destination teleportation', Nature **430**, 54 (2004).

[133] D. Leibfried, E. Knill, S. Seidelin, J. Britton, R. B. Blakestad, J. Chiaverini, D. B. Hume, W. M. Itano, J. D. Jost, C. Langer, R. Ozeri, R. Reichle, and D. J. Wineland, 'Creation of a six-atom 'Schrödinger cat' state', Nature **438**, 639 (2005).

[134] A. Ourjoumtsev, H. Jeong, R. Tualle-Brouri, and P. Grangier, 'Generation of optical 'Schrödinger cats' from photon number states', Nature **448**, 784 (2007).

[135] C.-Y. Lu, X.-Q. Zhou, O. Gühne, W.-B. Gao, J. Zhang, Z.-S. Yuan, A. Goebel, T. Yang, and J.-W. Pan, 'Experimental entanglement of six photons in graph states', Nat. Phys. **3**, 91 (2007).

[136] A. D. O'Connell, M. Hofheinz, M. Ansmann, R. C. Bialczak, M. Lenander, E. Lucero, M. Neeley, D. Sank, H. Wang, M. Weides, J. Wenner, J. M. Martinis, and A. N. Cleland, 'Quantum ground state and single-phonon control of a mechanical resonator', Nature **464**, 697 (2010).

[137] T. Gerrits, S. Glancy, T. S. Clement, B. Calkins, A. E. Lita, A. J. Miller, A. L. Migdall, S. W. Nam, R. P. Mirin, and E. Knill, 'Generation of optical coherent-state superpositions by number-resolved photon subtraction from the squeezed vacuum', Phys. Rev. A **82**, 031802 (2010).

[138] W.-B. Gao, C.-Y. Lu, X.-C. Yao, P. Xu, O. Gühne, A. Goebel, Y.-A. Chen, C.-Z. Peng, Z.-B. Chen, and J.-W. Pan, 'Experimental demonstration of a hyper-entangled ten-qubit Schrödinger cat state', Nat. Phys. **6**, 331 (2010).

[139] X.-C. Yao, T.-X. Wang, P. Xu, H. Lu, G.-S. Pan, X.-H. Bao, C.-Z. Peng, C.-Y. Lu, Y.-A. Chen, and J.-W. Pan, 'Observation of eight-photon entanglement', Nature Photon. **6**, 225 (2012).

[140] O. Morin, K. Huang, J. Liu, H. Le Jeannic, C. Fabre, and J. Laurat, 'Remote creation of hybrid entanglement between particle-like and wave-like optical qubits', Nature Photon. **8**, 570 (2014).

[141] K. Huang, H. Le Jeannic, J. Ruaudel, V. B. Verma, M. D. Shaw, F. Marsili, S. W. Nam, E. Wu, H. Zeng, Y. C. Jeong, R. Filip, O. Morin, and J. Laurat, 'Optical Synthesis of Large-Amplitude Squeezed Coherent-State Superpositions with Minimal Resources', Phys. Rev. Lett. **115**, 023602 (2015).

[142] C. Budroni and C. Emary, 'Temporal Quantum Correlations and Leggett-Garg Inequalities in Multilevel Systems', Phys. Rev. Lett. **113**, 050401 (2014).

[143] S. Foster and A. Elby, 'A SQUID No-Go theorem without macrorealism: What SQUID's really tell us about nature', Found. Phys. **21**, 773 (1991).

[144] F. Benatti, G. Ghirardi, and R. Grassi, 'On some recent proposals for testing macrorealism versus quantum mechanics', Found. Phys. Lett. **7**, 105 (1994).

[145] M. Reck, A. Zeilinger, H. J. Bernstein, and P. Bertani, 'Experimental realization of any discrete unitary operator', Phys. Rev. Lett. **73**, 58 (1994).

[146] P. Busch, 'Unsharp reality and joint measurements for spin observables', Phys. Rev. D **33**, 2253 (1986).

[147] P. Lahti, 'Coexistence and Joint Measurability in Quantum Mechanics', Int. J. Theo. Phys. **42**, 893 (2003).

[148] W. Son, E. Andersson, S. M. Barnett, and M. S. Kim, 'Joint measurements and Bell inequalities', Phys. Rev. A **72**, 052116 (2005).

[149] S. T. Ali, C. Carmeli, T. Heinosaari, and A. Toigo, 'Commutative POVMs and Fuzzy Observables', Found. Phys. **39**, 593 (2009).

[150] M. M. Wolf, D. Perez-Garcia, and C. Fernandez, 'Measurements Incompatible in Quantum Theory Cannot Be Measured Jointly in Any Other No-Signaling Theory', Phys. Rev. Lett. **103**, 230402 (2009).

[151] S. Yu, N.-l. Liu, L. Li, and C. H. Oh, 'Joint measurement of two unsharp observables of a qubit', Phys. Rev. A **81**, 062116 (2010).

[152] T. Heinosaari and M. M. Wolf, 'Nondisturbing quantum measurements', J. Math. Phys. **51**, 092201 (2010).

[153] M. Banik, M. R. Gazi, S. Ghosh, and G. Kar, 'Degree of complementarity determines the nonlocality in quantum mechanics', Phys. Rev. A **87**, 052125 (2013).

[154] A. Bhattacharyya, 'On a measure of divergence between two statistical populations defined by their probability distributions', Bull. Calcutta Math. Soc. **35**, 99 (1943).

[155] K. Husimi, 'Some Formal Properties of the Density Matrix', Proc. Phys.-Math. Soc. Jpn. **22**, 264 (1940).

[156] P. Busch and P. J. Lahti, 'The standard model of quantum measurement theory: History and applications', Found. Phys. **26**, 875 (1996).

[157] P. Busch, 'On the Sharpness and Bias of Quantum Effects', Found. Phys. **39**, 712 (2009).

[158] P. Busch and G. Jaeger, 'Unsharp Quantum Reality', Found. Phys. **40**, 1341 (2010).

[159] J. Ma, X. Wang, C. P. Sun, and F. Nori, 'Quantum spin squeezing', Phys. Rep. **509**, 89 (2011).

[160] L. Hyafil and R. L. Rivest, *Graph Partitioning and Constructing Optimal Decision Trees are Polynomial Complete Problems*, tech. rep. 33 (Laboratoire de Recherche en Informatique et Automatique, 1973).

[161] M. R. Garey, D. S. Johnson, and L. Stockmeyer, 'Some simplified NP-complete problems', in STOC '74 (1974), pp. 47–63.

[162] A. Buluc, H. Meyerhenke, I. Safro, P. Sanders, and C. Schulz, 'Recent Advances in Graph Partitioning', (2013), arXiv:1311.3144 [cs.DS].

[163] F. De Martini, F. Sciarrino, and C. Vitelli, 'Entanglement Test on a Microscopic-Macroscopic System', Phys. Rev. Lett. **100**, 253601 (2008).

[164] M. Born, *Natural Philosophy of Cause and Chance* (At The Clarendon Press, Oxford, 1949).

[165] S. B. Kochen and E. P. Specker, 'The problem of hidden variables in quantum mechanics', J. Math. Mech. **17**, 59 (1967).

[166] D. Avis, P. Hayden, and M. M. Wilde, 'Leggett-Garg inequalities and the geometry of the cut polytope', Phys. Rev. A **82**, 030102 (2010).

[167] M. Kleinmann, C. Budroni, J.-Å. Larsson, O. Gühne, and A. Cabello, 'Optimal Inequalities for State-Independent Contextuality', Phys. Rev. Lett. **109**, 250402 (2012).

[168] M. Araújo, M. T. Quintino, C. Budroni, M. T. Cunha, and A. Cabello, 'All noncontextuality inequalities for the n-cycle scenario', Phys. Rev. A **88**, 022118 (2013).

[169] J. V. Kujala, E. N. Dzhafarov, and J.-Å. Larsson, 'Necessary and Sufficient Conditions for Maximal Noncontextuality in a Broad Class of Quantum Mechanical Systems', (2014), arXiv:1412.4724 [quant-ph].

[170] E. N. Dzhafarov, J. V. Kujala, and J.-Å. Larsson, 'Contextuality in Three Types of Quantum-Mechanical Systems', Found. Phys. **45**, 762 (2015).

[171] A. Fine, 'Hidden Variables, Joint Probability, and the Bell Inequalities', Phys. Rev. Lett. **48**, 291 (1982).

[172] S. Mal and A. S. Majumdar, 'Optimal violation of Leggett-Garg inequality for arbitrary spin and emergence of classicality through unsharp measurement', (2015), arXiv:1506.00519 [quant-ph].

[173] J. J. Halliwell, 'The Leggett-Garg Inequalities and Linear Positivity: an Alternative to Non-Invasive Measurability', (2015), arXiv:1508.02271 [quant-ph].

[174] S. Pironio, 'Lifting Bell inequalities', J. Math. Phys. **46**, 062112 (2005).

[175] S. Pironio, 'All Clauser–Home–Shimony–Holt polytopes', J. Phys. A. **47**, 424020 (2014).

[176] B. S. Cirel'son, 'Quantum generalizations of Bell's inequality', Lett Math Phys **4**, 93 (1980).

[177] T. Fritz, 'Quantum correlations in the temporal Clauser–Horne–Shimony–Holt (CHSH) scenario', New J. Phys. **12**, 083055 (2010).

[178] S. V. Moreira, A. Keller, T. Coudreau, and P. Milman, 'Modeling Invasiveness in a Leggett-Garg Inequality', (2015), arXiv:1506.04993 [quant-ph].

[179] L. Clemente, 'Magnetically Levitated Micro-Objects in the Quantum Regime', Bachelor's thesis (Ludwig-Maximilians-Universität München, 2010).

[180] M. Cirio, G. Brennen, and J. Twamley, 'Quantum Magnetomechanics: Ultrahigh-Q-Levitated Mechanical Oscillators', Phys. Rev. Lett. **109**, 147206 (2012).

[181] D. Gevaux, 'Quantum mechanical resonators: Rising above the noise', Nat. Phys. **8**, 782 (2012).

[182] R. Schnabel, N. Mavalvala, D. E. McClelland, and P. K. Lam, 'Quantum metrology for gravitational wave astronomy', Nat. Commun. **1**, 121 (2010).

[183] J. D. Teufel, T. Donner, D. Li, J. W. Harlow, M. S. Allman, K. Cicak, A. J. Sirois, J. D. Whittaker, K. W. Lehnert, and R. W. Simmonds, 'Sideband cooling of micromechanical motion to the quantum ground state', Nature **475**, 359 (2011).

[184] J. Chan, T. P. M. Alegre, A. H. Safavi-Naeini, J. T. Hill, A. Krause, S. Gröblacher, M. Aspelmeyer, and O. Painter, 'Laser cooling of a nanomechanical oscillator into its quantum ground state', Nature **478**, 89 (2011).

[185] A. H. Safavi-Naeini, J. Chan, J. T. Hill, T. P. M. Alegre, A. Krause, and O. Painter, 'Observation of Quantum Motion of a Nanomechanical Resonator', Phys. Rev. Lett. **108**, 033602 (2012).

[186] F. Marquardt, J. P. Chen, A. A. Clerk, and S. M. Girvin, 'Quantum Theory of Cavity-Assisted Sideband Cooling of Mechanical Motion', Phys. Rev. Lett. **99**, 093902 (2007).

[187] I. Wilson-Rae, N. Nooshi, W. Zwerger, and T. J. Kippenberg, 'Theory of Ground State Cooling of a Mechanical Oscillator Using Dynamical Backaction', Phys. Rev. Lett. **99**, 093901 (2007).

[188] C. Genes, D. Vitali, P. Tombesi, S. Gigan, and M. Aspelmeyer, 'Ground-state cooling of a micromechanical oscillator: Comparing cold damping and cavity-assisted cooling schemes', Phys. Rev. A **77**, 033804 (2008).

[189] T. J. Kippenberg and K. J. Vahala, 'Cavity Optomechanics: Back-Action at the Mesoscale', Science **321**, 1172 (2008).

[190] M. Aspelmeyer and K. Schwab, 'Focus on Mechanical Systems at the Quantum Limit', New J. Phys. **10**, 095001 (2008).

[191] F. Marquardt and S. M. Girvin, 'Trend: Optomechanics', Physics **2**, 40 (2009).

[192] I. Favero and K. Karrai, 'Optomechanics of deformable optical cavities', Nature Photon. **3**, 201 (2009).

[193] M. Aspelmeyer, S. Gröblacher, K. Hammerer, and N. Kiesel, 'Quantum optomechanics—throwing a glance [Invited]', J. Opt. Soc. Am. B **27**, A189 (2010).

[194] M. Aspelmeyer, T. J. Kippenberg, and F. Marquardt, 'Cavity optomechanics', Rev. Mod. Phys. **86**, 1391 (2014).

[195] O. Romero-Isart, M. Juan, R. Quidant, and J. I. Cirac, 'Toward quantum superposition of living organisms', New J. Phys. **12**, 033015 (2010).

[196] D. E. Chang, C. A. Regal, S. B. Papp, D. J. Wilson, J. Ye, O. Painter, H. J. Kimble, and P. Zoller, 'Cavity opto-mechanics using an optically levitated nanosphere', Proc. Natl. Acad. Sci. U.S.A. **107**, 1005 (2010).

[197] P. F. Barker and M. N. Shneider, 'Cavity cooling of an optically trapped nanoparticle', Phys. Rev. A **81**, 023826 (2010).

[198] O. Romero-Isart, A. Pflanzer, M. Juan, R. Quidant, N. Kiesel, M. Aspelmeyer, and J. I. Cirac, 'Optically levitating dielectrics in the quantum regime: Theory and protocols', Phys. Rev. A **83**, 013803 (2011).

[199] A. Pflanzer, O. Romero-Isart, and J. I. Cirac, 'Master-equation approach to optomechanics with arbitrary dielectrics', Phys. Rev. A **86**, 013802 (2012).

[200] O. Romero-Isart, A. C. Pflanzer, F. Blaser, R. Kaltenbaek, N. Kiesel, M. Aspelmeyer, and J. I. Cirac, 'Large Quantum Superpositions and Interference of Massive Nanometer-Sized Objects', Phys. Rev. Lett. **107**, 020405 (2011).

[201] R. Kaltenbaek, G. Hechenblaikner, N. Kiesel, O. Romero-Isart, K. C. Schwab, U. Johann, and M. Aspelmeyer, 'Macroscopic quantum resonators (MAQRO)', Exp. Astron. **34**, 123 (2012).

[202] R. Kaltenbaek, M. Arndt, M. Aspelmeyer, P. F. Barker, A. Bassi, J. Bateman, K. Bongs, S. Bose, C. Braxmaier, Č. Brukner, B. Christophe, M. Chwalla, P.-F. Cohadon, A. M. Cruise, C. Curceanu, K. Dholakia, K. Döringshoff, W. Ertmer, J. Gieseler, N. Gürlebeck, G. Hechenblaikner, A. Heidmann, S. Herrmann, S. Hossenfelder, U. Johann, N. Kiesel, M. Kim, C. Lämmerzahl, A. Lambrecht, M. Mazilu, G. J. Milburn, H. Müller, L. Novotny, M. Paternostro, A. Peters, I. Pikovski, A. Pilan-Zanoni, E. M. Rasel, S. Reynaud, C. J. Riedel, M. Rodrigues, L. Rondin, A. Roura, W. P. Schleich, J. Schmiedmayer, T. Schuldt, K. C. Schwab, M. Tajmar, G. M. Tino, H. Ulbricht, R. Ursin, and V. Vedral, 'Macroscopic quantum resonators (MAQRO): 2015 Update', (2015), arXiv:1503.02640 [quant-ph].

[203] W. Meißner and R. Ochsenfeld, 'Ein neuer Effekt bei Eintritt der Supraleitfähigkeit', Naturwissenschaften **44**, 787 (1933).

[204] J. E. Mooij, T. P. Orlando, L. S. Levitov, L. Tian, C. H. van der Wal, and S. Lloyd, 'Josephson Persistent-Current Qubit', Science **285**, 1036 (1999).

[205] Y. Makhlin, G. Schön, and A. Shnirman, 'Quantum-state engineering with Josephson-junction devices', Rev. Mod. Phys. **73**, 357 (2001).

[206] M. H. Devoret, A. Wallraff, and J. M. Martinis, 'Superconducting Qubits: A Short Review', (2004), arXiv:cond-mat/0411174.

[207] J. Clarke and F. K. Wilhelm, 'Superconducting quantum bits', Nature **453**, 1031 (2008).

[208] J. Q. You and F. Nori, 'Atomic physics and quantum optics using superconducting circuits', Nature **474**, 589 (2011).

[209] J. Fortágh and C. Zimmermann, 'Magnetic microtraps for ultracold atoms', Rev. Mod. Phys. **79** (2007).

[210] A. Armour, M. Blencowe, and K. Schwab, 'Entanglement and Decoherence of a Micromechanical Resonator via Coupling to a Cooper-Pair Box', Phys. Rev. Lett. **88**, 148301 (2002).

[211] E. Il'ichev, N. Oukhanski, A. Izmalkov, T. Wagner, M. Grajcar, H. G. Meyer, A. Smirnov, A. Maassen van den Brink, M. Amin, and A. Zagoskin, 'Continuous Monitoring of Rabi Oscillations in a Josephson Flux Qubit', Phys. Rev. Lett. **91**, 097906 (2003).

[212] J. Hauss, A. Fedorov, C. Hutter, A. Shnirman, and G. Schön, 'Single-Qubit Lasing and Cooling at the Rabi Frequency', Phys. Rev. Lett. **100**, 037003 (2008).

[213] J. Hauss, A. Fedorov, V. Brosco, C. Hutter, R. Kothari, S. Yeshwant, and A. Shnirman, 'Dissipation in circuit quantum electrodynamics: lasing and cooling of a low-frequency oscillator', New J. Phys. **10**, 095018 (2008).

[214] P. Rabl, P. Cappellaro, M. Dutt, L. Jiang, J. Maze, and M. D. Lukin, 'Strong magnetic coupling between an electronic spin qubit and a mechanical resonator', Phys. Rev. B, 041302 (2009).

[215] M. Lindberg and S. Stenholm, 'The master equation for laser cooling of trapped particles', J. Phys. B: At. Mol. Phys. **17**, 3375 (1984).

[216] S. Stenholm, 'The semiclassical theory of laser cooling', Rev. Mod. Phys. **58**, 699 (1986).

[217] J. I. Cirac, R. Blatt, P. Zoller, and W. Phillips, 'Laser cooling of trapped ions in a standing wave', Phys. Rev. A **46**, 2668 (1992).

[218] M. Gehm, K. O'Hara, T. Savard, and J. Thomas, 'Dynamics of noise-induced heating in atom traps', Phys. Rev. A **58**, 3914 (1998).

[219] J. R. Clem and A. Sanchez, 'Hysteretic ac losses and susceptibility of thin superconducting disks', Phys. Rev. B **50**, 9355 (1994).

[220] C. P. Bean, 'Magnetization of Hard Superconductors', Phys. Rev. Lett. **8**, 250 (1962).

[221] E. H. Brandt, M. V. Indenbom, and A. Forkl, 'Type-II Superconducting Strip in Perpendicular Magnetic Field', Europhys. Lett. **22**, 735 (1993).

[222] A. M. Campbell and J. E. Evetts, 'Flux vortices and transport currents in type II superconductors', Advances in Physics **21**, 199 (1972).

[223] C. Y. Pang, A. Campbell, and P. McLaren, 'Losses in Nb/Ti multifilamentary composite when exposed to transverse alternating and rotating fields', IEEE Trans. Magn. **17**, 134 (1981).

[224] W. J. Carr, M. S. Walker, and J. H. Murphy, 'Alternating field loss in a multifilament superconducting wire for weak ac fields superposed on a constant bias', J. Appl. Phys. **46**, 4048 (1975).

[225] E. H. Brandt, 'The flux-line lattice in superconductors', Rep. Prog. Phys. **58**, 1465 (1995).

[226] F. Gömöry, M. Vojenčiak, E. Pardo, M. Solovyov, and J. Šouc, 'AC losses in coated conductors', Supercond. Sci. Technol. **23**, 034012 (2010).

[227] L. Hackermüller, K. Hornberger, B. Brezger, A. Zeilinger, and M. Arndt, 'Decoherence of matter waves by thermal emission of radiation', Nature **427**, 711 (2004).

[228] A. Vinante, A. Kirste, A. den Haan, O. Usenko, G. Wijts, E. Jeffrey, P. Sonin, D. Bouwmeester, and T. H. Oosterkamp, 'High sensitivity SQUID-detection and feedback-cooling of an ultrasoft microcantilever', Appl. Phys. Lett. **101**, 123101 (2012).

[229] A. Vinante, 'Superconducting inductive displacement detection of a microcantilever', Appl. Phys. Lett. **105**, 032602 (2014).

[230] J. Druge, C. Jean, O. Laurent, M.-A. Méasson, and I. Favero, 'Damping and nonlinearity of a levitating magnet in rotation above a superconductor', New J. Phys. **16**, 075011 (2014).

[231] M. T. Johnsson, G. K. Brennen, and J. Twamley, 'Macroscopic superpositions and gravimetry with quantum magnetomechanics', (2014), arXiv:1412.6864 [quant-ph].

[232] G. Via, G. Kirchmair, and O. Romero-Isart, 'Strong Single-Photon Coupling in Superconducting Quantum Magnetomechanics', Phys. Rev. Lett. **114**, 143602 (2015).

[233] S. Bera, B. Motwani, T. P. Singh, and H. Ulbricht, 'A proposal for the experimental detection of CSL induced random walk', Sci. Rep. **5**, 7664 (2015).

[234] O. Romero-Isart, C. Navau, A. Sanchez, P. Zoller, and J. I. Cirac, 'Superconducting Vortex Lattices for Ultracold Atoms', Phys. Rev. Lett. **111**, 145304 (2013).

[235] C. Navau, J. Prat-Camps, O. Romero-Isart, J. I. Cirac, and A. Sanchez, 'Long-Distance Transfer and Routing of Static Magnetic Fields', Phys. Rev. Lett. **112**, 253901 (2014).

[236] J. Prat-Camps, C. Navau, and A. Sanchez, 'A Magnetic Wormhole', Sci. Rep. **5**, 12488 (2015).

[237] J. W. Bull and A. Gordon, 'Schrödinger's microbe: implications of coercing a living organism into a coherent quantum mechanical state', Biol. Philos. **30**, 845 (2014).

[238] T. Li and Z.-Q. Yin, 'Quantum superposition, entanglement, and state teleportation of a microorganism on an electromechanical oscillator', (2015), arXiv:1509.03763 [quant-ph].

[239] R. Gasparovic and W. McLean, 'Superconducting Penetration Depth of Lead', Phys. Rev. B **2**, 2519 (1970).

[240] G. Chanin and J. Torre, 'Critical-Field Curve of Superconducting Lead', Phys. Rev. B **5**, 4357 (1972).

[241] V. Dikovsky, V. Sokolovsky, B. Zhang, C. Henkel, and R. Folman, 'Superconducting atom chips: advantages and challenges', Eur. Phys. J. D **51**, 247 (2008).

[242] J. D. Jackson, *Classical Electrodynamics, 2nd Edition* (John Wiley & Sons, 1975).

[243] Q.-G. Lin, 'Theoretical development of the image method for a general magnetic source in the presence of a superconducting sphere or a long superconducting cylinder', Phys. Rev. B **74**, 024510 (2006).